ABSTRACT

Title of Document: RELIABILITY TESTING & BAYESIAN MODELING OF HIGH POWER LEDS FOR USE IN A MEDICAL DIAGNOSTIC APPLICATION.

Milind Mahadeo Sawant,
Doctor of Philosophy, 2013

Directed By: Dr. Aristos Christou
Materials Science and Engineering
Reliability Engineering

While use of LEDs in fiber optics and lighting applications is common, their use in medical diagnostic applications is rare. Since the precise value of light intensity is used to interpret patient results, understanding failure modes is very important. The contributions of this thesis is that it represents the first measurements of reliability of AlGaInP LEDs for the medical environment of short pulse bursts and hence the uncovering of unique failure mechanisms. Through accelerated life tests (ALT), the reliability degradation model has been developed and other LED failure modes have been compared through a failure modes and effects criticality analysis (FMECA).

Appropriate ALTs and accelerated degradation tests (ADT) were designed and carried out for commercially available AlGaInP LEDs. The bias conditions were current pulse magnitude and duration, current density and temperature. The data was fitted to both an Inverse Power Law model with current density J as the accelerating

agent and also to an Arrhenius model with T as the accelerating agent. The optical degradation during ALT/ADT was found to be logarithmic with time at each test temperature. Further, the LED bandgap temporarily shifts towards the longer wavelength at high current and high junction temperature. Empirical coefficients for Varshini's equation were determined, and are now available for future reliability tests of LEDs for medical applications.

In order to incorporate prior knowledge, the Bayesian analysis was carried out for LEDs. This consisted of identifying pertinent prior data and combining the experimental ALT results into a Weibull probability model for time to failure determination. The Weibull based Bayesian likelihood function was derived. For the 1st Bayesian updating, a uniform distribution function was used as the Prior for Weibull α-β parameters. Prior published data was used as evidence to get the 1st posterior joint α-β distribution. For the 2nd Bayesian updating, ALT data was used as evidence to obtain the 2nd posterior joint α-β distribution. The predictive posterior failure distribution was estimated by averaging over the range of α-β values.

This research provides a unique contribution in reliability degradation model development based on physics of failure by modeling the LED output characterization (logarithmic degradation, TTF $\beta<1$), temperature dependence and a degree of Relevance parameter 'R' in the Bayesian analysis.

RELIABILITY TESTING & BAYESIAN MODELING OF HIGH POWER LEDS FOR USE IN A MEDICAL DIAGNOSTIC APPLICATION

By

Milind Mahadeo Sawant

Dissertation submitted to the Faculty of the Graduate School of the
University of Maryland, College Park, in partial fulfillment
of the requirements for the degree of
Doctor of Philosophy
2013

Advisory Committee:
Dr. Aristos Christou, Advisor and Chair
Dr. Martin Peckerar, Dean's Representative
Dr. Mohammad Modarres
Dr. Ali Mosleh
Dr. Jeffrey Herrmann

Preface

The topic of Bayesian analysis has been discussed and debated for a few centuries. Jacob Bernoulli developed the Binomial theorem and laid the rules of permutations and combinations in the 17th century. Reverend Thomas Bayes (after whom the Bayes' theorem is named) provided an answer to Bernoulli's inverse probability problem in the 18th century. Pierre Simon Laplace also referred to as the 'Newton of France' developed the 'Bayesian' interpretation of probability in the early 19th century. Bruno De Finitti published his two volume 'Theory of Probability' in the 20th century. This provided a further growth and interest in the topic of Bayesian approach to statistics.

In the Fall of 2009, when I took a course on Data Analysis taught by Dr. Ali Mosleh, UMD, I became interested in Bayesian analysis. In our day to day life, we take every action based on our previous experiences, bias and prejudice. Be it a short-term task such as driving a car or long-term assignment such as raising a child. While our brain performs these tasks by judgment and intuition, Bayesian analysis allows us to mathematically use our past experience to predict the probability of an event. I hereby caution the reader not to perform Bayesian computations while driving a car since these computations take time!

While working at Siemens, I was posed with the problem of testing the reliability of LEDs for use in a medical diagnostic application. Around the same time, I was researching a topic for my Ph.D. research. Considering my interest in Bayesian

analysis, my advisor Dr. Aristos Christou, UMD recommended that I use Bayesian approach for assessing the reliability of the LEDs. I am so grateful to him for that suggestion since this allowed me to do research on something that I thoroughly enjoyed.

Back in 1986, when I was in the 9^{th} grade, a friend of mine had given me a few RED colored LEDs to use as a light source in an electronic educational kit. LEDs were not affordable to school students then. I was very impressed with the LEDs since it did not drain my 'expensive' 1.5V battery compared to the mini light bulb. I also remember that I had to be careful with the polarity of the battery to avoid damage to the LED (from excessive reverse bias). Twenty-six years later, as I am writing this dissertation, I cannot help but think that my Ph.D. research on Bayesian analysis of LED reliability was destiny!

Milind Sawant

Newark DE.

September 2012.

Dedication

This is dedicated to my parents, my wife Sujata, sons Ashwin and Atharva and all my friends.

Acknowledgements

There are times in life when one feels a sense of accomplishment combined with a sense of gratitude. Writing the acknowledgement page of a Ph.D. dissertation is one of them. First and foremost, I must thank my advisor Dr. Aristos Christou at University of Maryland for his guidance. He helped me select the topic and also focus on it with ideas and concrete suggestions. I also thank Dr. Martin Peckerar, Dr. Mohammad Modarres, Dr. Ali Mosleh and Dr. Jeffrey Herrmann for giving me suggestions and their opinions on various aspects of this research.

The laboratory facilities for this research were provided by Siemens for which I sincerely thank Dr. Robert Hall, Carl Ford and Frank Krufka. I enjoyed technical discussions with my colleagues Dr. Lucian Kasprzak, Dr. Edward Gargiulo, Dr. C. C. Lee, Gregory Pease, Joe Marchegiano and Gregory Ariff. Charlotte Gonsecki, Dan West and Tan Bui provided invaluable support in building test fixtures where as Aleksey Karulin helped me take good photographs using a digital microscope.

My parents are responsible for my success. Their confidence in me makes me work harder. My wife Sujata took care of the home front while I spent long hours in the lab and on the PC. My in-laws provided encouragement whereas my friends helped me remain sane during stressful times. Thanking my family and friends will belittle their affection. Finally, I express my love for my sons Ashwin and Atharva who are a source of continuous joy, inspiration and at times perspiration for me!

Table of Contents

List of Tables

List of Figures

List of Symbols and Abbreviations

Symbols:

1. α - Failure mode ratio (section 7.1)
2. α - Scale parameter of Weibull Distribution
3. α – Significance level for Chi-square test (section 10.2)
4. β - Shape parameter of Weibull Distribution
5. β - Failure effect probability (section 7.1)
6. c - speed of light in vacuum (section 6.1)
7. c – Acceptance limit for Chi-square statistic (section 10.2)
8. C_m - Criticality of failure mode (section 7.1)
9. Ea – Activation Energy
10. eV – Electron Volts
11. Eg – Bandgap Energy
12. h - Plank's constant,
13. If or I – LED forward current
14. Jt – Junction temperature
15. λ - Wavelength
16. λ - Failure rate (section 7.1)
17. nm – Nanometer
18. Vf or V – LED forward voltage drop

Abbreviations:

1. AF – Acceleration Factor
2. Al - Aluminum
3. AlGaAs – Aluminum Gallium Arsenide
4. AlGaInP – Aluminum Gallium Indium Phosphide
5. ADT – Accelerated Degradation Test
6. ALT - Accelerated Life Test
7. CDF – Cumulative Distribution Function
8. CFL – Compact Fluorescent Light
9. COP - Chip on Plate
10. DBR - Distributed Bragg Reflector
11. DC – Direct Current
12. DH – Double Heterostructure
13. DLTS - Deep Level Transient Spectroscopy
14. EC - Electronic Components
15. EL - Electro-Luminescence
16. ES – End State
17. ESD – Event Sequence Diagram
18. FDA – Food and Drugs Administration
19. FLE - Fatigue Life Expended
20. FMECA - Failure Modes and Effects Criticality Analysis
21. GaAs – Gallium Arsenide
22. GaP –Gallium Phosphide

23. GaN – Gallium Nitride

24. HP – Hewlett Packard

25. IE – Initiating Event

26. IEEE – Institute of Electrical and Electronics Engineers

27. In - Indium

28. InGaN – Indium Gallium Nitride

29. IPL – Inverse Power Law

30. IQE - Internal Quantum Efficiency

31. ISDRS - International Semiconductor Device Research Symposium

32. LED - Light Emitting Diode

33. MLE – Maximum Likelihood Estimate

34. MOCVD - Metal Organic Chemical Vapor Deposition

35. MQW – Multi Quantum Well

36. MTTF – Mean Time to Failure

37. NASA – National Aeronautics and Space Administration

38. NIST – National Institute of Standards and Technology

39. QD - Quantum Dot

40. OP - Optical power

41. PDF – Probability Distribution Function

42. PE – Pivotal Event

43. PRA – Probabilistic Risk Assessment

44. RDT – Reliability Demonstration Test

45. ROCS - Reliability of Compound Semiconductors Workshop

46. SMD – Surface Mounted Device
47. SPIE - International Society for Optics and Photonics
48. TRC - Thermal Resistance Circuit
49. TTF – Time to Failure
50. VPE - Vapor Phase Epitaxy
51. WOCSDICE - Workshop on Compound Semiconductor Devices and Integrated Circuits

Chapter 1: Introduction

1.1 Background and Motivation

Recently introduced consumer products (LED light fixtures, LED flash lights etc) and automotive applications have driven the need for higher reliability of LEDs as a selling point against existing lighting technology [21]. In LED applications such as Fiber Optic Communications and Lighting (see Fig 1.1), the ability of the optical receiver or human eye to detect presence or absence of light is important. Slight intensity variation within limits is tolerated. In Medical diagnostic applications (see Fig 1.2), the light output travels through a lens/filter and then passes through an optical cuvette which contains the human sample (blood, urine etc) mixed with chemical reagents. The absorbance of light by the cuvette mixture at certain wavelengths depends on the patient's disease condition. Light intensity is then measured by a detector/receiver to interpret patient results. This makes the LED failure definition unique. Thus the reliability and risk analysis done for LEDs in non-medical applications cannot be directly used considering hazard to human life.

Most of recent literature on LED reliability focuses on white LEDs (lighting) or colored (blue, green and red) LEDs. In most cases, they were operated using dc bias [15-17, 19, 21, 22, 26-29, 32-34]. In a few cases, the LEDs were driven in a pulse mode with different on times and duty cycles [20, 35, 42, 43, 48]. The target medical application will require 640 nm AlGaInP LEDs operated at pulse currents (on time of 100us at 0.2% duty cycle) making this analysis inevitable. See Table 1.1 for a

comparison of Lighting/Fiber optic vs. a Medical diagnostic application for LEDs. Bayesian modeling can allow us to combine prior information from published data with medical application related test data to estimate posterior LED failure rates.

Commercially available wavelength-specific high power LEDs can provide a significant cost advantage compared to traditional high intensity sources (flash lamps). Some of the problems anticipated with use of LEDs were low efficiency of output optical power, output power reduction, spectral shift over operation time, and catastrophic failure due to thermal effects. The research of this thesis was to characterize LED performance over time, identify and characterize new failure mechanisms and finally, generate a model of time to failure. Successive Bayesian updating using Medical application related LED life test data was the key experimental component of this thesis.

Lighting/Fiber Optics Application	**Medical Diagnostics Application.**
Light is **Detected** for presence or absence	Light **Measured** and biologically correlated for medical interpretation.
Driving: DC or 1-100% duty cycle	**Driving:** 100us pulse (0.2% duty cycle)
Failure Definition: As defined by system performance requirements i.e. 3-6 db system power degradation.	**Failure Definition:** Only 20% decrease in LED output power allowed. No spectral shift is allowed.
Failure Mitigation: Part replacement or optical system redesign.	**Failure Mitigation:** System re-calibration is necessary if failure is not catastrophic. If failure is catastrophic, LED replacement is necessary.

Table 1.1: Comparison of Lighting/Fiber Optics vs. Medical Diagnostic application

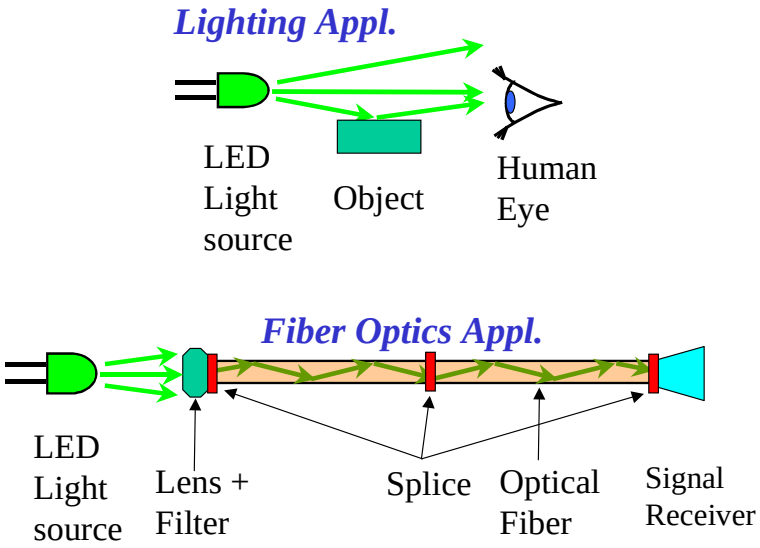

Fig. 1.1 LED in Lighting / Fiber Optics Application

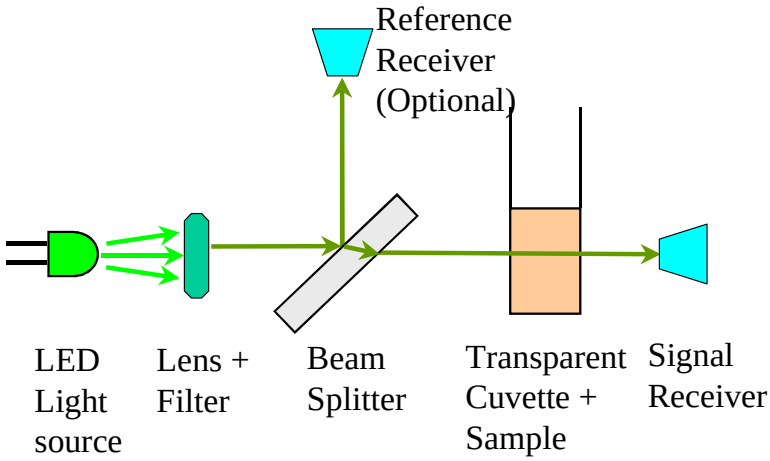

Fig. 1.2 LED in Medical Diagnostic Application

1.2 Goal, Objectives and Accomplishments of Research

This section summarizes the goals of the thesis and the approach taken as well as the summary of the results and the unique contributions. In subsequent chapters, the experimental and modeling approach is described in detail as well as the results of the research.

The goal of this research was to evaluate the reliability of 640 nm AlGaInP MQW LEDs in a medical diagnostic application using Accelerated Life testing and Bayesian modeling. The following questions needed answers:

1. Will the LED intensity remain within acceptable limits?
2. Will the LED wavelength remain stable?
3. Will the Time to Failure of LEDs exceed the Life of the Medical Instrument?
4. Will there be a cost benefit of using LEDs vs traditional light sources (flash lamps etc)?
5. Will there be any critical failure modes for the medical application?

The following section summarizes the specific accomplishments in order to meet the objectives stated above

1.2.1 FMECA for LED in Medical application

Failure Modes and Effects Criticality Analysis (FMECA) widely used for risk analysis was successfully applied to LED reliability and physics of failure investigation. FMECA was used to understand the criticality of LED failure modes when used in a medical diagnostic application. Failure modes of other components of the Medical device were not included in this study. The FMECA was repeated and refined after conducting accelerated life testing of LEDs. Degradation of the plastic encapsulation and the active region were found to be the critical failure modes. These failures could cause unscheduled calibration of the diagnostic instrument and could cause delay in patient medical test results.

1.2.2 Develop Test Setup

An experimental setup was developed for accelerated life testing of LEDs in environmental chambers. The test is automated by using test software, data acquisition/control boards and constant pulse current LED driver boards. The test SW makes the data acquisition board generate the necessary pulses, which trigger the LED driver board. The peak current through the LED is maintained constant while it is on. A separate signal conditioning circuit also measures the forward voltage Vf across the diode, which is fed back to the test SW to be written to a database. At regular intervals, the LEDs were removed from the environmental chambers and were characterized electrically and optically (using a Spectro-radiometer).

1.2.3 Perform Accelerated Life and Degradation Test

Accelerated Life Testing (ALT) and Accelerated Degradation Testing (ADT) of the LEDs in Pulse mode was conducted at 3 temperatures (35°C, 55°C and 75°C) and 2 Peak currents (Batch2: 483mA=418.1A/cm^2 and Batch3: 725mA=627.2A/cm^2). The optical power decreased with time due to degradation of the LED chip as well as the encapsulation. The rate of degradation followed a logarithmic function. 20% degradation was considered failure for the medical application. For LEDs that did not reach this failure threshold in a reasonable time (suspend data), the logarithmic function was used to extrapolate TTF. A log-linear model was used for analysis of degradation data and JMP software was used for this analysis.

1.2.4 Accelerating Agent Modeling

Prior published data and ALT data had to be converted to medical application conditions. This required the use of accelerating agent modeling. Inverse Power Law (IPL) model with J as the accelerating agent and the Arrhenius model with T as the accelerating agent were used. Regression analysis was used to estimate the parameter 'n' of the IPL model and activation energy 'Ea' of the Arrhenius model. An iterative regression analysis approach was used to get best possible regression fits thereby accommodating the effects of both current density and temperature.

1.2.5 Temperature dependence of Bandgap

Reliability testing of AlGaInP MQW LEDs resulted in a shift of Bandgap towards the longer wavelength when driven at high current. Characterization of the shift showed that it was temporary and dependent on the junction temperature Jt. The data was

further analyzed with respect to Varshini's equation, and the empirical coefficients were determined for the AlGaInP material.

1.2.6 Literature Survey for Bayesian Prior

The Bayesian analysis began by identifying published data, which can be used as prior information. From the published data, the time required for the optical power output to degrade by 20% was extracted. Analysis of published data for different LED Materials (AlGaInP, GaN, AlGaAs), Semiconductor Structures (DH, MQW) and driving (DC, Pulsed) was carried out.

1.2.7 Bayesian Likelihood Function

Many of the LED degradation mechanisms occur at the same temperature bias range. The mechanism with the lowest activation energy would dominate. The degradation mechanism of LEDs, published literature and our ALT data all indicate that Weibull is the most suitable model for this data analysis, as verified through a regression analysis. This rationale was used to develop the Weibull based Bayesian likelihood function. For the first Bayesian updating, uniform distribution was used as the Prior distribution for α-β parameters of the Weibull model.

1.2.8 Bayesian Updating

Starting with uniform prior for α-β values, prior published data was used as Evidence to get the first posterior joint α-β distribution. For the second Bayesian updating, the posterior from the first Bayesian updating was used as the prior. ALT data converted to medical application conditions was used as Evidence to get the second posterior joint α-β distribution. This joint α-β distribution gave a series of Weibull time to

failure distributions. The predictive posterior failure distribution for the LEDs was estimated by averaging over the range of α-β values. Software was written for performing various Bayesian computations.

1.2.9 Degree of Relevance in Bayesian modeling

An approach is proposed for using partially relevant data in Bayesian modeling. A new parameter 'R' (degree of relevance) is used to modify the likelihood function before using it in Bayesian updating. The 'R' value will be used such that the influence of evidence is decreased as R approaches zero.

1.3 Publications of Present Research

The research carried out as part of this thesis resulted in the publication of three research papers and one poster presentation. These are listed below:

1. International Semiconductor Device Research Symposium (ISDRS), College Park MD, Dec 2011 [11].
2. Workshop on Compound Semiconductor Devices and Integrated Circuits (WOCSDICE), Island of Porquerolles, France, May 2012 [12].
3. Reliability of Compound Semiconductors Workshop (ROCS), Boston MA, April 2012 [13]
4. Poster presented at ResearchFest, College Park, MD, March 2012.

1.4 Summary of Contribution

The contributions of this thesis is that it represents the first measurements of reliability of AlGaInP LEDs for the medical environment of short pulse bursts and hence the uncovering of unique failure mechanisms.

1.4.1 LED bias conditions are different

Published articles tried to characterize LEDs using DC bias (for reliability) and in some instances using pulsed bias (for performance evaluation rather than reliability). The target medical application does not require continuous optical output but only when the human test sample is provided (in fraction of ms). Failure mechanisms in this research were influenced by peak currents rather than average currents.

1.4.2 Application of LED is different

In Fiber Optics & Lighting applications, light is used for detection. In Medical diagnostic applications, the precise value of light intensity is used to interpret patient results. This research will allow replacement of traditional light sources (filament or flash lamps) with LEDs. The lamps degrade and have to be replaced 3-6 months causing a major inconvenience to the customer whereas LEDs will outlast the 7-year life of the medical diagnostic instrument.

1.4.3 Consequence of LED Failure is different

In Fiber Optics & Lighting applications, failures are usually significant loss of optical output. Failure usually means inconvenience and redundancy is a common mitigation. In medical diagnostic applications, calibration and referencing is used to mitigate LED failure. However, if a subtle change in optical intensity goes undetected, it could

cause erroneous patient results. This can cause erroneous diagnosis, incorrect treatment and possibly severe health complications. If this were to occur, apart from a possible litigation between patient, hospital and the medical equipment manufacturer, the FDA will start questioning the entire risk analysis done on the medical equipment.

1.4.4 Decreasing failure rate β of the Weibull TTF model

It was observed that the shape parameter β of the Weibull TTF model is less than one (implying a decreasing failure rate) in prior published data, ALT and Bayesian model. During ALT, the rate of optical output degradation was logarithmic and this rate varied significantly between different LEDs. Some LEDs cross the 20% degradation (failure threshold for this application) earlier than others. For LEDs that do survive this initial high rate of optical degradation, the probability that it will survive longer increases. This explains the decreasing failure rate.

1.4.5 Temperature dependence of bandgap characterized

It was found that the bandgap of AlGaInP MQW LEDs shifts towards the longer wavelength when driven at high current. Characterization of the shift showed that it was temporary and dependent on the junction temperature Jt. The data was further analyzed with respect to Varshini's equation, and the empirical coefficients were determined for the AlGaInP material. Since the spectral performance is critical for the medical application, my spectral shift investigation will provide immense value to the designer. The junction temperature will need to be maintained.

1.5 Dissertation Layout

Chapter 1 provides an introduction to this dissertation. It starts by giving a background and motivation. It specifically describes how a medical diagnostic application differs from a lighting or fiber optic application for LEDs. It then states the goals and objectives of this research. Work accomplished including publication of three research papers and a poster presentation is listed. Finally, it describes the contribution and why this research was necessary.

Chapter 2 provides a thorough literature review on the subject. It starts by listing various research groups who are working on the subject of LED reliability. It also lists various journals, which have published important articles on LED reliability. Thereafter it describes the work done on AlGaInP LEDs by various research groups. It briefly describes their work, their approach and their results. The same is then described for GaN LEDs. The chapter ends by describing a couple of articles on Bayesian analysis.

Chapter 3 covers the theory for LEDs. It describes the basic LED operation, the band structure in semiconductors and the relationship between the band gap energy and the wavelength of the photon emitted. It describes the radiative and non-radiative recombination process and its effect on LED reliability. Temperature dependence of the spectrum is briefly described. It then describes the basic LED degradation mechanisms and those specifically related to AlGaInP LEDs.

Chapter 4 describes Accelerated life modeling. Prior published data and ALT data had to be converted to medical application conditions. This required the use of accelerating agent modeling. Inverse Power Law (IPL) model with J as the accelerating agent and the Arrhenius model with T as the accelerating agent are described. Acceleration factors are derived. Parameter 'n' for the IPL model and activation energy 'Ea' for the Arrhenius model are estimated using regression analysis for various combinations of LED material and structure. After converting the published data to medical application conditions, it is subjected to Weibull analysis.

Chapter 5 describes the Accelerated Life Testing (ALT) performed during this research. It describes the materials and the methods used. ALT was performed at elevated temperature and current and the LEDs were driven in pulse mode. The test setup used is also described. This is followed by a detailed discussion on the results of ALT. It describes the LED optical power degradation, encapsulation degradation, and chip vs. lens degradation and spectral performance after ALT. The results of the ALT are then summarized.

Chapter 6 describes the thermal shift of the active layer band gap. It first describes the forward bias method used to establish the linear relationship between the forward voltage Vf of the diode and the junction temperature. A series of experiments are described which establish the relationship between Vf and the peak wavelength of the LED. It then describes the Varshini's model and estimates the parameters of this

model for the AlGaInP LED material. Findings of previous researchers are described and they are compared and contrasted with our results.

Chapter 7 describes the Failure Modes, Effects and Criticality Analysis (FMECA) performed during this research. Severity classification for a general and a medical diagnostic application are described. Various LED failure modes are discussed. FMECA table is constructed and critical failure modes are identified. The table is reconstructed after ALT and findings are discussed. Plastic encapsulation and active region degradation were estimated as the critical failure modes. Either of these failure modes will cause system level effects such as excessive drift requiring unscheduled calibration and delayed medical test results.

Chapter 8 describes Bayesian modeling of LED reliability. First, the basic Baye's theorem is derived. Then the likelihood function for α - β parameter based Weibull model is developed. Equation for the joint α - β posterior distribution is derived. Thereafter the results of our Bayesian modeling are discussed. The first posterior is generated using published data as evidence and the second posterior is generated using the ALT data as evidence. Predictive posterior estimates are derived by averaging over the range of α & β values.

Chapter 9 proposes the use of a new parameter Degree of Relevance (R) in Bayesian analysis. Life of LEDs varies significantly depending upon the LED material used, the semiconductor structure used and the mode of driving. Bayesian modeling

computes the LED reliability by combining prior published LED data with the current test data. It is very difficult to get prior for the exact same material, structure and driving. The ‘R’ value was used to modify the Bayesian model such that the influence of evidence is decreased as R approaches zero. This chapter discusses methods of obtaining the parameter R and one method of using it. Additional approaches are discussed in section 11.4 (Future research).

Chapter 10 covers the topic of Bayesian model selection and validation. The subjective nature of the prior distribution may raise doubts about the accuracy of Bayesian posterior distributions. Validation approach such as the chi-square statistic is described. Validation of Bayesian modeling for various phases is discussed. These include selection of the distribution for the underlying failure distribution, suitability of the prior information and appropriateness of predictive posterior distribution against the test data.

The final chapter 11 concludes this research. It reviews the objectives, accomplishments and future areas of research.

Chapter 2: Literature Review

2.1 Introduction

Various research groups are working on LED reliability and related topics:

- Osram, HP, Philips R&D groups: High brightness AlGaInP LEDs [15-24]
- University of Padova, Italy: Reliability & Life testing of GaN LEDs [32-41]
- LRC, Rensselaer Polytechnic Institute, Troy, NY: LED Life Testing, [49-50]
- Sandia National Laboratories, NM: AlGaN/InGaN/GaN Life testing [42-44]
- Nakamura, Yanagisawa, other Japanese groups: GaN LEDs [3, 46-48]
- NIST: Calibration / LED measurement Standards, [52-57]
- Miscellaneous / Bayesian [5, 25-27, 58-63]

Articles related to LED reliability have been published in various journals such as IEEE, SPIE, Microelectronic Reliability, Applied Optics, Electronics Letters, Electronic Materials & Packaging etc. Ott [14] has written a review article on capabilities and reliability of LEDs as a part of a NASA report, which summarizes some of the degradation modes. Vanderwater, Kish et al. [15] have written a nice review article on high brightness AlGaInP LEDs whereas Meneghini et al. [32] have reviewed reliability of GaN LEDs. Work by Nakamura [3] and Fukuda [2] served as good references for this dissertation. Research is this dissertation relied heavily on work by Mosleh [8] for concepts on Bayesian reliability (explained in chapter 8). A few examples of use of Bayesian analysis in reliability applications are discussed at the end of this literature review.

LEDs used in this research used AlGaInP material and the Multi Quantum Well (MQW) semiconductor structure. AlGaInP is a mature technology developed in the early-mid-nineties compared to GaN, which is still evolving. It was interesting to observe that a lot of published AlGaInP related articles focused on performance improvement [15-23, 25-27, 30] compared to articles on AlGaInP Reliability & Life testing [15-17, 21, 22, 24, 26-30]. On the other hand, we found many recent articles on GaN LEDs which specifically focus on Reliability and Life testing [32-43, 47-51]. A possible explanation for this could be that since last 5 years, LEDs are being considered as serious competitors to compact florescent lamps (CFL) which will soon replace incandescent lamps. LED based 'bulbs', which fit in regular electrical fixtures, have started appearing in retail stores since 2011. LED based break lights and indicator lights are available in recent automobile models. Many of the flashlights sold in retail stores since 2009 use LEDs. Such automotive applications and consumer products [16, 21, 32] may have driven the need for higher reliability as a selling point against existing lighting technology.

2.2 AlGaInP LEDs

Per Vanderwater, Kish et al. [15, 17], attainment of high efficiency performance in AlGaInP LEDs is a result of the development of advanced Metal Organic Chemical Vapor Deposition (MOCVD) crystal growth techniques. $(Al_xGa_{1\_x})_{0.5}In_{0.5}P$ Double-Heterostructure (DH) active layers are grown lattice-matched on GaAs substrates by MOCVD. To improve current spreading and light-extraction, a p-type GaP window is grown by Vapor Phase Epitaxy (VPE) on the device layers. Subsequently, the absorbing GaAs substrate is selectively removed and a transparent n-type GaP substrate is substituted in its place by semiconductor wafer bonding at elevated temperature and under applied uni-axial pressure. An important step is matching of the crystallographic orientations of the bonded wafers to facilitate low-resistance (low-voltage, high efficiency) operation. After wafer bonding, patterned alloyed ohmic contact metallization is applied to both the p and n sides of the wafer, and the devices are diced and packaged into standard LED lamps.

A recent review article by Streubel et al [22] mention further advancements in the AlGaInP LED technology such as texturing the surface of the chips to improve extraction efficiency. They provide a schematic drawing of the layer structure of a typical high brightness LED. The outer layers are used to optimize carrier confinement and decrease leakage. The Setback layers are used to control doping and diffusion of dopants Mg, Zn and Te. Window layers on top are used to improve current spreading where as an optional DBR layer is used to recover the light emitted in the direction of the substrate.

Grillot et al [16] used both fixed and variable current density stress conditions to study light output degradation of AlGaInP LEDs as functions of LED stress current and LED stress time. For stress times long enough and current densities high enough to saturate any short-term effects, quantification of the resulting data indicated that the LED degradation is a linear function of current density and a logarithmic function of stress time for as long as 60 000 hours. They show that LED degradation can be caused by changes in Extraction efficiency $C_{ex}(t)$, Defect concentration $N_T(t)$ and Leakage current density $J_L(t)$. They argue that monotonic increase or decrease in LED light output is likely due to corresponding increase or decrease in $N_T(t)$ whereas short term degradation is due to changes in $N_T(t)$ as well as changes in $J_L(t)$ that saturate for sufficiently long stress time or high current density.

Lacey et al [28] studied the reliability of AlGaInP DH LEDs operating typically at 600 nm. To investigate degradation, accelerated aging at ambient temperatures of 50, 75 and 125 C was carried out for over 5000 hrs. The activation energy of homogeneous degradation was determined to be 0.8 eV and an extrapolated half-life in excess of 1.0E6 hrs was estimated at an ambient temperature of 20 C. Nogueira et al [30] performed accelerated life testing on AlGaInP LEDs at high temperatures (120C to 140C). Open circuit catastrophic failures were observed and the root cause was due Anode corrosion caused by moisture penetrating the package. The data was analyzed using Inverse Power Law model for current and Arrhenius reaction rate model for temperature. The data was also fitted to Weibull distribution.

Hofler et al [18] concluded that for AlGaInP LEDs, increasing the junction area (from 210 x 210μm^2 to 500 x 500μm^2) without changing the aspect ratio results in ~25% decrease in extraction efficiency. They also saw significant color shifts and decrease in luminous efficiency as junction temperature is increased. Liang et al [25] specifically compared temperature performance for InGaN and AlGaInP LEDs. In case of GaN MQW LEDs, the Electro-Luminescence (EL) main peak increased monotonically with temperature from 10 to 200 K and slightly decreased with further temperature increase in the 200 K range. This is in contrast with the monotonic decrease of EL with increasing temperature for conventional AlGaInP QW red LEDs. The anomalous temperature dependence of the InGaN/GaN LEDs was attributed to the barrier caused by Quantum Dot (QD) like structure.

Kish et al [20] studied high luminous flux AlGaInP/GaP large area emitters with currents as high as 7A. Although heating is significant in these devices, their performance was primarily limited by light extraction. Under pulsed operation (1 μs, 0.1 % duty cycle), a conventional TS AlGaInP LED lamp (213 x 213μm^2 chip) exhibited an external efficiency of ~9.1% (415 A/cm^2) compared to ~3.1% for the large-area LED (375 x 4500μm^2 chip) where both chips were fabricated from the same wafer. Under DC operation, the external efficiency of the large-area LED further decreases to ~1.9%.

Chang et al [19] reviewed the luminescence properties of various AlGaInP LEDs using Double Heterostructure (DH), Distributed Bragg Reflector (DBR) and various Multi Quantum Well (MQW) structures. They found that MQW LEDs are brighter than DH and DBR LEDs, particularly under low current injection. For the MQW LEDs, their Electro-Luminescence (EL) increases as the number of wells increase. They found that MQW LEDs are more reliable than DH and DBR LEDs. Under pulse operation, they found that, as the number of wells increases, the amount of decay becomes smaller.

Altieri et al [23] studied internal quantum efficiency of high brightness AlGaInP LEDs. One approach to improve the LED efficiency is to improve the light extraction efficiency by means of new device concepts comprising wafer bonding, chip geometry or surface texturing. However, with decreasing emission wavelength, a strongly temperature dependent loss of LED External Quantum Efficiency (EQE) is observed. This short wavelength behavior indicates the existence of loss mechanisms originating from the active layer itself. E.g. Nonradiative recombination and carrier leakage into the confining layers reduce the internal quantum efficiency (IQE). From a more detailed analysis of the wavelength dependence of the non-radiative recombination, they assign the loss to the electron transfer from the quantum well Γ-band to the confinement layer X-band (Γ-X transfer), dominating over other defect related mechanisms.

Krames et al [21] review the status of LEDs for Solid state lighting applications. The AlGaInP (red to yellow) and InGaN-GaN (blue to green) material systems dominate the field. Sophisticated device structures based on these material systems result in light extraction efficiencies of 60% and 80%, for AlGaInP and InGaN-GaN, respectively. At the time of their writing, commercially available high-power white LEDs based on phosphor down-conversion provided luminous efficacies of 70 lm/W. Recent improvements in LED luminance place them brighter than halogen filaments, making LEDs attractive for use in automotive headlamps for the first time. The challenge for solid-state lighting now is clearly in internal quantum efficiency, which for the InGaN-GaN and AlGaInP (at operating temperatures) is far below what has been achieved in other III-V systems such as (Al)GaAs. Breakthroughs in internal quantum efficiency would result in high-power phosphor-white LEDs with efficiencies reaching 160 lm/W or more, a performance level surpassing anything known to date for a practical white light source.

2.3 GaN LEDs

Meneghini et al [32] review the degradation mechanisms that limit the reliability of GaN-based light-emitting diodes (LEDs). They propose a set of specific experiments for separately analyzing the degradation of the active layer, ohmic contacts and the package/phosphor system. They show that Low-current density stress can determine the degradation of the active layer of the devices, implying modifications of the charge/deep level distribution with subsequent increase of the nonradiative recombination components. High-temperature storage can significantly affect the properties of the ohmic contacts and semiconductor layer at the p-side of the devices,

thus determining emission crowding and subsequent optical power decrease. High-temperature stress can significantly limit the optical properties of the package of high-power LEDs for lighting applications.

Levada et al. [34] carried out accelerated life tests on plastic transparent encapsulation and pure metallic package GaN LEDs. Parameters chosen as representative of the observed failure modes were Optical power (OP) measured at 20 mA, Reverse current (Irev) measured at −5 V and Series resistance Rs (differential at 40mA & 10mA). The failure criteria were 20% decrease in OP, Irev increase by factor of 2.5 and 7% increase in Rs. A consistent Weibull based statistical model was found for MTTF and the accelerating factors of high current stresses were estimated.

Buso et al. [35] experimentally investigated the performance of commercially available high brightness GaN LEDs under DC and pulsed bias. Electrical, Thermal resistance and Optical characterization was done to see the effects of stress. The authors conclude that square-wave driving can be efficient only for high duty cycles. For low duty cycles, worse performance was detected due to the saturation of efficiency at high peak current levels. Three families of devices submitted to dc and pulsed stresses showed different behaviors, indicating that stress kinetics strongly depends on the LED structure and package thermal design.

Osinski et al [42] focused on the performance of commercial AlGaN/InGaN/GaN blue LEDs under high current pulse conditions. The results of deep level transient

spectroscopy (DLTS), thermally stimulated capacitance, and admittance spectroscopy measurements performed on stressed devices, showed no evidence of any deep-level defects that may have developed as a result of high current pulses. Physical analysis of stressed LEDs indicated a strong connection between the high intrinsic defect density in these devices and the resulting mode of degradation.

Following the initial studies of rapid LED failures due to metal migration under high current pulses, Barton et al. [43] placed a number of Nichia NLPB-500 LEDs (InGaN/AlGaN) on a series of life tests. The life tests did not produce significant degradation at currents less than 60 mA indicating a remarkable longevity in spite of their high density of defects. One of the older technology, double heterostructure Nichia LEDs showed a greater than 50% light output degradation after 1200 hours. Failure analysis revealed that a crack had isolated part of the junction and was the cause of the degradation. Two of the newer generation LEDs showed a greater than 40% loss in output intensity after 3600 and 4400 hours. The LEDs did not exhibit any significant change in its I-V characteristics indicating that the failure mechanism may be related to the plastic encapsulation material.

Yanagisawa [48] performed long-term accelerated degradation tests on GaAlAs red LEDs under continuous and low-speed pulse operation and studied the differences in the degradation and lifetime. The major factor causing the degradation was decrease in the radiative recombination probability due to defect generation. In an earlier paper, Yanagisawa [47] investigated the long-term accelerated degradation of GaN

blue LEDs under current stress. From the degradation pattern of optical output over time, the dependence on current stress was studied and an equation for estimation of the half-life of the diode was obtained.

Getty et al [56] demonstrated a method for the determination of internal quantum efficiency (IQE) in III-nitride-based light-emitting diodes. LED devices surrounded with an optically absorbing material were fabricated to limit collected light to photons emitted directly from the quantum wells across a known fraction of the recombination area. The emission pattern for this device configuration was modeled to estimate the extraction efficiency. IQE was then be calculated from the measured input current and output power. This method was applied to c-plane InxGa1−xN-based LEDs emitting at 445 nm. Initial measurements estimated an IQE of 43% + 1% at a current density of 7.9 A/cm2.

Chen et al. [31] evaluated the thermal resistance and reliability of high power Chip on Plate (COP) LEDs. The techniques used were Thermal Resistance Circuit (TRC) method, Finite Element Method (2D Ansys) and Experimental using Wet High Temperature Operation life (WHTOL) conditions (85°C/85%RH, 350mA) for 1008 hrs. Results from 2D Ansys were closer to experimental data than TRC since real heat flow paths are difficult to be completely evaluated by TRC. During WHTOL, all COP packages with phosphorus in the silicone encapsulant failed after 309 hrs. The failure sites were located at aluminum wire bonding to the chip and copper pad of the substrate. For the passing packages (without phosphorus), junction to air thermal

resistances increased with time by up to 12 °C/W due to decrease in thermal conductivity of die attach (from moisture absorption).

Narendran et al. [49] conducted two experiments. In the first experiment, several white LEDs (same make/model) were subjected to life tests at different ambient temperatures (35, 45, 50, 55, & 60 ^{o}C). A temperature sensor was placed on the cathode lead (T-point). The environment chambers also acted as light integrator boxes. The drive current was 350mA and the light was measured by a photodiode. The exponential decay of light output over time was used to estimate life. The life also decreased exponentially with increasing temperature. In a second experiment, several high-power white LEDs from different manufacturers were life-tested under similar conditions (35 ^{o}C, 350mA). Results showed that different products have significantly different life values.

In an earlier paper [50], Narendran et al. measured light output degradation and color shift over time for commercially available high flux LEDs. From one manufacturer (single die per package), red, green, blue and white LEDs were used. From a second manufacturer (multiple dies per package), a different high flux white LED was used. The LED arrays were tested under three sets of conditions: Normal current (350 mA) / normal temperature (35 ^{o}C), 350 mA / 50 ^{o}C and 450 mA / 35 ^{o}C. The LEDs were characterized optically by NIST accredited 2 meter integration spheres. Overall, the single die green and white LED arrays showed very little light loss after 2000 hours even though the current and temperature were increased. The red LED seemed to

have a high degradation rate. The white LEDs had a significant color variation (total 12 step MacAdam ellipse, 2 step during initial 2000 hours).

Tsai et al. [51] aged samples from different manufacturers at 65, 85, and 95^{o}C under a constant driving current of 350 mA. The results showed that the optical power of the LED modules at the two view angles of ± (45^{o}~75^{o}) decreased more than the other view angles as the aging time increased. This was due to the reduction of radiation pattern from the corner effect of lens shape, resulted in lower output power. Results also showed that the center wavelength of the LED spectrum shift 5 nm after thermal aging 600 hours at 95^{o}C because of degradation in the lens material.

Wang et al [45] developed a comprehensive optical model for dual wavelength LEDs using optical ray tracing programs. Optical dispersion of GaN, InGaN, and AlGaN was also included in this numerical model. Per the authors, the light extraction efficiency of LEDs can be calculated based on LED structure and material properties. The LED device structure can be optimized to improve the light extraction efficiency.

2.4 LED measurements

Yoshi Ohno [52] reviewed photometric, radiometric, and colorimetric quantities used for LEDs and discussed CIE standardization efforts. A large variation in LED measurements is reported (40-50 % due to spectral/spatial characteristics) compared with traditional lamps (within a few %). The Averaged LED Intensity is defined by CIE127 publication and involves measuring the intensity by a circular photometer head (100 sq.mm) at a distance of 316 mm (condition A, 0.001 steridians) or 100 mm

(condition B, 0.01 steridians). This is recommended for individual LEDs having a lens optic (such as a 5 mm epoxy type) since they do not behave as a point source. CIE127 also revised total luminous flux measurements and spectral measurements to include backward and sideways emissions of LEDs by mounting it in the center of the integrating sphere. For applications where backward or sideways emissions are not useful, a new quantity 'Partial LED Flux' is proposed.

Miller et al. [53] cover the capabilities and services provided by NIST for calibration of LEDs. Services include official color calibrations, radiometric calibration and total spectral radiant flux standards. In two earlier papers [54, 55], the authors discuss the uncertainty in LED measurement. For Average LED Intensity (photometric bench / alignment procedures), uncertainty range was 0.8 % to 3 %. For total luminous flux measurement (mounting geometry, backward emission, integrating sphere designs, including baffles and auxiliary LEDs) the expanded uncertainty range was 0.6 % to 2.3 %. Park et al. [57] also evaluated the uncertainty in measurement of Average LED Intensity by using a spectral Irridiance standard lamp as a calibration source for the spectro-radiometer and 12 uncertainty components with correlation taken into account. The relative uncertainties for the test samples were determined to be in a range from 4.1% to 5.5%.

2.5 Bayesian analysis

Brian Hall [58] published his Ph.D. dissertation titled 'Methodology for evaluating reliability growth programs of discrete systems'. The purpose of this area of research is to quantify the reliability that could be achieved if failure modes observed during

testing are corrected via a specified level of fix effectiveness. New reliability growth management metrics are prescribed for one-shot systems under two corrective action strategies. The first is when corrective actions are delayed until the end of the current test phase. The second is when they are applied to prototypes after associated failure modes are first discovered. Statistical procedures (i.e., classical and Bayesian) for point-estimation, confidence interval construction, and model goodness-of-fit testing are also developed. In particular, a new likelihood function and maximum likelihood procedure is derived to estimate model parameters.

Hurtado-Cahuao [60] published his Ph.D. dissertation titled ‘Airframe Integrity Based on Bayesian Approach'. A probabilistic based method has been proposed to manage fatigue cracks in the fastener holes. As the Bayesian analysis requires information of a prior initial crack size pdf, such a pdf is assumed and verified to be lognormally distributed. The prior distribution of crack size as cracks grow is modeled through a combined Inverse Power Law (IPL) model and lognormal relationships. The first set of inspections is used as the evidence for updating the crack size distribution at the various stages of aircraft life. After the updating, it is possible to estimate the probability of structural failure as a function of flight hours for a given aircraft in the future. The results show very accurate and useful values related to the reliability and integrity of airframes in aging aircrafts.

Wang et al. [61] propose a Lognormal distribution model to relate crack-length distribution to fatigue damage accumulated in aging airframes. The fatigue damage is

expressed as fatigue life expended (FLE) and is calculated using the strain-life method and Miner's rule. A 2-stage Bayesian updating procedure is used to determine the unknown parameters in the proposed semi-empirical model of crack length versus FLE. At the first stage, the crack closure model is used to simulate the crack growth. The results are then used as data to update the un-informative prior distributions of the unknown parameters of the proposed semi-empirical model. At the second stage, the crack-length data collected from field inspections are used as evidence to further update the posteriors. Two approaches are proposed to build the crack-length distribution for the fleet based on individual posterior crack distribution of each aircraft. These can be used to analyze the reliability of aging airframes by predicting, the probability that a crack will reach an unacceptable length after additional flight hours.

R. Bris et al [62] demonstrates the use of Bayesian approach to estimate the acceleration factor in the Arrhenius reliability model based on long-term data given by a manufacturer of electronic components (EC). Using the Bayes approach they consider failure rate and acceleration factor to vary randomly according to some prior distributions. Bayes approach enables for a given type of technology, the optimal choice of test plan for RDT under accelerated conditions when exacting reliability requirements must be met.

Anduin E. Touw [63] use Bayesian estimation procedure for mixed Weibull distributions. Estimation of mixed Weibull distribution by MLE and other methods is

frequently difficult due to unstable estimates arising from limited data. Bayesian techniques can stabilize these estimates through the priors, but there is no closed-form conjugate family for the Weibull distribution. This paper reduces the number of numeric integrations required for using Bayesian estimation on mixed Weibull situations from five to two, thus making it a more feasible approach to the typical user. It also examines the robustness of the Bayesian estimates under a variety of different prior distributions.

Chapter 3: Theory of Light Emitting Diodes

3.1 Basic LED Operation

A light Emitting Diode (LED) is a semiconductor diode, which emits light when current passes through it in the forward direction. See Fig 3.1 [5] and Fig 3.2 [5]. When the diode is forward biased [9], electrons are able to recombine with holes and energy is released in the form of light. This effect is called electro-luminescence and the color of the light is determined by the energy gap of the semiconductor. Like a normal diode, the LED consists of a chip of a semiconductor material impregnated, or doped, with impurities to create a p-n junction which conducts when forward biased (P-type Anode is +ve with respect to N-type cathode).

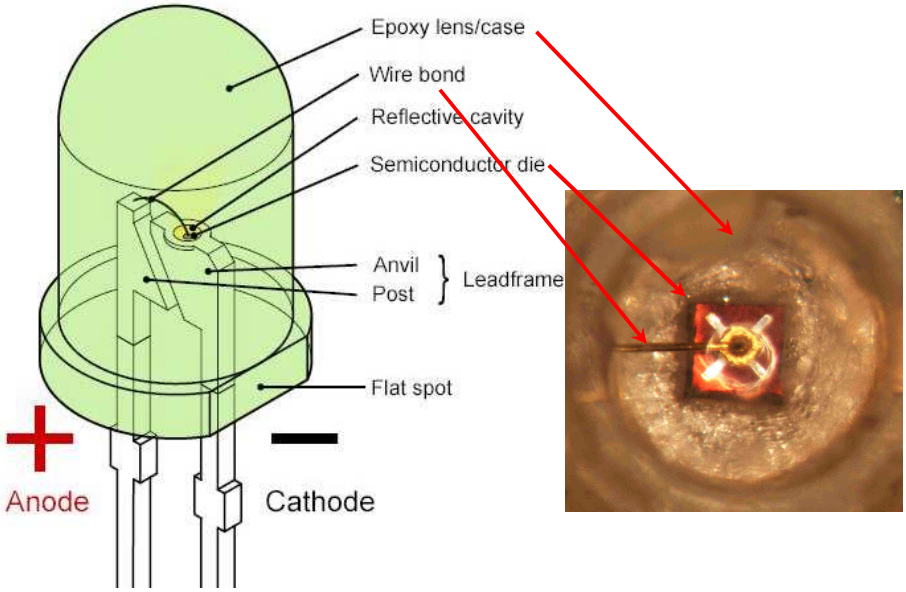

Fig. 3.1 Construction of Common LED [5] vs. LED used in this research

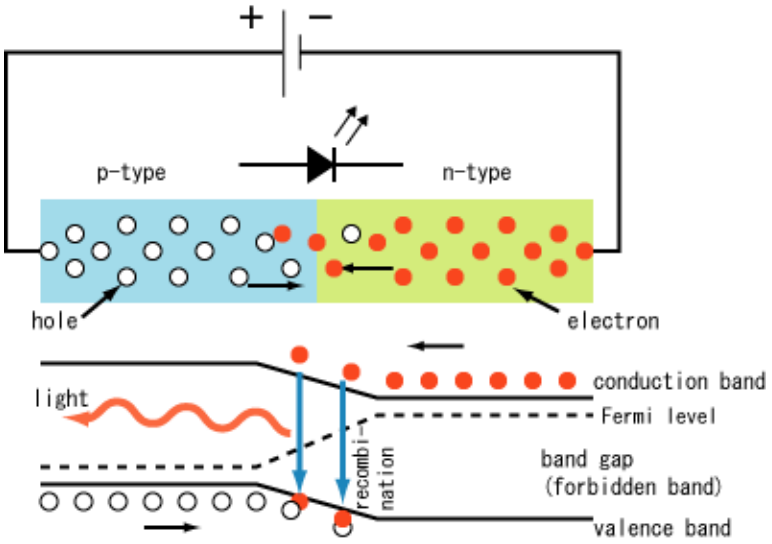

Fig. 3.2 LED Operation [5]

3.2 Band Structure in Semiconductors

The electrons of a single isolated atom occupy atomic orbitals, which form a discrete set of energy levels [9]. If several atoms are brought together into a molecule, their atomic orbitals split, as in a coupled oscillation. This produces a number of molecular orbitals proportional to the number of atoms. When a large number of atoms ($>10^{20}$) are brought together to form a solid, the number of orbitals becomes exceedingly large. The difference in energy between them becomes very small, so the levels may be considered to form continuous bands of energy rather than the discrete energy levels of the atoms in isolation. However, some intervals of energy contain no orbitals, no matter how many atoms are aggregated, forming band gaps.

The band gap of a semiconductor is either direct or indirect. The minimal-energy state in the conduction band, and the maximal-energy state in the valence band, are each

characterized by a certain k-vector in the Brillouin zone [9]. If the k-vectors are the same, it is called a "direct gap". If they are different, it is called an "indirect gap". For an indirect band gap, an electron cannot shift from the lowest-energy state in the conduction band to the highest-energy state in the valence band without a change in momentum. Hence direct band gap semiconductors are preferred for LEDs.

3.3 Wavelength of emitted light

When an LED is forward biased, the electrons in the conduction band recombine with holes in the valence band. In the recombination process, energy Eg corresponding to the band gap is emitted in the form of a photon whose wavelength λ (in nm) is given by

$$\lambda = h\,c / Eg = 1239.8 / Eg \qquad \text{- (3.1)}$$

where h = Plank's constant, c = speed of light in vacuum and Eg = band gap in eV.

3.4 Radiative and Non-radiative recombination in semiconductors

During a radiative recombination [9], an electron in the conduction band annihilates a hole in the valence band, releasing the excess energy as a photon. This process is possible in a direct band gap semiconductor. In contrast, the energy produced in a non-radiative recombination does not create photons, but is released by lattice vibration (phonon) in the semiconductor and finally changed to heat [2]. This non-emitted energy enhances the rate of degradation of optical devices. Thus the non-radiated recombination process plays a very important role in the device degradation and hence device reliability.

3.5 Light output vs. Junction temperature

Temperature dependence of semiconductor device characteristics is very important from a reliability standpoint [2]. During operation, heat is generated in the active layer (also in other parts having ohmic resistance) which raises the junction temperature. As the junction temperature increases, the internal quantum efficiency η_i decreases due to the reduction of the radiative recombination coefficient and increase in overflow of injected carrier from the active layer. Both of these changes cause the light output of an LED to decrease rapidly. Moreover, the influence of Auger recombination becomes large in the high-injected region. Thus the suppression or removal of the heat generated in the active region during operation is very important to obtain high radiative efficiency. Thermal shift of active layer bandgap was studied in detail during this research and is discussed in Chapter 6.

3.6 Basic LED degradation mechanisms

Various degradation modes of LEDs have been classified [2] as rapid, gradual and sudden. Different parts in LEDs prone to degradation are Active region, P-N Contacts, Indium Tin Oxide layer, Plastic encapsulation and Packaging (Bond wires and internal Heat Sink). These are described in detail in section 7.2.

3.7 Degradation of AlGaInP LEDs

The resistance to degradation of AlGaInP LEDs has been attributed by Streubel et al [22] to a decreased sensitivity of the devices to oxidation. This is due to reduced Al content in the active zone if compared to AlGaAs devices. Also, growth and mobility of dark line defects is decreased owing to incorporation of In in the compound. Per

Vanderwater et al [15], neither the mismatched GaP window layer nor the presence of the wafer-bonded GaP substrate adversely affects the reliability characteristics. Similarly Grillot et al [16] feel that Auger recombination does not affect long term reliability of AlGaInP LEDs. They attribute decrease in light output over time to changes in Extraction efficiency, Leakage current density out of the active region and Defect concentration.

Gradual degradation in LEDs causes the light output to decrease over its lifetime. Arrhenius reaction rate model has been used to describe this process. Catastrophic degradation could be due to an electrical surge during device handling, setting and operating. In those cases, the active layer and the p-n junction corresponding to a part or the entire light emitting region are catastrophically destroyed. The dark spots or dark regions corresponding to the damaged part of the p-n junction can be observed by EL topographs.

Chapter 4: Development of Empirical Modeling for Test Data Analysis

During review of published literature on LED reliability and also during accelerated life testing, both current and temperature were simultaneously used as accelerating variables. In order to estimate LED life under nominal conditions (no life acceleration), models for current and temperature acceleration were used. A method was also developed to evaluate the combined effect of both of these accelerating variables.

4.1 Current density: Inverse Power Law model

Inverse Power Law (IPL) model with current density J as the accelerating variable was used in this analysis. Since the prior published data spans over decades, use of current density (instead of current) normalizes the effect of die size increase to a great extent. The IPL model is given as

$$TTF = A.J^{-n} \qquad \text{-(4.1)}$$

Where TTF=Time to failure in hrs, J=LED Current density in Amps/cm^2, A & n are +ve constants. Taking Ln on both sides,

$$Ln(TTF) = LnA - nLn.J \qquad \text{-(4.2)}$$

Equation 4.2 gives a straight line relationship where '-n' is the slope and J is the accelerating variable. The negative slope implies that as the current density increases, the TTF decreases.

4.2 Temperature: Arrhenius Reaction Rate model

For temperature acceleration, the Arrhenius reaction rate model was used.

$$Rate = Be^{-\left(\frac{Ea}{KT}\right)} \quad \text{-(4.3)}$$

Where T=Temperature in °K, Ea=Activation energy of the LED degradation, K=Boltzmann's constant, B=constant. Taking a reciprocal of 'rate' gives 'time to failure' as given by

$$TTF = Ce^{\left(\frac{Ea}{KT}\right)} \quad \text{- (4.4)}$$

Where TTF=Time to failure in hrs, C=1/B is another constant. Taking Ln on both sides,

$$Ln(TTF) = LnC + \frac{Ea}{KT} \quad \text{- (4.5)}$$

This is a straight line relationship where Ea is the slope and 1/KT as the accelerating variable. The positive slope implies that as temperature increases, 1/KT and TTF decrease.

4.3 Computation of Acceleration Factors

From equation 4.1, Acceleration Factor for Inverse Power Law Model is given by

$$AF_1 = \frac{TTF_{Use}}{TTF_{Acc}} = \left(\frac{J_{Acc}}{J_{Use}}\right)^n \quad \text{- (4.6)}$$

From equation 4.4, Acceleration Factor for Arrhenius Reaction Rate Model is given by

$$AF_2 = \frac{TTF_{Use}}{TTF_{Acc}} = e^{\frac{Ea}{K}\left(\frac{1}{T_{Use}} - \frac{1}{T_{Acc}}\right)} \quad \text{- (4.7)}$$

Since multiple data points at different temperatures and currents were available, regression analysis was performed to accommodate the results of both the accelerating variables. The overall Acceleration Factor is given by

$$AF = AF_1 x AF_2 = \left(\frac{J_{Acc}}{J_{Use}}\right)^n e^{\frac{Ea}{K}\left(\frac{1}{T_{Use}} - \frac{1}{T_{Acc}}\right)} \quad \text{- (4.8)}$$

4.4 Regression Analysis of Prior Published Data

4.4.1 LED classification

Previously published data [10-51] in which LEDs were put on long term reliability tests were identified. See Table 4.1. From the graphs or tabular data, the time required for the optical power output to degrade by 20% was extracted. This is the failure criterion for the medical diagnostic application. Analysis of published data for different LED Materials (AlGaInP, GaN, GaAlAs), the Semiconductor Structures (DH, MQW) and the mode of testing (DC, Pulsed) was carried out. The data was categorized for various combinations such as AlGaInP-DH-DC, AlGaInP-MQW-DC, GaN-DH-DC, GaN-DH-DC etc. Further, their testing was done at different temperature and current. This data was converted to application conditions of the medical environment. This was done by assessing the acceleration factors, which in turn required estimating the ‘n’ parameter of the IPL model and the activation energy ‘Ea’ of the Arrhenius model.

4.4.2 Iterative Regression Analysis

Regression analysis on the prior published data was done as follows. The activation energy, Ea value provided/estimated from the published data was used or if not available a value of 0.43eV was used (based on MIL-HDBK-217C for optical components). The activation energy, Ea was the same for identical LEDs in an article. Similarly, if any article had data at different J (but same temperature), the n value was estimated. For all other reported data, where Ea or n was unavailable, iterative regression approach was used as follows. Using equation 4.7 and assumed/estimated Ea, all TTF data was converted to use Temperature T_{Use}. Linear regression for equation 4.2 was used to estimate n. Using this n value and equation 4.6, all TTF data was re-converted to use current density J_{Use}. Now linear regression for equation 4.5 was used to improve our estimate of Ea. It is quickly evident that normalizing the data for temperature, affects the regression analysis for n and normalizing the data for current density, affects the regression analysis of Ea. Thus an iterative approach was used to get best possible regression fits thereby accommodating the effects of both current density and temperature.

See Fig 4.1 for effect of current density J on LED category AlGaInP-DH-DC and Fig 4.2 for effect of temperature on LED category AlGaInP-DH-DC.

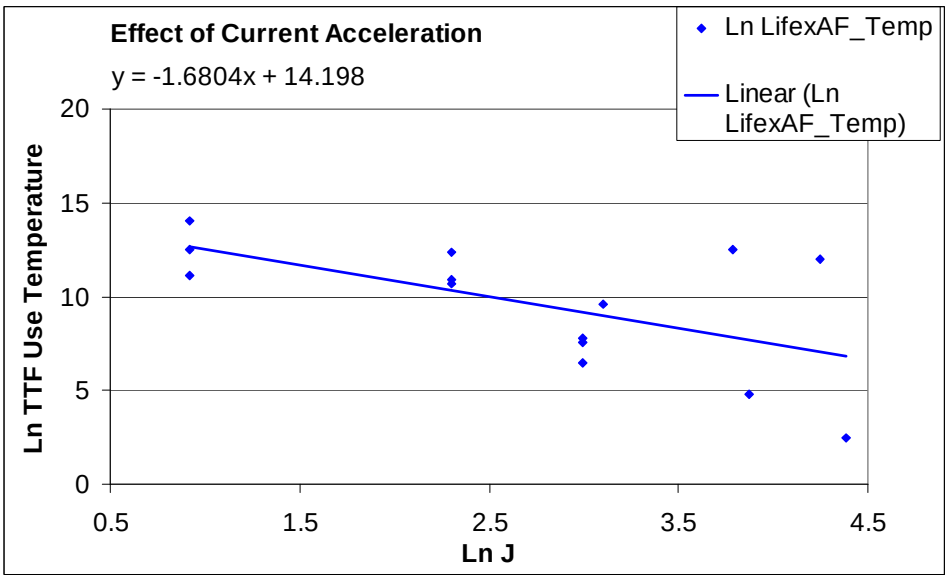

Fig 4.1 Effect of Current density J: AlGaInP-DH-DC

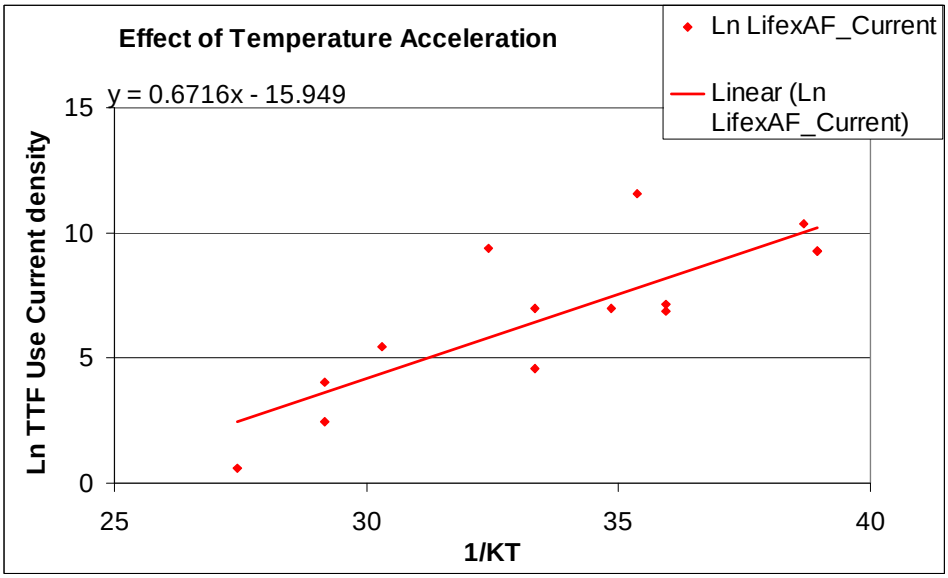

Fig 4.2 Effect of Temperature: AlGaInP-DH-DC

See Fig 4.3 for effect of current density J on LED category AlGaInP-MQW-DC and Fig 4.4 for effect of temperature on LED category AlGaInP-MQW-DC.

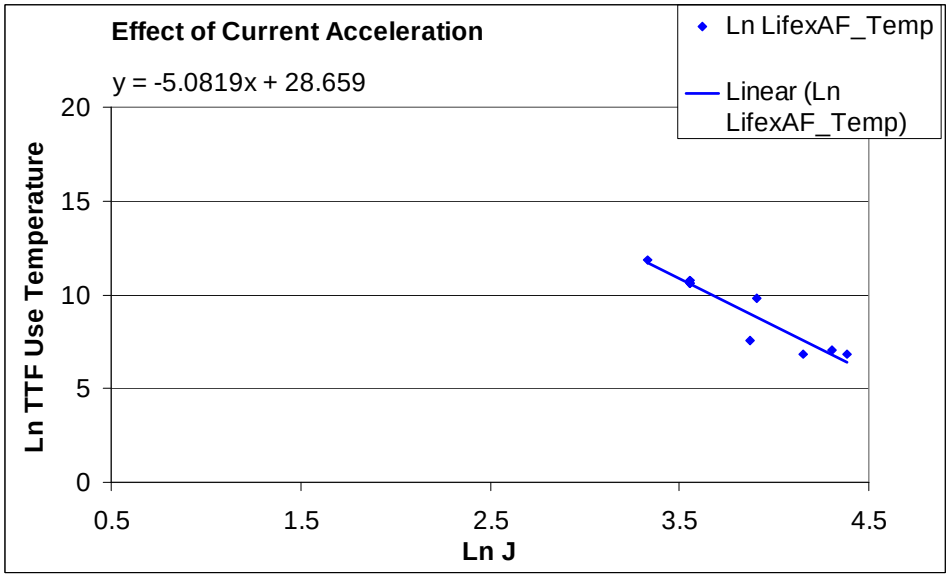

Fig 4.3 Effect of Current density J: AlGaInP-MQW-DC

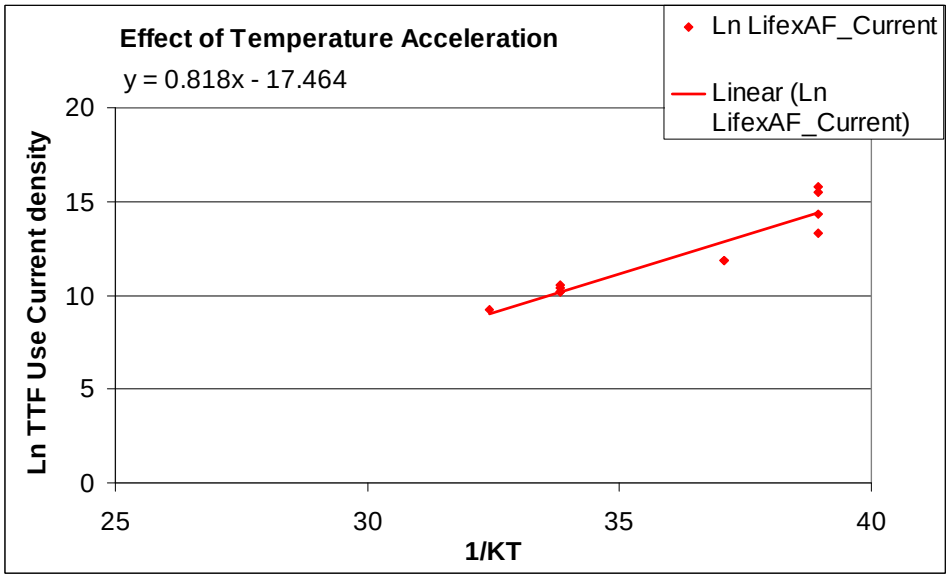

Fig 4.4 Effect of Temperature: AlGaInP-MQW-DC

See Fig 4.5 for effect of current density J on LED category GaN-DH-DC and Fig 4.6 for effect of temperature on LED category GaN-DH-DC.

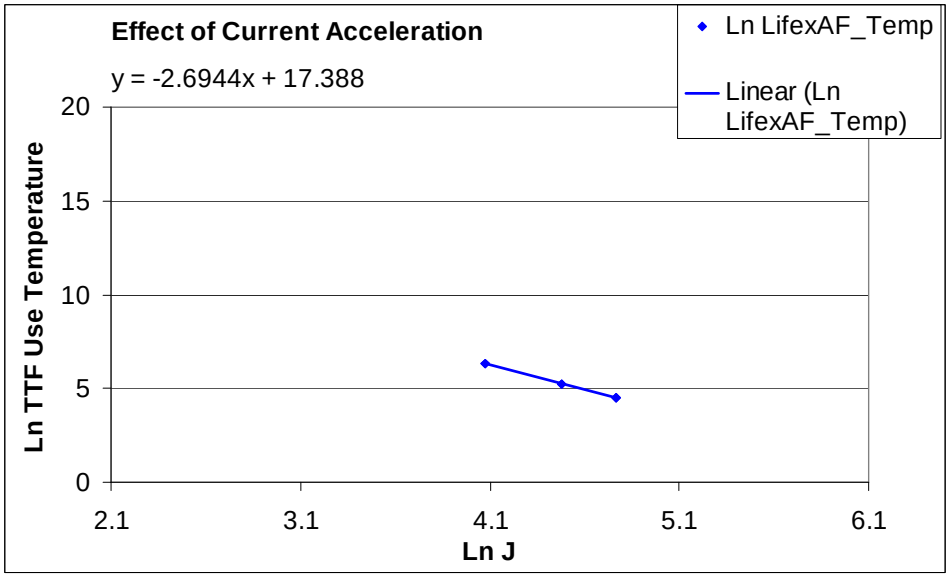

Fig 4.5 Effect of Current density J: GaN-DH-DC

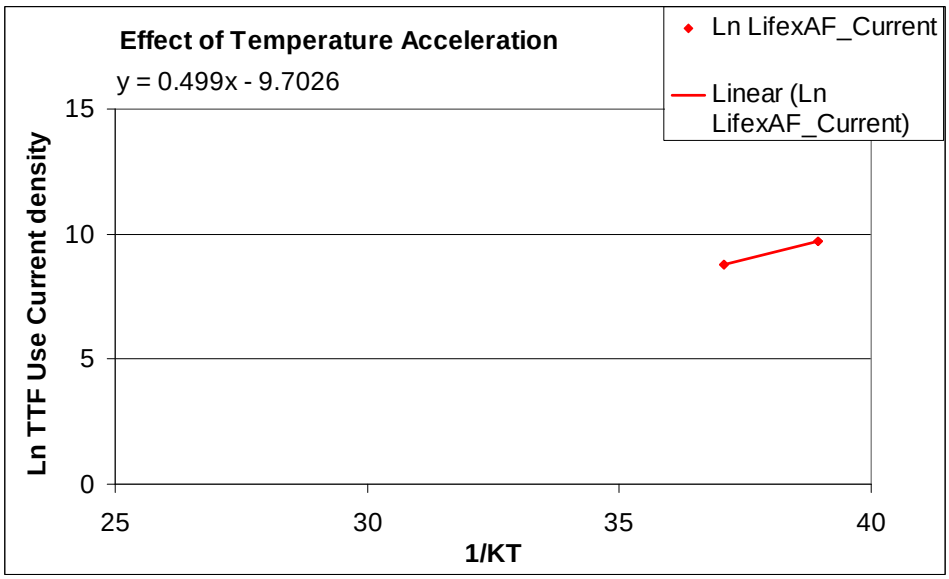

Fig 4.6 Effect of Temperature: GaN-DH-DC

See Fig 4.7 for effect of current density J on LED category GaN-MQW-DC and Fig 4.8 for effect of temperature on LED category GaN-MQW-DC.

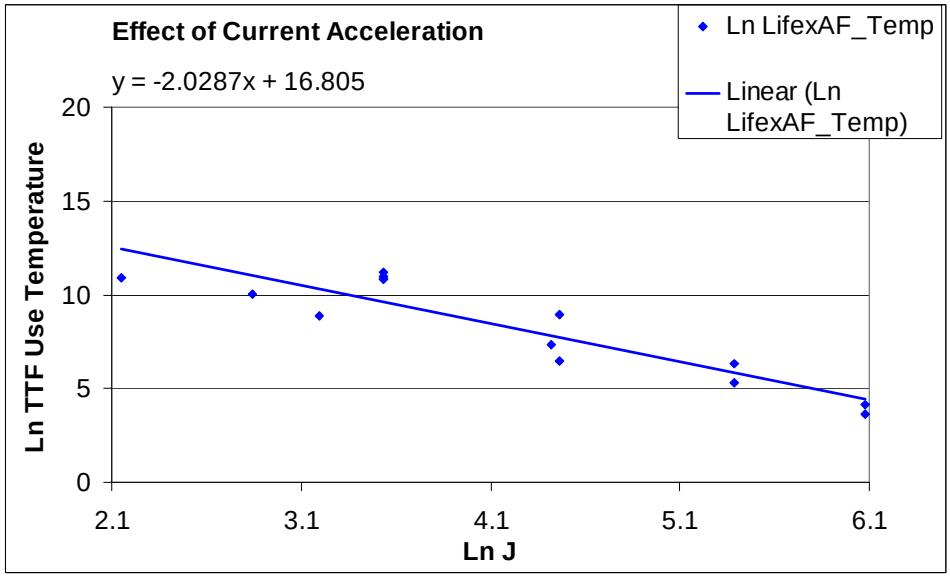

Fig 4.7 Effect of Current density J: GaN-MQW-DC

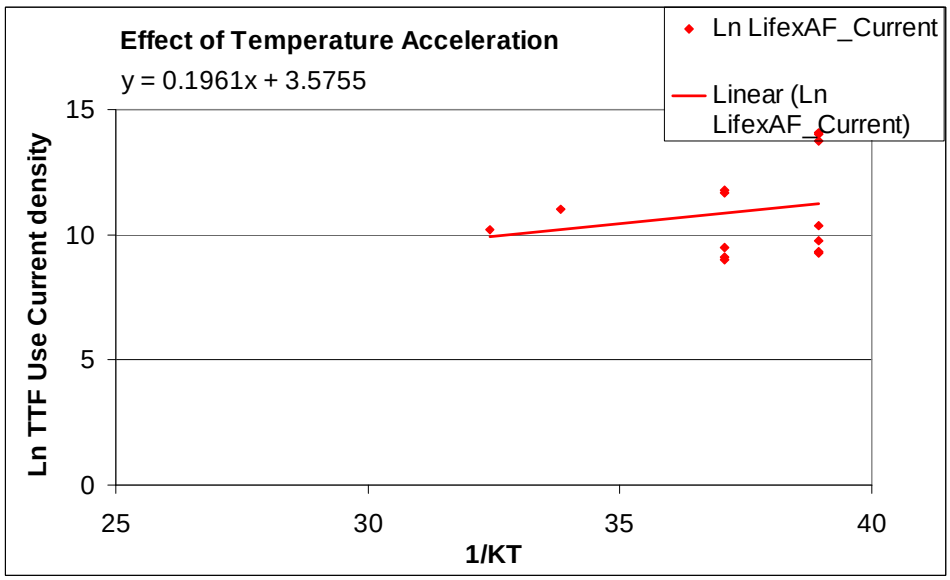

Fig 4.8 Effect of Temperature: GaN-MQW-DC

4.4.3 Weibull Analysis of Prior Published data

Equation 4.8, published data and use conditions of the medical device application (i.e. temperature = 35°C and current density = 21.6Amps/cm^2) were used to obtain the TTF distributions (given in Table 4.1) for AlGaInP-DH-DC, AlGaInP-MQW-DC, GaN-DH-DC, GaN-DH-DC etc. and was previously reported, Sawant et al [11]. The last 6 columns give the parameters for Weibull and Logarithmic distribution fit and the corresponding Mean Time to Failure (MTTF). Accelerated Life Test data in pulse mode (described in chapter 5) is also included as Sr. # 5 for comparison with Prior published DC driving data in Sr. # 2.

Sr. #	LED Material Structure Driving	Source of Data [Ref.]-Fig	IPL n	Act. E. eV	Weibull (Converted to application conditions) α	β	MTTF Hrs	Lognormal (Conv. to appl. Conditions) μ	σ	MTTF Hrs
1	AlGaInP-DH-DC	[17]-2/4, [19]-9a/9b, [26]-3, [28]-3a/3b [29]-5	1.68	0.67	2.76E4	0.50	1.33E4	9.1	2.30	9.41E3
2	AlGaInP-MQW-DC	[19]-9a/9b, [22]-16, [24]-6/8/10 [27]-2	5.08	0.82	7.82E5	0.89	5.17E5	13	1.25	4.27E5
3	GaN-DH-DC	[47]-1	2.69	0.50	-	-	-	-	-	-
4	GaN-MQW-DC	[24]-7/9/11 [33]-5, [34]-2/6	2.02	0.20	1.61E5	0.57	8.47E4	11.0	2.06	6.22E4
5	ALT: AlGaInP-MQW-Pulsed (0.2%)	ALT performed for this study	4.48	1.15	1.55E9	0.50	7.50E8	20.0	2.50	5.23E8

Table 4.1 Regression Analysis of Prior Published Data

Chapter 5: Accelerated Life and Degradation Testing

Present commercial LEDs have reported extrapolated MTTFs in the range of 1.0E6 hours [28, 29]. For a medical diagnostic application, 20% decrease in light output is considered to be the failure threshold at the device level. However their low duty cycle will still allow them to operated for longer time period at derated bias conditions. In order to determine LED life (MTTF), accelerated life testing (ALT) and accelerated degradation testing (ADT) was carried out. Acceleration is achieved either by increasing the LED current or the temperature. Care should be taken that the acceleration is not so high that it introduces unrelated failure modes. Computation of acceleration factors (described in chapter 4) allows the calculation of LED life in use conditions.

ALT and ADT was performed on LEDs under various conditions and in different batches. Some of these results were also published by the author in Sawant et al [11]. However, Section #, Figure #, Table # and References have been rearranged as necessary.

5.1 Materials

Commercially procured AlGaInP 640nm MQW LEDs were used in this research. The structure and material combinations of these LEDs have been previously reported [15, 19, 21, and 22].

5.2 Methods

AlGaInP LEDs were tested simultaneously in 3 Environment Chambers. The LEDs were tested in batches with 15 LEDs in each batch. See Fig 5.1.

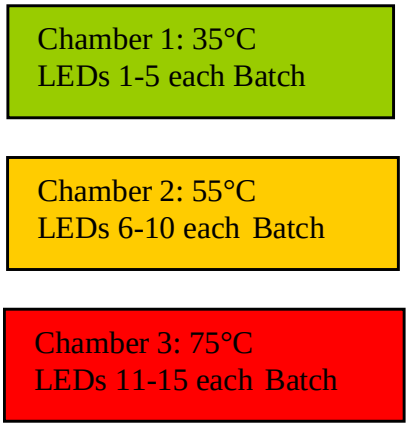

Fig 5.1 Environmental Test

Per the need of the medical application in Fig 1.2, the LEDs were driven in burst mode where each burst consists of 100 pulses. A single pulse corresponds to the time during which light passes though a single medical test sample. See Fig 5.2 for details of the timing diagram.

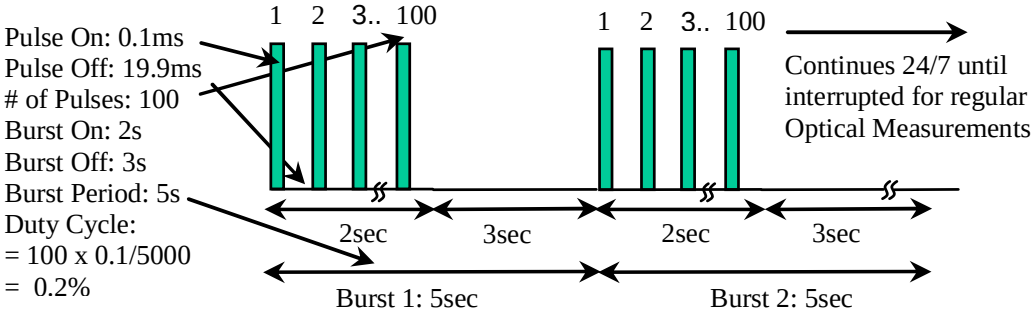

Fig 5.2 Pulse/Burst mode timing
Note: 1 hr = 1200pulses/min x 60min = 7.2E4 pulses

5.3 Test Setup

The test is automated by using test software, data acquisition/control boards and constant current LED driver boards. The test SW makes the data acquisition board generate the necessary pulses, which trigger the LED driver board. The peak current through the LED is maintained constant while it is on. A separate signal conditioning circuit also measures the forward voltage Vf across the diode, which is fed back to the test SW to be written to a database. At regular intervals, the LEDs were removed from the chambers and were characterized electrically and optically (using a Spectro-radiometer). See Fig 5.3 for LED ALT/ADT and Fig 6.1 (in chapter 6) for Electrical and Optical Characterization of LEDs .

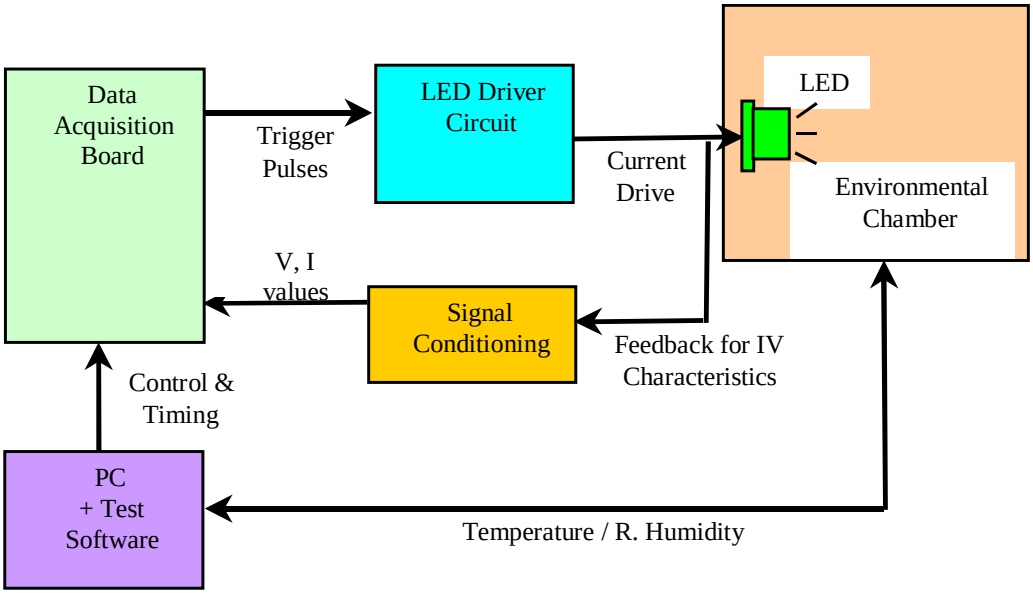

Fig. 5.3 Setup for LED Testing

5.4 ALT/ADT Results

5.4.1 LED optical power degradation

ALT/ADT of the LEDs in Pulse mode was conducted at 3 temperatures (35°C, 55°C and 75°C) and 2 Peak currents (Batch2: 483mA=418.1A/cm^2 and Batch3: 725mA=627.2A/cm^2). The optical power (measured by averaging over 10nm around peak wavelength) decreased with time due to degradation of the LED chip as well as the encapsulation. See Fig 5.4 and Fig 5.5. The optical power degradation followed a logarithmic function in agreement with Yanagisawa et al [47] and Grillot et al [16]. 20% degradation was considered failure for the medical application. For LEDs that did not reach 20% degradation in a reasonable time (suspend data), the logarithmic function was used to extrapolate TTF. Using regression analysis of ALT data, the activation energy 'Ea' was found to be 1.15eV and 'n' for IPL was 4.48. Note that a few LEDs showed extremely low degradation rates (due to different failure mechanisms with much higher activation energies). LEDs not failed during ALT/ADT were excluded from the analysis since the focus was FMECA for a medical application.

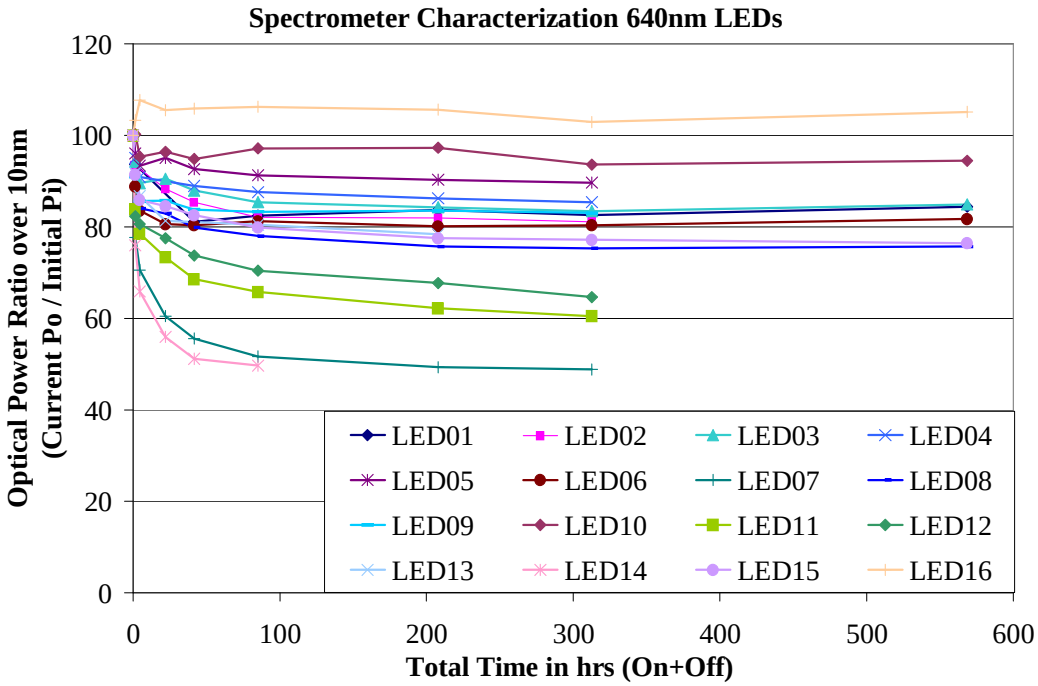

Fig. 5.4 ALT/ADT for Batch2, 483mA
Note: 1 hr = 1200pulses/min x 60min = 7.2E4 pulses

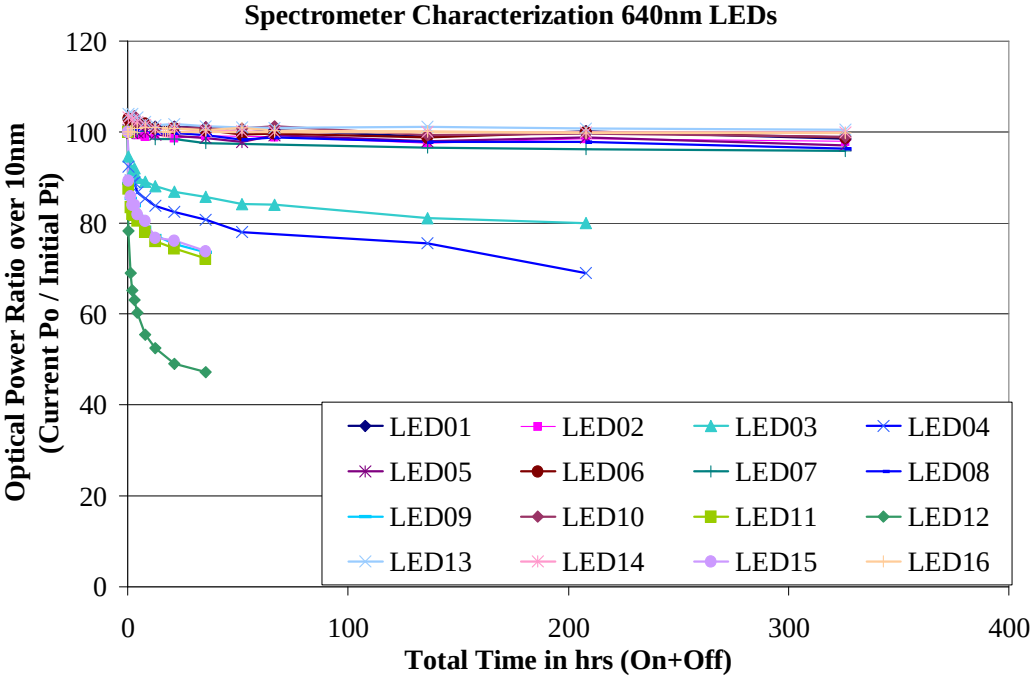

Fig. 5.5 ALT/ADT for Batch3, 725mA
Note: 1 hr = 1200pulses/min x 60min = 7.2E4 pulses

5.4.2 Encapsulation degradation

LED Photographs were taken before and after the ALT/ADT using a digital microscope. See Fig 5.6. The most obvious failure mode was found to be encapsulation (lens) degradation. The lens degradation after the ALT/ADT varied from minor to moderate too severe, which can be attributed to variations in LED lens material and manufacturing process. A new and a used LED chip were also photographed by illuminating the LED at 40 uA dc. These photos indicate that the LED chip also degrades during ALT/ADT.

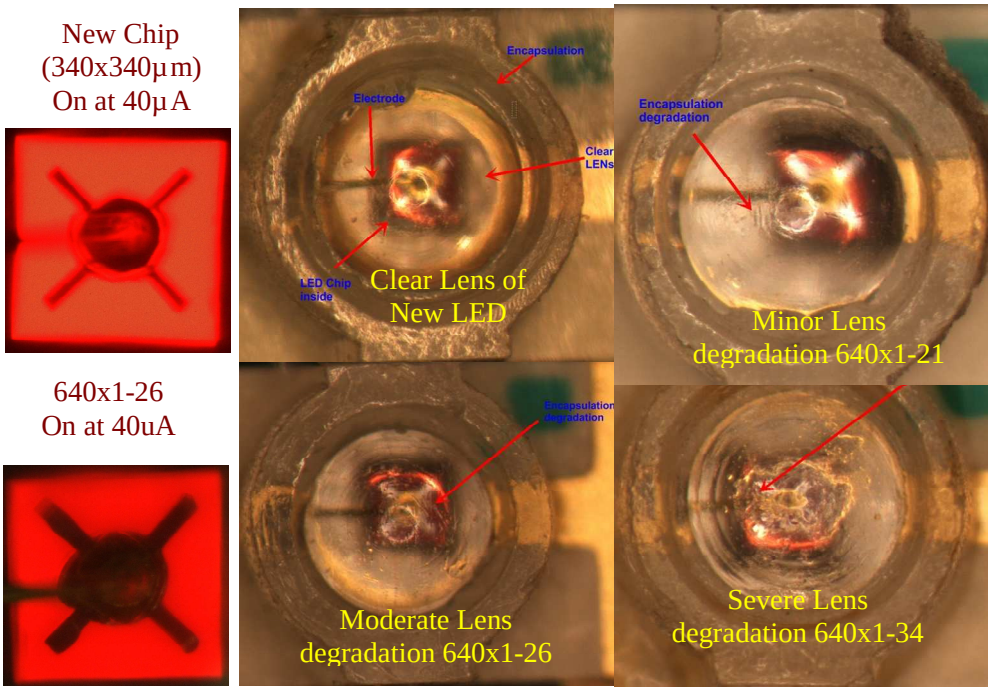

Fig 5.6 Photos of Minor, Moderate & Severe Lens degradation

5.4.3 Chip vs. Lens degradation

At regular intervals within the ALT/ADT, optical power and diode forward voltage Vf were measured. See Fig 5.7. The Vf (y-axis on right) and Optical power (y-axis on left) appear like inverted images of each other. The chip degradation (interpreted from Vf) dominated the initial period whereas the lens degradation will occur during the entire period of the test.

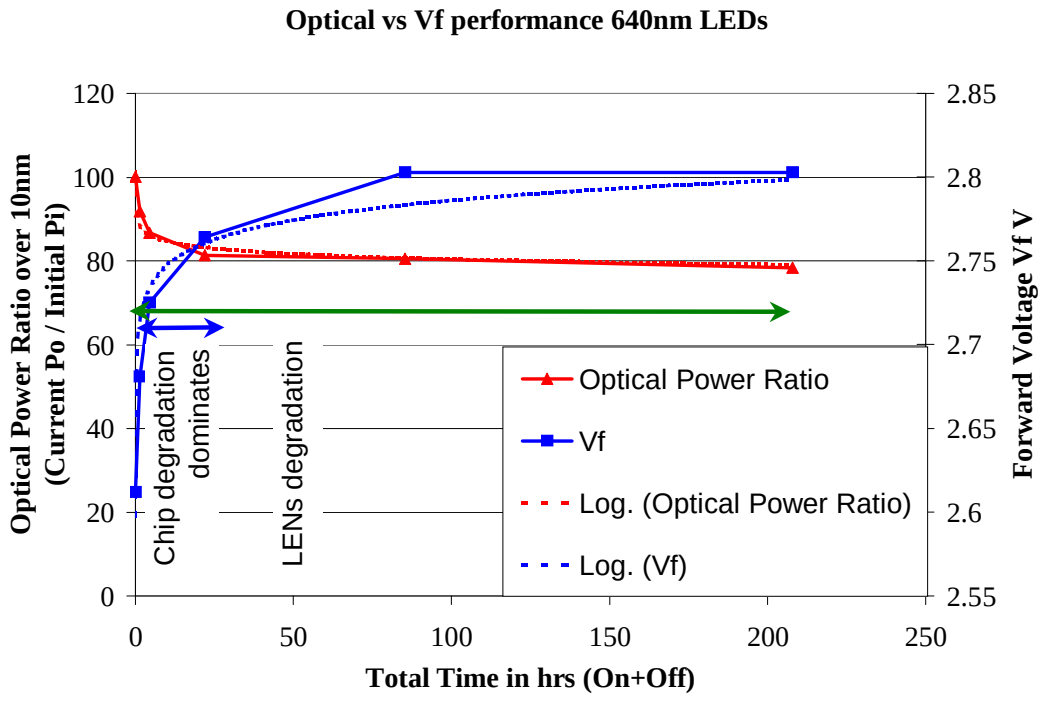

Fig 5.7 Chip (Vf) vs. Lens degradation
Note: 1 hr = 1200pulses/min x 60min = 7.2E4 pulses

5.4.4 Spectral Performance after ALT/ADT

A slight change in spectral performance after the ALT was detected in some of the tested LEDs. See Fig 5.8 and Fig 5.9. Where the peak wavelength changed by 1-2nm, changes in the active region were speculated to be the major cause. Where the optical power drop at 650nm was different than that at 630nm, changes in the plastic encapsulation were suggested. The shift is minor and acceptable for the medical application. For larger shifts, see Chapter 6. In Fig 5.8, the peak wavelength of one LED decreased by 2nm (0.3%). The optical power drop at 650nm was higher than that at 630nm.

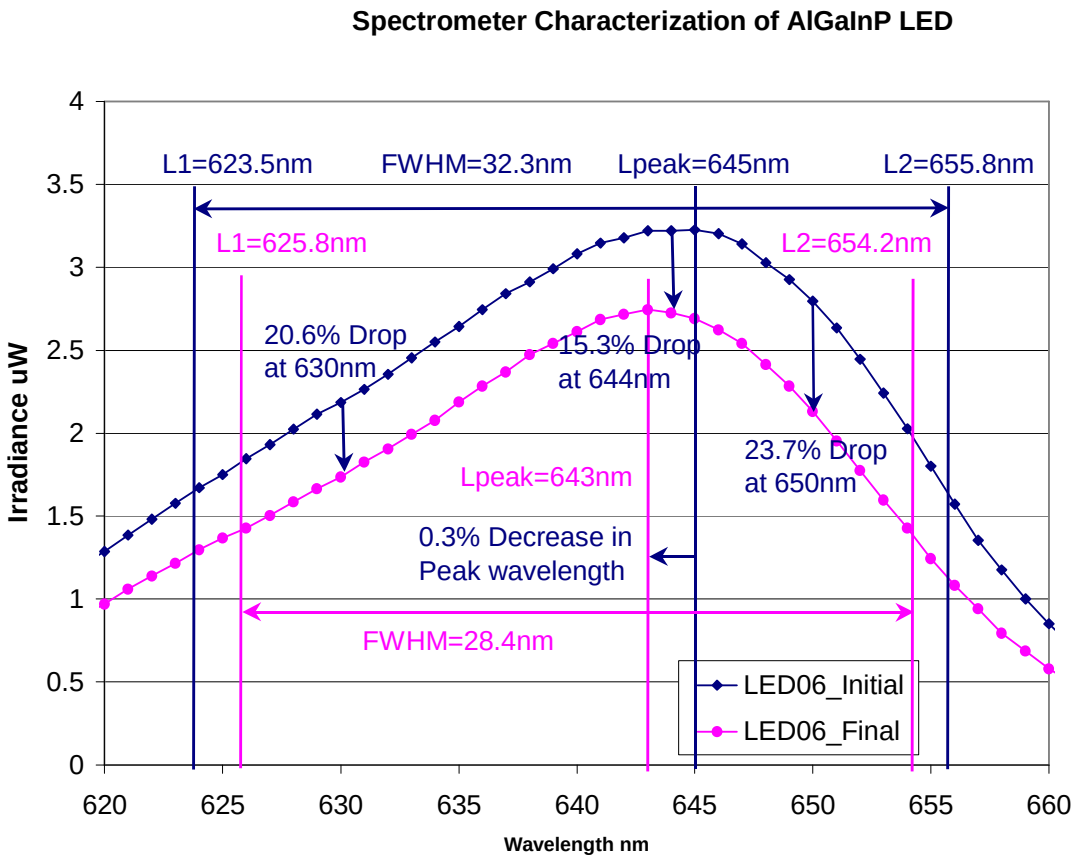

Fig 5.8 Spectral shift to lower wavelength after ALT/ADT

In Fig 5.9, the peak wavelength of another LED increased by 1nm (0.15%). The optical power drop at 650nm was lower than that at 630nm.

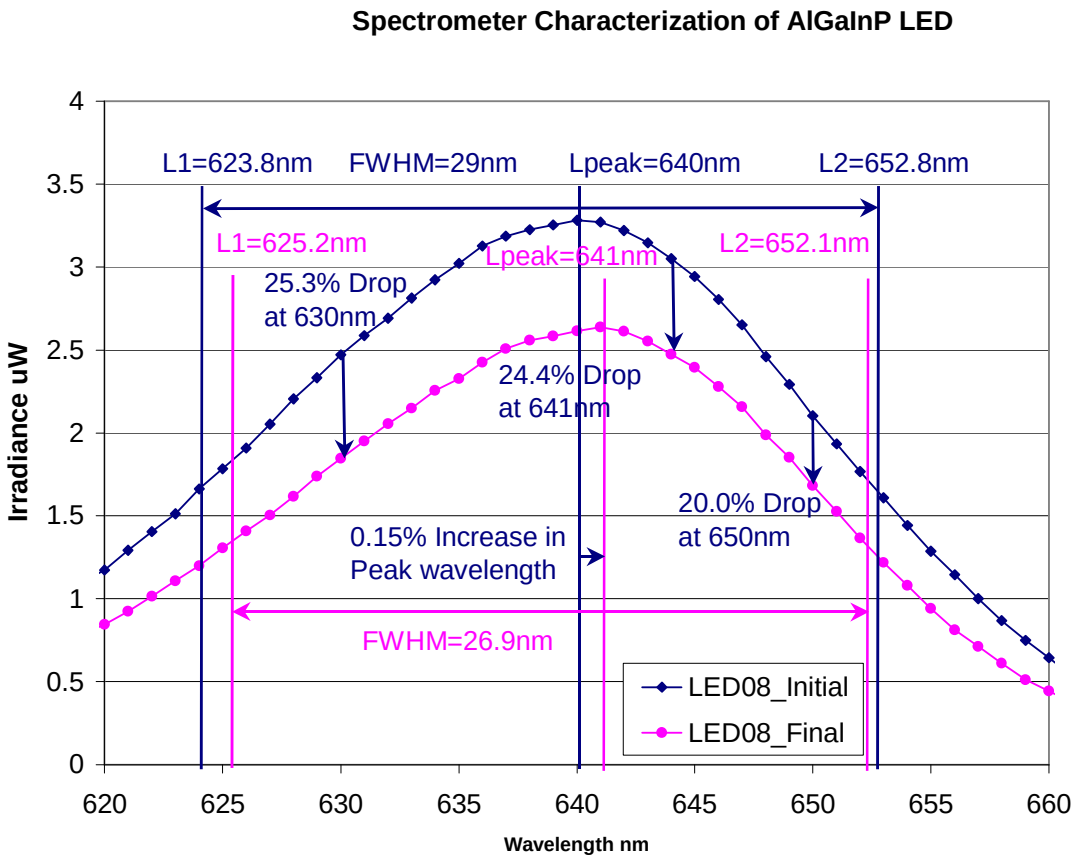

Fig 5.9 Spectral shift to higher wavelength after ALT/ADT

5.4.5 Summary of Test results

Table 5.1 summarizes the test results for Batch 2 (15 LEDs at 483 mA) and Table 5.2 summarizes the test results for Batch 3 (15 LEDs at 725 mA). Various columns are Sr.# of UUT, Chamber Temperature in deg C, Estimated Time to Failure based on the equation of logarithmic degradation model, Equation for the logarithmic degradation model, Severity of Lens degradation, % change in forward voltage Vf and the last 3 columns indicate whether the optical power drop is occurring at lower wavelength or higher.

UUT	Temp C	TTF hrs Estimated 20% degrd	Equation for Logarithmic degradation model	LENs degradation	Vf Increase %	% Drop @ 630nm rel to 640nm	% drop 640nm	% Drop @ 650nm rel to 640nm
640x1-21	35	1755.6	y = -1.4537Ln(x) + 90.86 R2 = 0.8617	Minor Surface	4.0	3.2	12.2	-0.2
640x1-22	35	335.9	y = -2.8548Ln(x) + 96.606 R2 = 0.9119	Minor Few Bubbles	4.6	4.4	12.9	0.4
640x1-23	35	8282.1	y = -1.4323Ln(x) + 92.922 R2 = 0.9367	Minor Surface	6.5	4.6	10.4	1.0
640x1-26	55	195.0	y = -1.5697Ln(x) + 88.277 R2 = 0.9025	Moderate Surface	2.9	5.2	13.2	9.6
640x1-27	55	0.3	y = -4.3842Ln(x) + 73.933 R2 = 0.9732	Moderate Surface	7.9 -> 6.4	4.9	45.8	2.1
640x1-28	55	38.7	y = -1.9411Ln(x) + 87.094 R2 = 0.9864	Minor Few Bubbles	7.5	5.6	21.6	0.8
640x1-29	55	1225.0	y = -1.4315Ln(x) + 90.179 R^2 = 0.9535	Minor Few Bubbles	2.5	3.8	10.7	12.5
640x1-31	75	1.5	y = -3.2403Ln(x) + 81.238 R^2 = 0.9684	Moderate Surface+Bubles	3.6	6.0	33.3	2.6
640x1-32	75	3.2	y = -2.748Ln(x) + 83.18 R^2 = 0.9754	Minor Few Bubbles	11.7 -> 7.0	6.1	28.9	3.2
640x1-33	75	125.9	y = -1.8618Ln(x) + 89.002 R^2 = 0.9464	Minor Very Few Bubbles	8.8	4.1	18.1	2.3
640x1-34	75	0.2	y = -4.6769Ln(x) + 71.53 R^2 = 0.9691	Severe Surface	8.6 -> 4.5	4.6	42.0	3.5
640x1-35	75	113.4	y = -1.9047Ln(x) + 89.011 R2 = 0.9633	Minor Few Bubbles	11.5 -> 7.8	4.2	19.6	4.1

Table 5.1 Summary of ALT/ADT results for Batch 2

UUT	Temp C	TTF hrs Estimated 20% degrd	Equation for Logarithmic degradation model	LENs degradation	Vf Increase %	% Drop @ 630nm rel to 640nm	% drop 640nm	% Drop @ 650nm rel to 640nm
640x1-43	35	316.3	y = -2.339Ln(x) + 93.465 R2 = 0.9704	Moderate Bubles	8.6	5.0	20.6	-0.8
640x1-44	35	34.1	y = -2.5448Ln(x) + 88.985 R2 = 0.8966	Minor Surface	5.6	5.7	31.0	0.0
640x1-49	55	6.0	y = -2.7834Ln(x) + 84.99 R2 = 0.9781	Minor Surface	7.5	6.6	25.7	0.0
640x1-51	75	3.8	y = -2.8983Ln(x) + 83.881 R2 = 0.9886	Minor Surface	7.5	6.8	27.3	0.1
640x1-52	75	0.1	y = -5.7886Ln(x) + 68.472 R2 = 0.986	Minor Surface	6.6	6.5	52.7	0.0
640x1-55	75	7.0	y = -2.7536Ln(x) + 85.365 R2 = 0.9692	Minor Surface	10.1	6.2	25.8	0.5

Table 5.2 Summary of ALT/ADT results for Batch 3

5.4.6 Additional ALT/ADT testing

In addition to Batch 2 (483mA, 0.2% duty cycle) and Batch 3 (725mA, 0.2% duty cycle), other LED testing included Batch 4 (483mA, 50% duty cycle) and Batch 5 (26mA, 50% duty cycle). The failure times during Batch 4 were significantly lower due to the high current and high duty cycle. See Table 5.3.

UUT	Temp C	TTF hrs Observed 20% degrd	MTTF	Acc Factor	Act. Energy eV	Equation for Logarithmic degradation model	LENs degradation	Vf Increase %	% Drop @ 630nm rel to 640nm	% Drop @ 650nm rel to 640nm
640x1-61	35	20.56	15.5			N/A	N/A	40.0		
640x1-62	35	10.25				N/A	N/A	67.0		
640x1-63	35	20.79				N/A	N/A	38.7		
640x1-64	35	5.22				N/A	N/A	10.2		
640x1-65	35	20.79				N/A	N/A	96.8		
640x1-66	55	5.58	9.2	1.7	0.23	N/A	N/A	33.0		
640x1-67	55	12.79				N/A	N/A	0.4 -> -35		
640x1-68	55	13.87				N/A	N/A	1 -> -28		
640x1-69	55	5.61				N/A	N/A	2.1		
640x1-70	55	8.03				N/A	N/A	13.4		
640x1-71	75	3.77	4.7	3.3	0.28	N/A	N/A	0.7		
640x1-72	75	1.65				N/A	N/A	1.5		
640x1-73	75	33.30				N/A	N/A	5.6		
640x1-74	75	2.26				N/A	N/A	-0.6		
640x1-75	75	11.06				N/A	N/A	-1.7		

Table 5.3 Summary of ALT/ADT results for Batch 4

Batch 5 testing was done to see performance at a lower current of 26mA. In order to get failures in a reasonable amount of time, the duty cycle was increased to 50%. See Fig 5.10. A larger number of LEDs were used (10 at 35°C in blue plots, 10 at 55°C in green plots, 9 at 75°C in orange plots and 3 Reference LEDs which were not stressed). However, even after 3000 hours of testing, no failure was observed and the test had to be suspended. With acceleration factors for Temperature (14 at 55°C and 144 at 75°C) and Duty cycle (250 at 50% duty cycle), the life of the LED for the medical application exceeds 1.0E8 hrs as predicted by ALT (in section 5.4.7) and ADT (in section 5.4.8). Batch5 testing provides a sanity check for the previous conclusions that the LEDs will have a very high TTF.

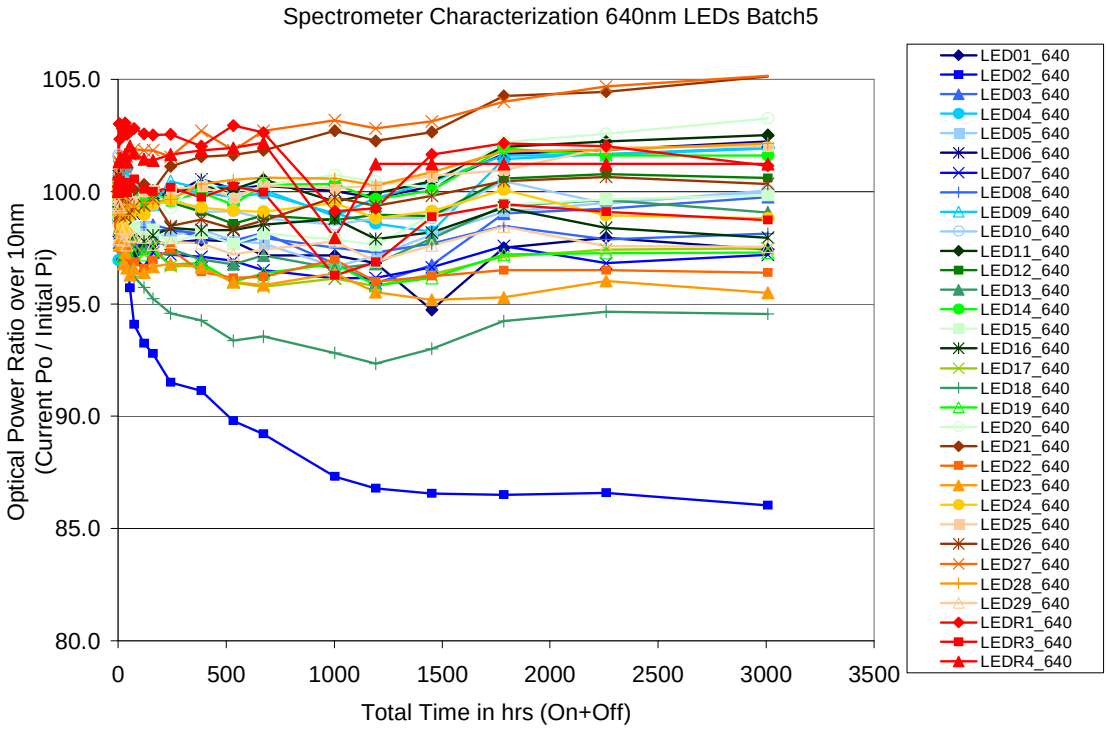

Fig. 5.10 ALT/ADT for Batch5, 26mA, 50% duty cycle
Note: 1 hr = 1200pulses/min x 60min = 7.2E4 pulses

5.4.7 Weibull analysis of ALT data

Pior published data and accelerated life test data were subjected to Weibull analysis. This required the estimation of the parameter n for the Inverse Power Law model and the activation energy for the Arrhenius reaction rate model (described in chapter 4). Next, the overall acceleration factor was calculated (using equation 4.8). Now the entire ALT data from both the batches was converted to medical application conditions (i.e. temperature = 35°C and current density = 21.6Amps/cm^2) by multiplying the TTF data with the acceleration factors. This converted data was subjected to Weibull analysis to estimate the Weibull parameters α and β. This was shown in Table 4.1 in chapter 4. A portion of Table 4.1 is repeated as Table 5.4 for convenience. The activation energy 'Ea' and 'n' value during ALT are comparable with values for prior published data. However, the time to failure predicted by ALT is much higher compared to published data. This is due to the extremely low duty cycle (0.2%) at which the LEDs were driven during ALT to simulate the medical diagnostic application. The published data is at dc bias conditions (100% duty cycle).

Sr. #	**LED Material Structure Driving**	**Source of Data [Ref.]-Fig**	**IPL n**	**Act. E. eV**	**Weibull** (Converted to application conditions) α	β	**MTTF Hrs**	**Lognormal** (Conv. to appl. Conditions) μ	σ	**MTTF Hrs**
2	AlGaInP-MQW-DC	[19]-9a/9b, [22]-16, [24]-6/8/10 [27]-2	5.08	0.82	7.82E5	0.89	5.17E5	13	1.25	4.27E5
5	ALT: AlGaInP-MQW-Pulsed (0.2%)	ALT performed for this study	4.48	1.15	1.55E9	0.50	7.50E8	20.0	2.50	5.23E8

Table 5.4 Regression Analysis of ALT Data

5.4.8 Analysis of ADT data

In section 5.4.7, ALT data was analyzed which involved Weibull analysis of TTF data. In this section, the data was analyzed based on the power degradation pattern of the LEDs. Two common approaches to degradation analysis are the Non-linear reaction rate model and the Linear (or Log-linear) model. As mentioned in section 5.4.1, during ALT/ADT, the optical power degraded as a logarithmic function of time in agreement with Yanagisawa et al [47] and Grillot et al [16]. This property was used to select Log-linear degradation model. The slope of the straight line (with time on log scale) will depend on the degradation rate which is a function of the LED current density and temperature. We used the Inverse Power Law model (IPL) and the Arrhenius reaction rate models to modify the slope. Equations 4.6 and 4.7 for acceleration factors (AF) still hold good. However, the AF is calculated as a ratio of reaction rates (accelerated rate to use rate) rather than time to failure (at a specific value of 20% degradation). Consequently, the parameters 'n' and 'Ea' for corresponding IPL and Arrhenius models will have different values than those calculated for ALT.

The ADT analysis created a degradation equation of the form

$$Y = Po(t)/Pi(t=0) = \frac{m}{AF_J x AF_T} Ln(t) + C \qquad \text{- (5.1)}$$

Where t = LED test time in hrs, C = y-intercept

Y = Po/Pi = Normalized optical power at time t and

Slope at use conditions = Slope m at accelerated T and J / (AF_T x AF_J)

The statistical analysis for degradation was done using JMP software created by SAS Institute Inc. This resulted in Table 5.5 below with the first row representing use conditions of the medical environment and average values for various parameters.

Condition	Temp °C	J A/cm^2	LnJ	JMP Slope m	JMP Y-intercept C	AF_Temp w.r.t. T=35C	AF_J w.r.t J=418.1	eV	n	% Optical o/p at t=7.5E8
Use	35	21.6	3.07		84.79	1.0	NA	0.39	0.82	
Batch2	35	418.1	6.04	-0.7	85.5	1.0	NA		NA	
Batch2	55	418.1	6.04	-2.3		3.4	NA	0.53	NA	80.2
Batch2	75	418.1	6.04	-3.0		4.4	NA	0.34	NA	84.5
Batch3	35	627.2	6.44	-1.1	84.1	1.0	1.6		1.19	
Batch3	55	627.2	6.44	-2.7		2.4	1.2	0.38	0.38	78.5
Batch3	75	627.2	6.44	-4.4		3.9	1.4	0.31	0.91	83.0

Table 5.5 Degradation Analysis using JMP software

The JMP software fitted a straight line for optical power degradation with time in log scale. This was done for Batch2 (J=418.1A/cm^2) and Batch3 (J=627.2A/cm^2) with temperatures 35ºC, 55 ºC and 75 ºC for each batch. A common y-intercept was estimated for each batch and its average (84.79) was used as 'C' in equation 5.1. The slope was calculated separately for each batch at each of the three temperatures. The acceleration factors AF_Temp were calculated for temperatures 55 ºC and 75 ºC by taking a ratio of slopes with respect to 35 ºC. This was done separately for Batch2 and Batch3. Using equation 4.7, the corresponding activation energies Ev were estimated and the average was found to be 0.39eV. The acceleration factors AF_J for current

density were calculated by taking a ratio of slopes between Batch3 and Batch2. Note that Batch2 is also at an accelerated condition of J and AF_J values are only used to estimate parameter ‘n’ of IPL model using equation 4.6. Once ‘n’ and ‘Ev’ were available, AF_J and AF_T were calculated and equation 5.1 was developed for various conditions. From table 5.4, MTTF of the LEDs (at use conditions) estimated from ALT was 7.5E8 hrs. The last column in Table 5.5 gives optical output at t=7.5E8 hrs for various conditions. This value was found to be close to 80% implying a 20% degradation which was the failure criterion for the ALT. Thus, the results from ALT and ADT agree with each other. Further, equation 5.1 for ADT can be used to calculate LED TTF if the degradation threshold is changed.

Chapter 6: Thermal Shift of Active layer Bandgap

Reliability testing of AlGaInP MQW LEDs resulted in a shift of Bandgap towards the longer wavelength when driven at high current and high duty cycles. The spectral FWHM also increased. Characterization of the shift showed that it was temporary and dependent on the junction temperature. Some of these results were also published by the author in Sawant et al [12]. However, Section #, Figure #, Table # and References have been rearranged as necessary.

6.1 Background on Spectral Shifts

The band gap of a semiconductor is either direct or indirect. For an indirect band gap, an electron cannot shift from the lowest-energy state in the conduction band to the highest-energy state in the valence band without a change in momentum [9]. Hence direct band gap semiconductors are preferred for LEDs. When an LED is forward biased, the electrons in the conduction band recombine with holes in the valence band. In the recombination process, energy Eg corresponding to the band gap is emitted in the form of a photon whose wavelength λ (in nm) is given by

$$\lambda = h c / Eg = 1239.8 / Eg \qquad - (6.1)$$

where h = Plank's constant, c = speed of light in vacuum and Eg = band gap in eV.

Temperature dependence of semiconductor device characteristics is very important from a reliability standpoint [2]. During operation, heat is generated in the active layer (also in other parts having ohmic resistance) which raises the junction

temperature. This research tried to characterize the shift in the spectrum resulting from elevated junction temperature.

6.2 Methods

The forward bias method was used to establish the linear relationship between the forward voltage Vf and the junction temperature Jt for a given forward current. See section 6.3.1 for details on this. The Shockley diode equation [10] relates the diode current I of a p-n junction diode to the diode voltage Vf:

$$I = Is\left(e^{Vf/nVt} - 1\right)$$

$$= Is\left(e^{Vf\,q/nKT} - 1\right)$$

$$= Is\,e^{Vf\,q/nKT} \quad \text{for } e^{Vf\,q/nKT} >> 1 \qquad \text{- (6.2)}$$

where Is is the saturation current or scale current of the diode (the magnitude of the current that flows for negative Vf in excess of a few Vt, typically 10-12 A). The scale current is proportional to the diode area. Vt is the thermal voltage, and n is known as the diode ideality factor. Thus if I is maintained constant, junction temperature Jt can be directly interpreted in terms of forward voltage Vf which typically decreases between 1 and 3mV per 1 deg C rise in temperature. See details in section 6.3.1.

To measure the spectral response, the LEDs were driven at different currents and measured the optical output of the LED using a Spectro-Radiometer. While measuring the spectrum, the Vf was also measured thereby allowing us to estimate Jt during those conditions. The data was further analyzed with respect to Varshini's equation, and the empirical coefficients were determined.

6.3 Experimental

6.3.1 Forward Bias Method

The LED is connected to a constant current source (turned off) and kept in an environmental chamber set to 25deg C. Once the chamber temperature stabilises, the current source was turned On for 0.3ms and the voltage drop Vf across the diode was measured. Since the LED is on for a very short time, it does not significantly heat itself and junction temperature Jt is same as ambient temperature T. This was repeated for ambient temperatures (Jt = T) of 35, 45 and 55 °C. Temperature Jt (= T) against Vf was plotted. Now the junction temperature at any other temperature could be estimated by measuring the Vf under operating conditions and intercepting it with the plot above.

6.3.2 Spectral Measurement

The LEDs were driven in burst mode where each burst consists of 90909 pulses at 45KHz and 50% duty cycle. The test was automated by using test software, data acquisition/control boards and constant current LED driver boards. The test SW makes the data acquisition board generate the necessary pulses, which trigger the LED driver board. The peak current through the LED was maintained constant while it was on. A separate signal conditioning circuit also measured the forward voltage Vf across the diode. This was fed back to the test SW to be written to a database. The LEDs were characterized optically using a Spectro-radiometer. See Fig. 6.1 for details of the LED characterization setup.

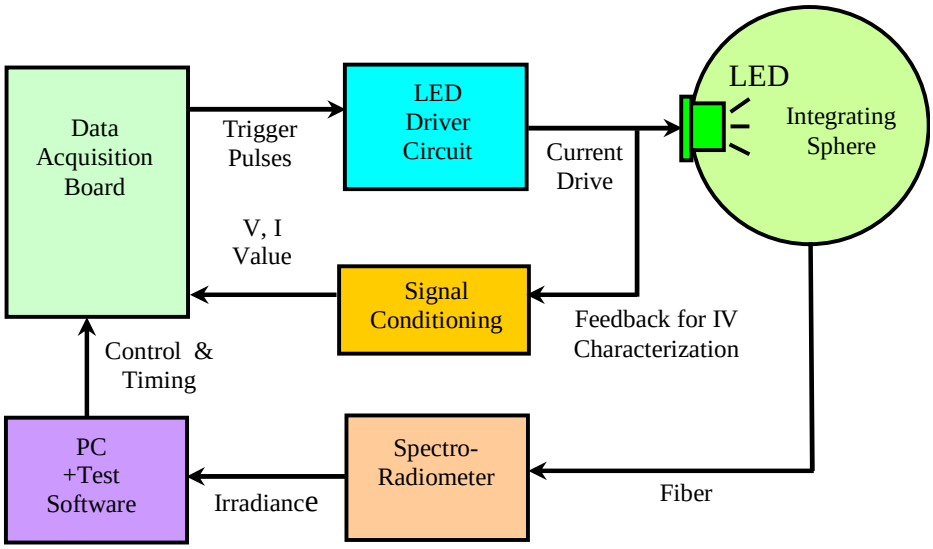

Fig 6.1 Electrical and Optical Characterization of LEDs

6.4 Results and Discussion of Spectral Shift

6.4.1 Vf-Jt Linear Relationship

Linear relationship between the forward voltage Vf and Junction Temperature Jt was established for 2 LEDs (640x1-57 and 640x1-58) for a given forward current value. This was repeated at different currents (26mA, 58mA, 483mA and 725mA). See Fig. 6.2 and Fig. 6.3 for details.

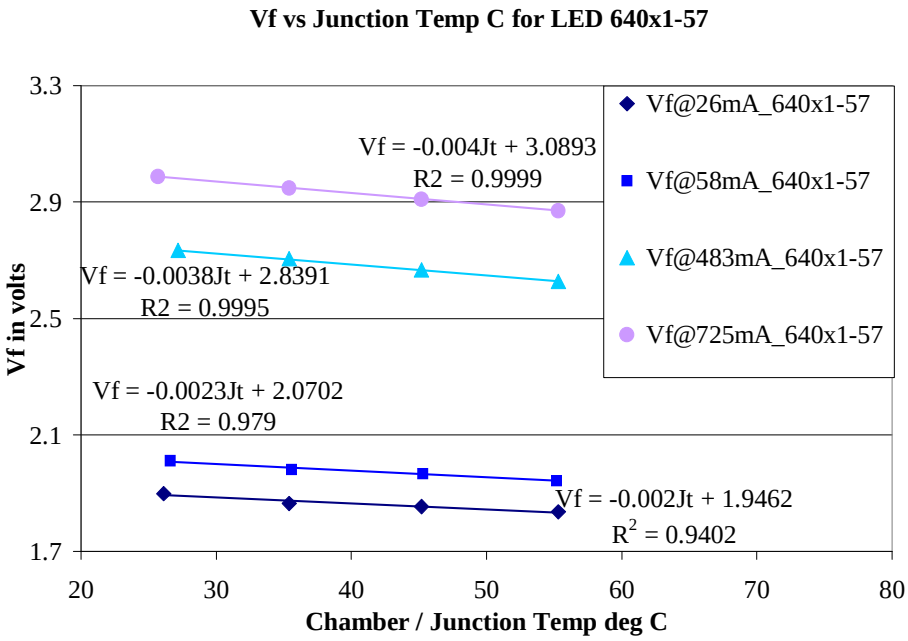

Fig. 6.2 Vf-Jt relationship for LED 640x1-57
Vf-Jt relationship is plotted for 26, 58, 483 and 725mA.

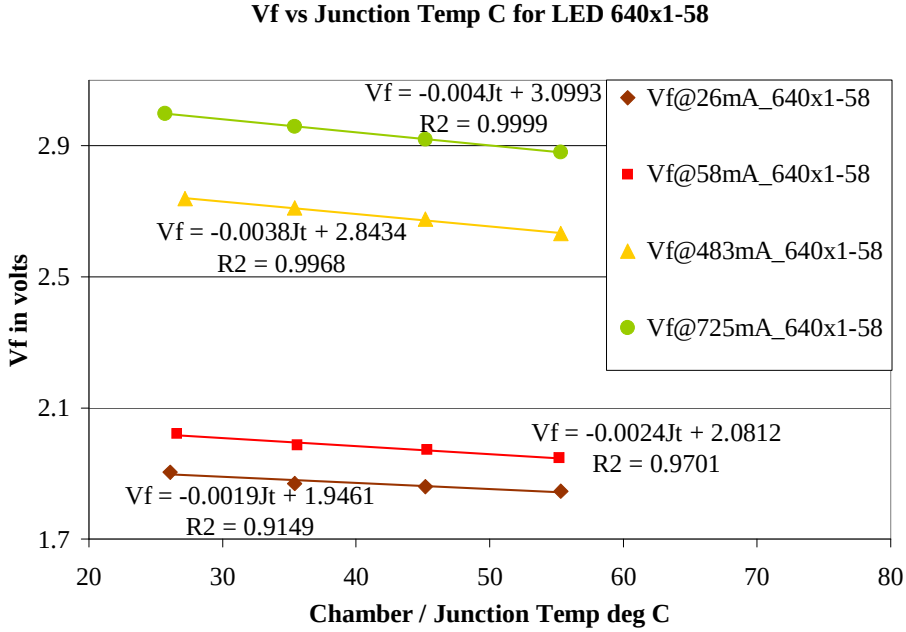

Fig. 6.3 Vf-Jt relationship for LED 640x1-58
Vf-Jt relationship is plotted for 26, 58, 483 and 725mA.

6.4.2 Spectral shift in Bandgap

There was a prominent shift in the spectral output of the LEDs towards the longer wavelength at higher current (which caused higher junction temperatures). The peak wavelength λpeak returned to normal values when the current was decreased suggesting that this shift was temporary. There was no permanent degradation. See Fig 6.4 and Fig 6.5 for the spectral performance of LEDs 640x1-57 and 640x1-58 respectively. Table 6.1 captures the details of the Peak wavelength and the estimated junction temperature for different values of forward current If.

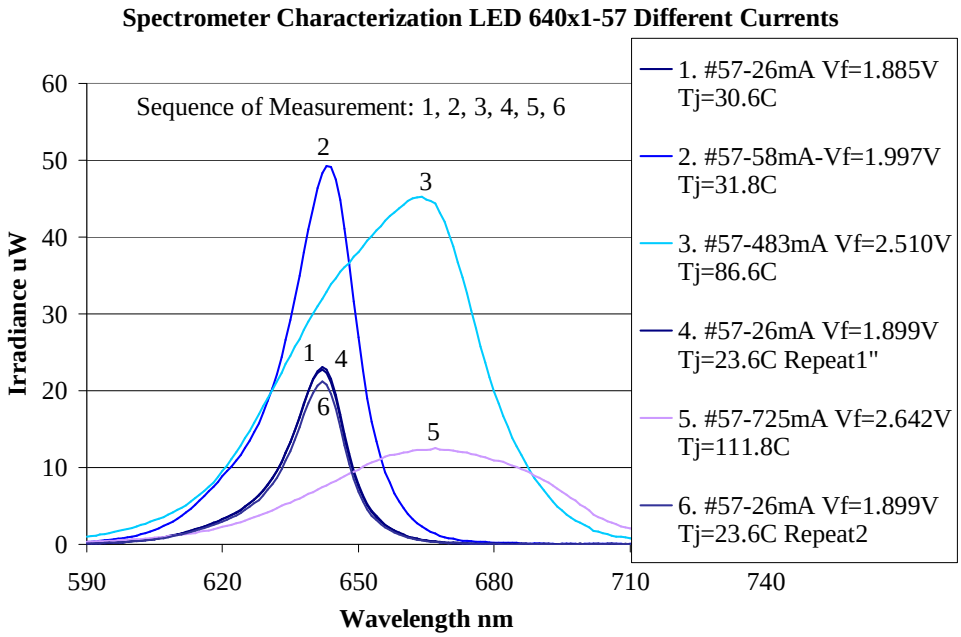

Fig. 6.4 Spectral Shift in Bandgap at higher Jt for LED 640x1-57
Note the sequence of measurements. λpeak returned to normal values indicating that the shift is temporary. There is no permanent degradation.

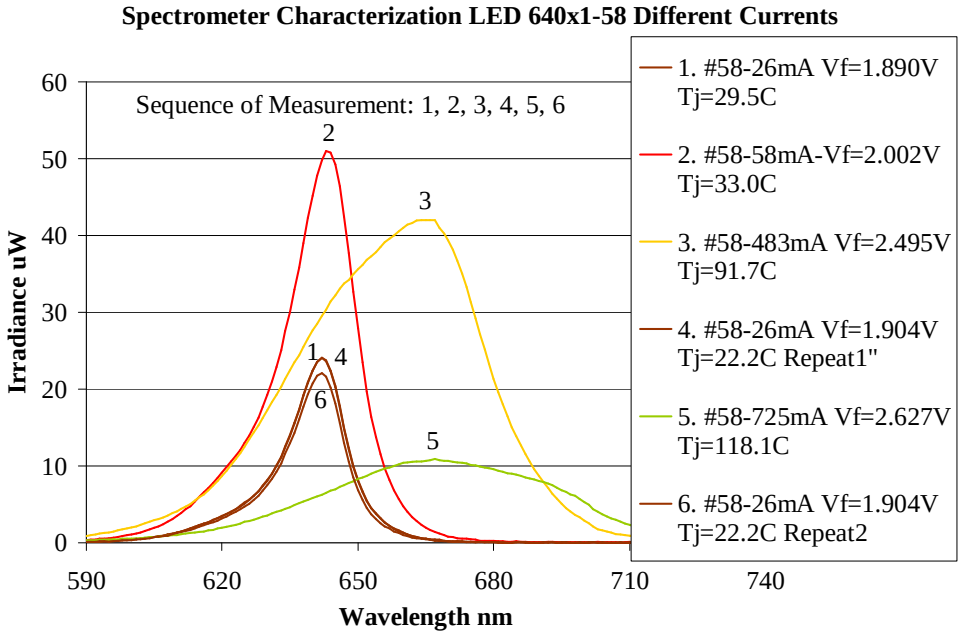

Fig. 6.5 Spectral Shift in Bandgap at higher Jt for LED 640x1-58
Note the sequence of measurements. λpeak returned to normal values indicating that the shift is temporary. There is no permanent degradation.

LED	If mA	Equation	Vf Volts	Jt C Estimated	Peak nm
640x1-57	26	Vf = -0.002Jt + 1.9462	1.885	30.6	642
640x1-57	58	Vf = -0.0023Jt + 2.0702	1.997	31.8	643
640x1-57	483	Vf = -0.0038Jt + 2.8391	2.510	86.6	664
640x1-57	26	Vf = -0.002Jt + 1.9462	1.899	23.6	642
640x1-57	725	Vf = -0.004Jt + 3.0893	2.642	111.8	667
640x1-57	26	Vf = -0.002Jt + 1.9462	1.899	23.6	642
640x1-58	26	Vf = -0.0019Jt + 1.9461	1.890	29.5	642
640x1-58	58	Vf = -0.0024Jt + 2.0812	2.002	33.0	643
640x1-58	483	Vf = -0.0038Jt + 2.8434	2.495	91.7	665
640x1-58	26	Vf = -0.0019Jt + 1.9461	1.904	22.2	642
640x1-58	725	Vf = -0.004Jt + 3.0993	2.627	118.1	667
640x1-58	26	Vf = -0.0019Jt + 1.9461	1.904	22.2	642

Table 6.1 Spectral Shift in Bandgap at higher temperatures

6.4.3 Varshini's empirical model

The relationship between peak wavelength and current/junction temperature has been published in various articles. Our research findings agree with Kish et al [20] for the AlGaInP LEDs. They studied high luminous flux AlGaInP/GaP large area emitters with currents as high as 7A. The peak wavelength shifted from 602nm to 614nm when the current was increased to 7A corresponding to a 120°C rise in junction temperature. Similar results have been observed by Nakamura et al [3] for InGaN MQW LEDs. The peak wavelength changed from 409nm at 25°C to 410.5nm at 55°C.

Nakamura et al [46] also found an anomaly while testing InGaN DH LEDs. The peak wavelength shifted to the shorter-wavelength region with increasing forward current. The peak wavelengths were 458 nm at 0.1 mA, 449 nm at 1 mA and 447 nm at 20mA. They suggested that this anomaly was due to donor-acceptor (DA) pair recombination in the InGaN active layer co-doped with both Si and Zn. At 20 mA, a narrower, higher-energy peak emerged around 385 nm. This peak was due to band-to-band recombination in the InGaN active layer. This peak became resolved at injection levels where the impurity related recombination was saturated. H. Morkoc [6] shows current and temperature dependence of Spectra for Green Nichia GaN LEDs. A clear shift to higher energies was observed (532nm at 0.1mA to 519nm at 10mA). For pulsed current, EL changed from 534nm at 0.1mA to 492nm at 2000mA. For the same LEDs, the peak decreases from 541nm at 50°K (-223°C) to 534nm at 300°K (27°C) whereas the band edge increases from 535nm to 544nm.

Dependence of the bandgap on the temperature has been determined for various materials. The relationship can be described by Varshini's empirical equation given below.

$$Eg(T) = Eg(0) - \frac{\alpha T^2}{T + \beta} \qquad \text{-(6.3)}$$

where Eg(0), α and β are the fitting parameters, T is temperature in °K and Eg(T) is the bandgap in eV. These fitting parameters are listed in Zeghbroeck et al [7], which we have reproduced in Table 6.2 for Ge, Si and GaAs. Based on our test results, we have included estimated values for AlGaInP in this table.

	Ge	**Si**	**GaAs**	**AlGaInP**
E_g**(0) [eV]**	0.7437	1.166	1.519	2.11
α[eV/K]	4.77 x10^4	4.73 x10^4	5.41 x10^4	1.02 x10^3
β [K]	235	636	204	199

Table. 6.2 Varshini's coefficients: Ge, Si, GaAs & AlGaInP

6.4.4 Effect on LED life testing

We see in section 6.4.2 that the shift in the peak wavelength at high junction temperature is temporary. There is no permanent degradation. Published literature [2, 27] on LED life testing reveals that there may be an increase in junction temperature during LED life testing. The heat may either be due to increase in ohmic resistance of the contacts or it may be due to defect generation leading to an increase in non-radiative recombinations. The published research establishes that the light output will eventually decrease during life testing [16, 17, 26, 27]. Our research proposes that there might also be a shift in the peak wavelength as a secondary effect. To assess such shifts, the forward bias method should be employed to characterize the Vf-Jt

relationship before the start of Accelerated Life testing (ALT) and Accelerated Degradation Test (ADT). Varshini's model may also be used to establish the Jt-λpeak relationship. During the ALT/ADT, the Vf measured will allow us to estimate the actual Jt and its contribution towards λpeak.

6.5 Effect of Spectral Shift on Medical application

Wavelength shifts are more critical for Medical applications compared to Lighting applications of LEDs. In principle, the shift will have 2 consequences.

6.5.1 Decrease in net optical output

As described in Fig 1.2 in Chapter 1, the light from the LED passes through a sharp optical filter, which has a bandwidth of only few nano-meters. If the peak wavelength of the LED shifts, a part of the spectrum will shift outside the bandwidth of the optical filter causing a decrease in the net optical power as shown in Fig 6.6. This decrease will depend on the shape of the LED spectrum, the filter bandwidth and the actual shift of the LED spectrum, which will depend on junction temperature.

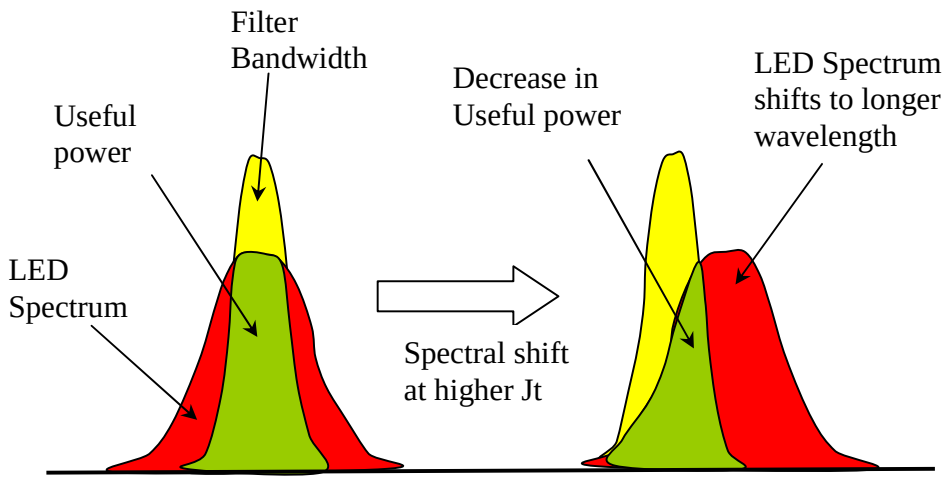

Fig. 6.6 Effect of Spectral Shift on useful optical power

6.5.2 Change in the Absorbance Chemistry

As described in section 1.1 in Chapter 1, the absorbance of light by the cuvette mixture at certain wavelengths depends on patient's disease condition. Beer's law [1] gives a relationship between the transmission T of light through a substance and the product of the absorption coefficient of the substance, α, and the distance the light travels through the material (i.e. the path length), ℓ. For a given medical instrument, the path length is constant and the absorption of light can be calculated from the incident and transmitted light. Further, the same medical diagnostic instrument performs various tests (called assays) such as Clinical Chemistry, Drugs of abuse, therapeutic drug monitoring (TDM) and specific proteins etc. Depending upon the actual diagnostic test to be performed, the human sample is mixed with proprietary chemical reagents. The relationship between the light absorbed and the disease condition is pre-determined by Chemists for all the diagnostic tests that the medical instrument supports. Some of these tests are very sensitive to the peak wavelength whereas others are less sensitive. A shift in peak wavelength of the LED light source will have different consequences depending upon the specific diagnostic test being conducted, its sensitivity to wavelength and the actual spectral shift. Much of this information is proprietary and beyond the scope of this research.

6.6 Conclusions of Spectral Shift

Reliability testing of AlGaInP MQW LEDs resulted in a shift of Bandgap towards the longer wavelength when driven at high current. Characterization of the shift showed that it was temporary and dependent on the junction temperature Jt. The data was further analyzed with respect to Varshini's equation, and the empirical coefficients were determined. Published research establishes that the light output will eventually decrease during life testing. This research proposes that there might also be a shift in the peak wavelength as a secondary effect if the LED operates at a high junction temperature Jt. This research will also help in evaluating LED performance during ALT/ADT and while choosing LEDs for applications (such as medical diagnostics) where λpeak needs to be stable. The junction temperature Jt will need to be maintained within limits to achieve spectral stability.

Chapter 7: Failure Modes and Effects Criticality Analysis (FMECA)

7.1 Introduction

Failure Modes Effects and Criticality Analysis (FMECA) was used as a risk analysis tool for use of LEDs in a medical diagnostic application. Probabilistic Risk Assessment (PRA) with Event Sequence Diagrams (ESD) is also used for performing risk analysis. While the focus of this chapter is FMECA, PRA/ESD is discussed briefly in section 7.5. FMECA is a bottom up approach used to separate critical failure modes from the rest. The segregation is done based on the approximate probabilities of the failure modes and the severity of the outcomes. It identifies failure modes at a component level (LED in this context), and analyzes the system level effects (failure or partial failure of the medical diagnostic instrument in this case). Some of these results were also published by the author in Sawant et al [11]. However, Section #, Figure #, Table # and References have been rearranged as necessary.

A FMECA table was constructed for various LED failure modes (described in section 7.2) and the criticality is calculated for different severity levels as

$C_m = \beta\alpha\lambda t$ - (7.1)

where

1. Failure effect probability (β) is the conditional probability that the failure effect will result in the identified severity classification, given that the failure mode occurs. It represents the analyst's best judgment as to the likelihood that the loss will occur.

2. Failure mode ratio (α) is the ratio of the probability of the current failure mode to the failure probability due to all the failure modes,

3. Failure rate (λ) is the ratio the total failures observed during a test to the total time of all the devices under test and

4. Operating time (t) is the time during which the test is performed.

Table 7.1 below describes the severity classification for a general application and a medical diagnostic application.

Level	**Rating**	**Severity description for General application**	**Severity for Medical Diagnostic application**
Catastrophic	1	A failure mode that may cause death, complete system or mission loss	Inaccurate medical test result, May lead to death of patient or user or Serious deterioration in their state of health
Critical	2	A failure mode that may cause severe injury, major system degradation, damage or reduction in mission performance	Incorrect diagnosis, Inappropriate treatment
Marginal	3	A failure mode that may cause minor injury or degradation in system or mission performance	Inaccurate Medical test result, But test is used in conjunction with other diagnostic information.
Minor	4	A failure mode that does not cause injury or system degradation, but may cause a minor inconvenience such as unscheduled maintenance or repair	Delayed or no medical test result, Incorrect result. But no difference in diagnosis or treatment, Incorrect result requiring confirmatory testing.
None	5	---	---

Table 7.1 Failure Severity classification for general and medical diagnostic application

7.2 LED Failure Modes

The first step in FMECA was identification of various LED failure modes. Fig 7.1 shows various failure modes that were identified for this analysis.

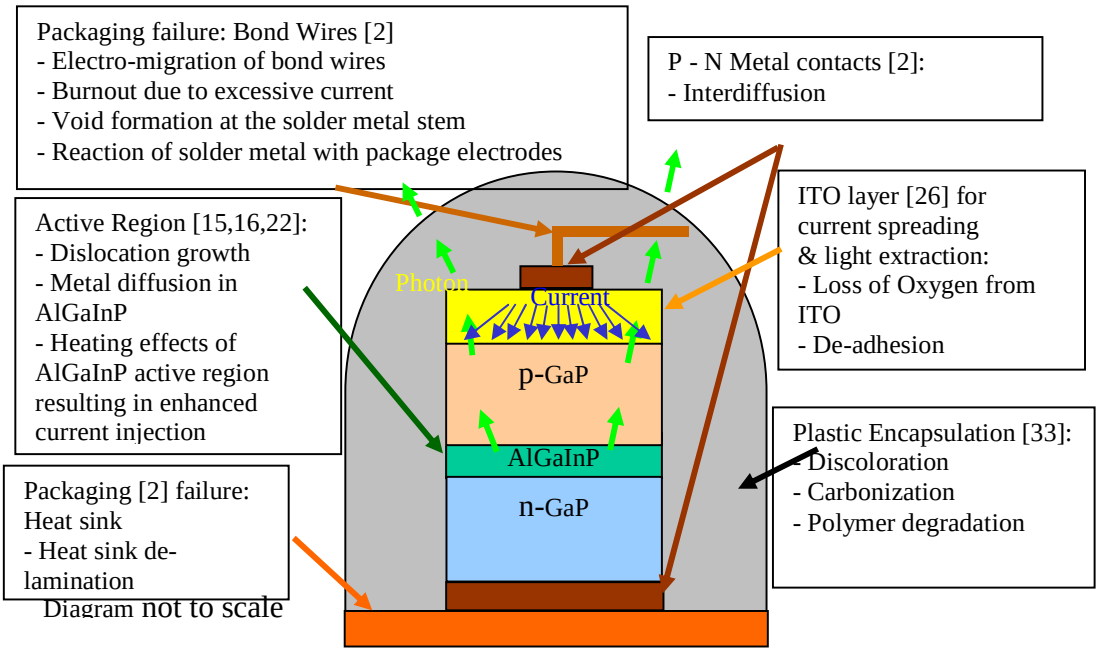

Fig 7.1 LED Failure modes

7.2.1 Active Region failure

Active layer is the region where electrons and holes recombine to emit photons. The degradation is mainly related to the property of semiconductor crystals [2]. Dislocation growth, in-diffusion and precipitation of a host atom are typical modes in such degradation. Enhancement factors include injected current (electron and hole), Joule heating by injected current, ambient temperature and emitted light.

7.2.2 P-N Contacts failure

Degraded contacts [2] generally correspond to p-side electrodes because ordinary devices are composed of n-type substrates and the p-side electrodes exist near the active region of the devices. For devices with a p-type substrate, the degradation is in n-type electrode. The main mechanism is caused by metal diffusion in to the inner region (outer diffusion of semiconductor material) and is enhanced by injected current, joule heating and ambient temperature.

7.2.3 Indium Tin-Oxide failure

Indium Tin-Oxide layer is used for current spreading and improvement of light extraction [26]. Failure modes are related to loss of oxygen from the ITO layer and de-adhesion.

7.2.4 Plastic encapsulation failure

Plastic encapsulation (lens) is usually a polymer used to protect the LED chip from external atmosphere and to direct the extracted light. Typical failure modes are discoloration, carbonization and polymer degradation [33].

7.2.5 Packaging failures

Packaging failure is either related to Bond Wires or the Heat Sinks [2]. The bonding part corresponds to the interface between an LED chip – heat sink and between heat sink – package stem [2]. Usually some type of solder is used at the interface as a bonding metal. The degradation is mainly caused by Electro-migration (transport of metal atoms under high current stress) and is related to the properties of the solder metal. The main mode is void formation through the migration of the solder metal

stem or reaction of solder metal with electrodes / the plated metal on the heat sink / the stem. The migrated solder often shows a whisker growth. The factors that enhance this type of degradation are current flow and ambient temperature. Heat sink degradation is not degradation of the heat sink itself, but the separation of the metal used for metallization of the heat sink. The generation of this degradation depends on the heat sink material, the metal used for metallization and the metallization process. The enhancement factor is not clear but ambient temperature and current flow are estimated to be factors.

7.3 FMECA before ALT/ADT

During initial FMECA (done before Accelerated Life/Degradation Test based on literature review and knowledge of the medical diagnostic instrument), packaging (heat sink de-lamination) and degradation of the active region were estimated as the critical failure modes. See Table 7.2 for details

Sr.#	Failure Modes/Mechanisms	Causes	Local Effects at LED level	System Effects in Medical equipment	Severity	Failure Effect Probability (ß)	Failure Mode Ratio (a)	Failure Rate	Operating Time (T) in hrs	Criticality #
1	Packaging failure (Heat Sink)	Heat sink de-lamination	- Decrease of optical output - Local heating effects	- Unscheduled module replacement - Delayed medical test results	3	0.4	0.3	1.8E-11	31500	6.7E-08
2	Degradation of plastic encapsulation	- Discoloration - Carbonization - Polymer degradation at high temperature	- Gradual decrease of optical output	- Excessive drift requires unscheduled calibration - Delayed medical test results	3	0.4	0.2	1.8E-11	31500	4.5E-08
3	Degradation of ITO layer	- Loss of Oxygen from ITO - De-adhesion	- Decrease of optical output - Non-uniform light emission	- Unscheduled module replacement - Delayed medical test results	4	0.3	0.1	1.8E-11	31500	1.7E-08
4	Packaging failure (Bond Wires)	- Electro-migration of bond wires - Burnout due to excessive current - Void formation at the solder metal stem - Reaction of solder metal with package electrodes	- Abrupt LED failure	- Unscheduled module replacement - Delayed medical test results	4	0.9	0.1	1.8E-11	31500	5.0E-08
5	Degradation of active layer	- Dislocation growth - Metal diffusion in AlGaInP - Heating effects of AlGaInP active region resulting in enhanced current injection	- Gradual decrease of optical output	- Excessive drift requires unscheduled calibration - Delayed medical test results	4	0.4	0.4	1.8E-11	31500	9.0E-08
6	Degradation of P-N metal contacts	- Interdiffusion	- Change in IV characteristics	- Design will accommodate minor changes in IV characteristics	5	0.4	0.2	1.8E-11	31500	4.5E-08

Table 7.2 FMECA table before ALT/ADT

7.4 FMECA after ALT/ADT

After Accelerated Life Test was performed, plastic encapsulation and active region degradation are estimated as the critical failure modes. Either of these failure modes will cause system level effects such as excessive drift requiring unscheduled calibration and delayed medical test results. See Table 7.3 for details.

Sr.#	Failure Modes/Mechanisms	Causes	Local Effects at LED level	System Effects in Medical equipment	Severity	Failure Effect Probability (ß)	Failure Mode Ratio (a)	Failure Rate (?)	Operating Time (T) in hrs	Criticality #
1	Packaging failure (Heat Sink)	Heat sink de-lamination	- Decrease of optical output - Local heating effects	- Unscheduled module replacement - Delayed medical test results	3	0.4	0.3	1.8E-11	31500	6.7E-08
2	Degradation of plastic encapsulation	- Discoloration - Carbonization - Polymer degradation at high temperature	- Gradual decrease of optical output	- Excessive drift requires unscheduled calibration - Delayed medical test results	3	0.6	0.7	1.8E-11	31500	2.3E-07
3	Degradation of ITO layer	- Loss of Oxygen from ITO - De-adhesion	- Decrease of optical output - Non-uniform light emission	- Unscheduled module replacement - Delayed medical test results	4	0.3	0.1	1.8E-11	31500	1.7E-08
4	Packaging failure (Bond Wires)	- Electro-migration of bond wires - Burnout due to excessive current - Void formation at the solder metal stem - Reaction of solder metal with package electrodes	- Abrupt LED failure	- Unscheduled module replacement - Delayed medical test results	4	0.9	0.1	1.8E-11	31500	5.0E-08
5	Degradation of active layer	- Dislocation growth - Metal diffusion in AlGaInP - Heating effects of AlGaInP active region resulting in enhanced current injection	- Gradual decrease of optical output	- Excessive drift requires unscheduled calibration - Delayed medical test results	4	0.6	0.6	1.8E-11	31500	2.0E-07
6	Degradation of P-N metal contacts	- Interdiffusion	- Change in IV characteristics	- Design will accommodate minor changes in IV characteristics	5	0.4	0.2	1.8E-11	31500	4.5E-08

Table 7.3 FMECA table after ALT/ADT

7.5 Probabilistic Risk Assessment and Event Sequence Diagrams

Probabilistic Risk Assessment (PRA) starts with critical end states (ES). For the medical diagnostic application, critical end states are

1. Correct Medical Test Results,
2. Correct but Delayed Medical Test Results,
3. Incorrect Medical Test Results but Detected before Reporting and
4. Erroneous but Believable Medical Test Results

Once the ES are defined, all possible Initiating Events (IE) are identified which could create such ES. The propagation of an IE in to an ES is called a scenario. The scenario is shown graphically in the form of an Event Sequence Diagram (ESD) in Fig 7.2 below [4].

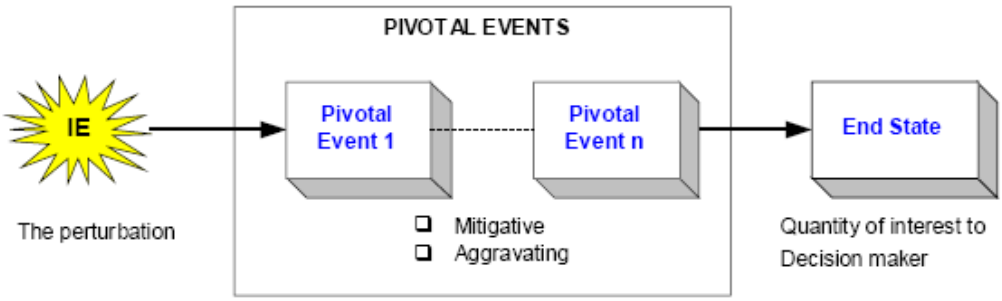

Fig 7.2 Scenario / Event Sequence Diagram [4]

A scenario contains an IE and one or more pivotal events leading to an end state. As modeled in most PRAs, an IE is a perturbation (such as LED degradation) that requires some kind of response from the Medical instrument (such as detection of the LED degradation and correction using calibration). The Pivotal Events (PE) include

successes or failures of these responses. Simple pivotal events may be expressed as a block with numerical probability for occurrence of each response. Complicated pivotal events may be expressed as a Fault Tree (FT) for calculation of probabilities of the responses. Once the probabilities of all the Initiating Events and Pivotal Events are known (or estimated), the probability of all the End States can be calculated. Fig 7.3 gives an example of an ESD for the medical diagnostic application. Many such ESDs need to be created before the probabilities of critical End States can be calculated.

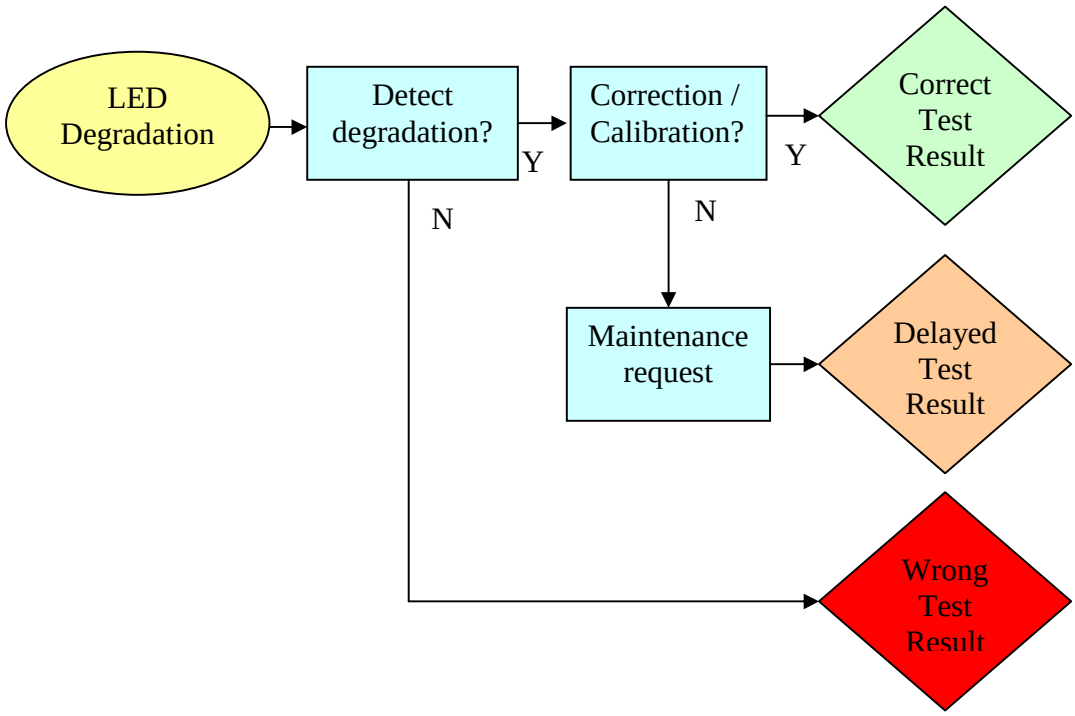

Fig 7.3 ESD for LED degradation in Medical application

7.6 Conclusions

FMECA approach, widely used for risk analysis, has been successfully applied to LED reliability and physics of failure investigation. In this study, we used FMECA to understand the criticality of LED failure modes when used in a medical diagnostic application. Failure modes of other components of the Medical device were not included in this study. The FMECA was repeated and refined after conducting accelerated life testing of LEDs. Degradation of the plastic encapsulation and the active region were found to be the critical failure modes. These failures could cause unscheduled calibration of the diagnostic instrument and would cause delay in patient medical test results. Probabilistic Risk Assessment using Event Sequence Diagrams is also briefly discussed. An example ESD describing LED degradation as an initiating event and its progression towards critical end states is provided.

Chapter 8: Bayesian Modeling of LED Reliability

Bayesian Analysis allowed us to combine prior published data with Accelerated Life Test (ALT) performed to verify the Medical diagnostic application. Bayesian Analysis involves compiling 'Prior' information, generating the 'Likelihood' function (probability of seeing the Evidence in terms of test data given a specific underlying failure distribution) and then estimating the 'Posterior' distribution. Some of these results were also published by the author in Sawant et al [13]. However, Section #, Figure #, Table # and References have been rearranged as necessary. The general scheme of Bayesian modeling of LED reliability is as shown in Fig 8.1

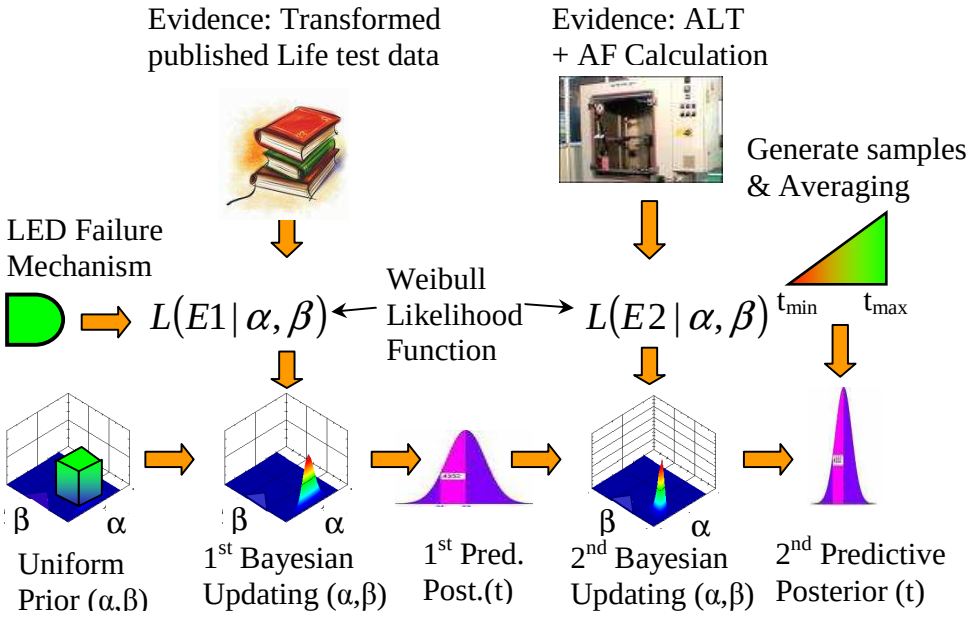

Fig 8.1 Bayesian modeling of LED Reliability

8.1 Baye's theorem

For two events X and E, the probability of X AND E occurring simultaneously (represented by X•E) is the product of probability of X given E has occurred and probability of E

$$Pr(X \bullet E) = Pr(X|E)Pr(E) \quad \text{- (8.1)}$$

$$Pr(E \bullet X) = Pr(E|X)Pr(X) \quad \text{- (8.2)}$$

Since Pr(X•E) = Pr(E•X), we have

$$Pr(X|E)Pr(E) = Pr(E|X)Pr(X) \quad \text{- (8.3)}$$

Rearranging the terms gives the Baye's Theorem

$$\Pr(X \mid E) = \frac{\Pr(E \mid X)\Pr(X)}{\Pr(E)} \quad \text{- (8.4)}$$

Now Pr(E) = Σ Pr(E|X)Pr(X) for all possible values of X, this gives

$$\Pr(X \mid E) = \frac{\Pr(E \mid X)\Pr(X)}{\sum \Pr(E \mid X)\Pr(X)} \quad \text{- (8.5)}$$

In Reliability applications, events X and E are represented by distributions. Summation is used for discrete distributions and integration is used for continuous distributions as shown below.

$$\pi_1(X \mid E) = \frac{L(E \mid X)\pi_0(X)}{\int L(E \mid X)\pi_0(X)\,dX} \quad \text{- (8.6)}$$

where L(E/X) is the likelihood of seeing the evidence E given that X is the random variable of interest,

$\Pi_0(X)$ is the prior distribution of the random variable of interest and

$\Pi_1(X/E)$ is the posterior distribution of the random variable of interest given that evidence E was observed.

8.2 Bayesian Modeling of LED data

Many of the LED degradation mechanisms occur simultaneously. The weakest link causes the actual failure. This leads us to believe that Weibull distribution (with parameters α & β) is the most suitable distribution for time to failure of the LEDs. Levada et al. [34] carried out accelerated life tests on plastic transparent encapsulation and pure metallic package GaN LEDs. A consistent Weibull based statistical model was found for MTTF. When the data from ALT performed in this research was analyzed, it revealed that Weibull is a slightly better fit compared to the Lognormal fit. Thus the degradation mechanism, published literature and our ALT data all point to Weibull as a most suitable model for this data analysis. See section 10.3.1 for a detailed discussion on the subject.

For the first posterior, using Uniform Prior distribution for α & β is a good choice. Since only MTTF values were available, min-max values for α & β were estimated using engineering judgment. Test data was used as Evidence and a joint α-β posterior distribution was calculated using Bayesian updating. This joint α-β distribution gave a series of Weibull time to failure distributions. The predictive posterior failure distribution for the LEDs was estimated by averaging over the range of α-β values. Numerical techniques were used for various computations.

8.2.1 Likelihood function for LED reliability

Consider a life test in which *n* LEDs are put on test and *r* out of *n* fail at failure times *t1, t2,…,tr*. The test is terminated at time *tc* at which point *n-r* LEDs did not fail. The only thing we know about these 'survived' LEDs is that their failure time is greater than *tc*. The failure times *t1, t2,…,tr* and the suspend time *tc* is the Evidence for the Bayesian Analysis.

The likelihood of r LEDs failing at ti (i = 1 to r) and n-r LEDs surviving time tc is given in (8.7) and (8.8) below

$$L(E \mid \alpha, \beta) = \prod_{i=1}^{r} f(t_i \mid \alpha, \beta) \prod_{i=1}^{n-r} R(t_c \mid \alpha, \beta) \qquad \text{- (8.7)}$$

$$L(E \mid \alpha, \beta) = \beta^r \alpha^{-\beta r} \left(\prod_{i=1}^{r} t_i\right)^{\beta-1} \exp\left(-\alpha^{-\beta} T\right) \qquad \text{- (8.8)}$$

where $T = \sum_{i=1}^{r} t_i^{\beta} + \sum_{i=1}^{n-r} t_c^{\beta} = \sum_{i=1}^{r} t_i^{\beta} + (n-r) t_c^{\beta}$

8.2.2 Uniform Prior distribution for α & β

The Uniform Prior distribution for α & β is given by equation below

$$\pi_0(\alpha, \beta) = \begin{cases} \dfrac{1}{(\alpha \max - \alpha \min)(\beta \max - \beta \min)}, & \alpha \min \le \alpha \le \alpha \max, \\ & \beta \min \le \beta \le \beta \max \\ 0, & \textit{otherwise} \end{cases} \qquad \text{- (8.9)}$$

8.2.3 Posterior distribution for α & β

The posterior distribution for α and β can be estimated by using the Baye's theorem given is equation

$$\pi\ (\alpha,\beta \mid E) = \frac{L(E \mid \alpha,\beta)\pi_0(\alpha,\beta)}{\int_{\beta}\int_{\alpha} L(E \mid \alpha',\beta')\pi_0(\alpha',\beta')d\alpha' d\beta'} \quad \text{- (8.10)}$$

8.2.4 Predictive Posterior distribution for LED life

Our final goal is to estimate the Weibull distributed time to failure. The joint posterior distribution of α and β then allows the posterior predictive distribution to be calculated as given by PDF equation (8.11) and CDF equation (8.12)

$$\overline{f}(t) = \int_{\beta}\int_{\alpha} f(t \mid \alpha',\beta')\pi_1(\alpha',\beta' \mid E)d\alpha' d\beta' \quad \text{- (8.11)}$$

$$\overline{F}(t) = \int_{\beta}\int_{\alpha} F(t \mid \alpha',\beta')\pi_1(\alpha',\beta' \mid E)d\alpha' d\beta' \quad \text{- (8.12)}$$

8.3 Results of Bayesian modeling

8.3.1 Compiling the Prior Data

Results of prior published data and ALT as reported in Sawant et al [11] will be used in the Bayesian modeling. Table 4.1 was modified to get Table 8.1 where Sr.# 1-4 represents prior data (normalized to current density and temperature values) under dc driving conditions. Sr.#5 represents ALT data (normalized to current density and temperature values) under pulse (0.2% duty cycle) driving conditions. Since LED life under dc conditions was much shorter compared to pulse conditions, we had to

transform Sr#.1-4 data in to Sr.#:1A-4A to allow using in our Bayesian model. This also seems reasonable from the fact that during pulse driving, the LED gets time to cool off. This increases the time to failure of the LEDs during pulse driving compared to DC driving. The exact method of transformation will be covered in chapter 9. For now, a simple multiplier of 500 is assumed (1 hr at 100% duty cycle is equivalent to 500hrs at 0.2% duty cycle).

Sr. #	LED Material Structure Driving	Source of Data [Ref.]-Fig	IPL n	Act. E. eV	**Weibull** (Converted to application conditions) α	β	MTTF Hrs	**Lognormal** (Conv. to appl. Conditions) μ	σ	MTTF Hrs
1	AlGaInP-DH-DC	[17]-2/4, [19]-9a/9b, [26]-3, [28]-3a/3b [29]-5	1.68	0.67	2.76E4	0.50	1.33E4	9.1	2.30	9.41E3
2	AlGaInP-MQW-DC	[19]-9a/9b, [22]-16, [24]-6/8/10 [27]-2	5.08	0.82	7.82E5	0.89	5.17E5	13	1.25	4.27E5
3	GaN-DH-DC	[47]-1	2.69	0.50	-	-	-	-	-	-
4	GaN-MQW-DC	[24]-7/9/11 [33]-5, [34]-2/6	2.02	0.20	1.61E5	0.57	8.47E4	11.0	2.06	6.22E4
5	ALT: AlGaInP-MQW-Pulsed (0.2%)	ALT performed for this study	4.48	1.15	1.55E9	0.50	7.50E8	20.0	2.50	5.23E8
1A	AlGaInP-DH-Pulse-Transformed	Sr. # 1	1.68	0.67	1.38E7	0.5	6.65E6			
2A	AlGaInP-MQW-Pulse-Transformed	Sr. # 2	5.08	0.82	3.91E8	0.89	2.59E8			
3A	GaN-DH-Pulse-Transformed	Sr. # 3	2.69	0.50	-	-	-			
4A	GaN-MQW-Pulse-Transformed	Sr. # 4	2.02	0.20	8.07E7	0.57	4.24E7			

Table 8.1 Prior Published Data Transformed for Bayesian Analysis

Bayesian updating involves computation of posterior joint α-β distribution by combining the prior joint α-β distribution with new Evidence/Likelihood function. Bayesian analysis started with a Uniform prior joint α-β distribution with α taking values between 5E7 to 9E9 and β taking values between 0.1 to 2. Uniform distribution implies that the probabilities are constant for the entire range. Further, since the Bayesian updating was done using a SW program written for this research (to implement equation 8.10), the α & β values had to discretized.

8.3.2 Computation of 1st Posterior Distribution

The data represented by Sr.# 2A in Table 8.1 was used as evidence to compute the 1st posterior joint α-β distribution as shown in Fig 8.2.

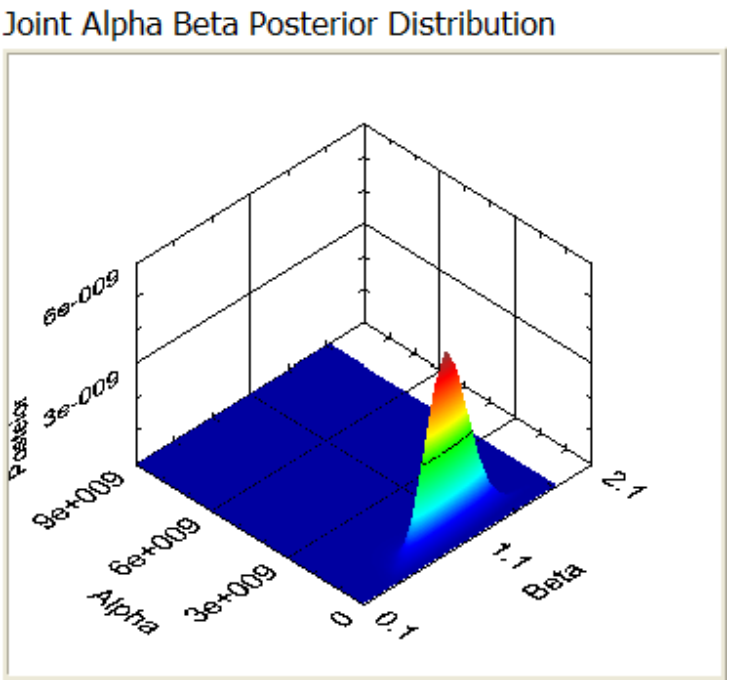

Fig 8.2 1st Posterior Joint α-β distribution for AlGaInP-MQW-Pulse-Transformed

The 1st posterior joint α-β distribution was used to compute the Average Predictive distribution of the LED time to failure (TTF) using equations 8.11 and 8.12. See Fig 8.3 for the CDF of LED TTF.

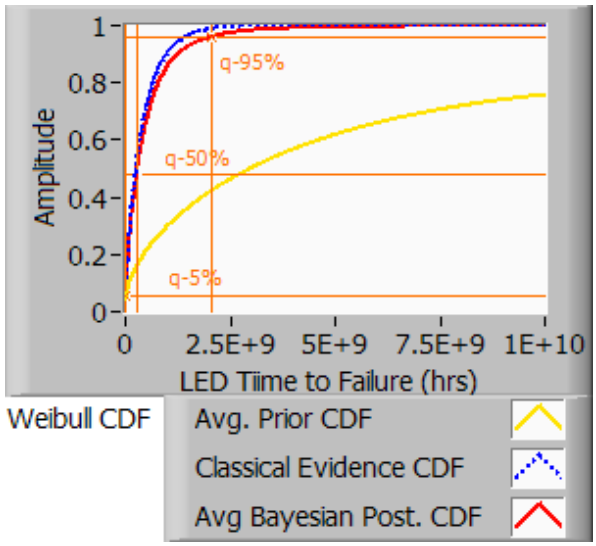

Fig 8.3 1st Average Predictive Posterior of LED TTF.
"Amplitude" refers to the magnitude of the cumulative distribution function

8.3.3 Computation of 2nd Posterior Distribution

For the 2nd Bayesian updating, the 1st posterior joint α-β distribution was used as the prior distribution and the data representing Sr.# 5 in Table 8.1 was used as evidence. Fig 8.4 shows the 2nd Posterior Joint α-β distribution for AlGaInP-MQW-Pulse-ALT. Comparing Fig.8.2 and Fig.8.4, quickly reveals that the uncertainty in the Joint α-β distribution has decreased after 2nd Bayesian updating.

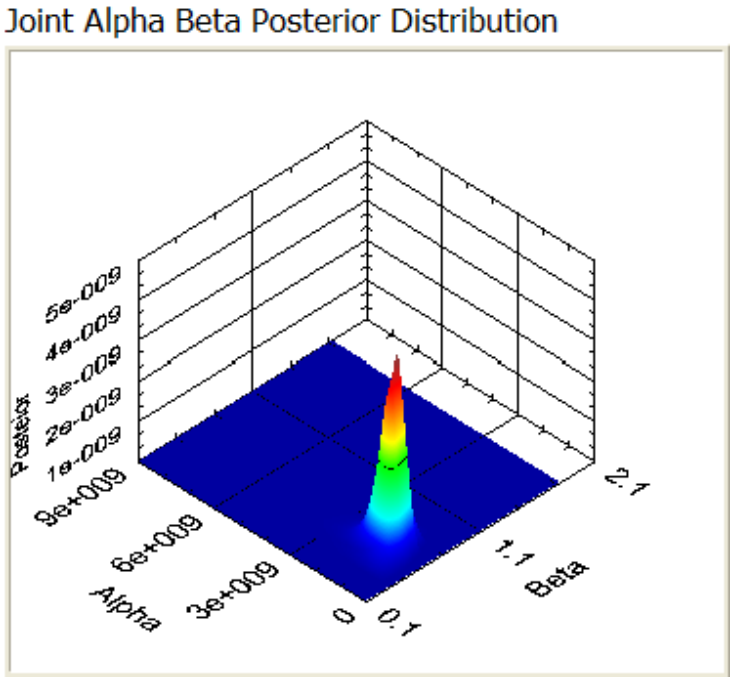

Fig 8.4 2nd Posterior Joint α-β distribution for AlGaInP-MQW-Pulse-ALT

The 2nd Average Predictive posterior distribution of the LED time to failure (TTF) was computed using equations 8.11 and 8.12. See Fig 8.5 for the CDF of LED TTF. Again, comparing Fig 8.3 and Fig.8.5 reveals that 50th percentile of LED TTF changed from 2.75E8 to 6.00E8 hrs between 1st and 2nd Bayesian updating.

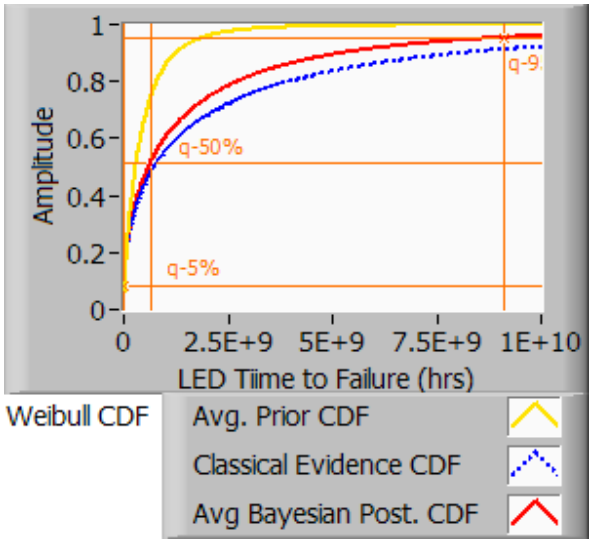

Fig 8.5. 2nd Average Predictive Posterior of LED TTF
"Amplitude" refers to the magnitude of the cumulative distribution function.

8.3.4 Conclusion from Prior data, ALT and Bayesian analysis

Prior published LED data is given in Table 8.1 (Sr.# 2A), ALT results in Table 8.1 (Sr.# 5) and Bayesian updating results are described is described in section 8.3.3. All sources indicate that the MTTF of AlGaInP-MQW LEDs when used in this specific medical application (pulse mode 0.2% duty cycle, temperature = 35°C and current density = 21.6Amps/cm^2) is in excess of 1E8 hrs. This exceeds the life of the medical diagnostic instrument by orders of magnitude and as such is suitable for the application. It is also interesting to observe that the shape parameter β of the Weibull model is less than 1 in all cases implying a decreasing failure rate. This is not by

coincidence. In section 5.4.1, we had observed during ALT that the rate of optical output degradation is logarithmic and that this rate varies significantly between different LEDs (even if taken from same manufacturing batch). Some LEDs cross the 20% degradation (failure threshold for this application) earlier than others. For LEDs that do survive this initial high rate of optical degradation, the probability that it will survive longer increases. This explains the decreasing failure rate.

Chapter 9: Degree of Relevance in Bayesian modeling

Chapter 8 treats Bayesian modeling of LEDs for a medical diagnostic application. It allowed us to combine prior available data with accelerated life test data to predict the reliability (time to failure) of the AlGaInP LEDs. That is the main approach adopted in this dissertation and has been published in Sawant et al [13]. In this chapter, an alternate method for performing Bayesian modeling of LED reliability is proposed. This is additional work that has not been published by the author yet. This approach may also be used in other applications of Bayesian analysis.

9.1 The Problem: Partially relevant prior data

LED families are made from different material systems such as AlGaInP, GaN, GaAs etc. Further, LEDs are manufactured using different semiconductor structures such as Double Heterostructure (DH) and Multi Quantum Well (MQW). Depending upon the application, LEDs may be driven in a DC mode (typically lighting or indicator applications), Pulse mode with high duty cycle (Fiber optic applications) or Pulse mode with very low duty cycle (our current medical diagnostic application). From Table 8.1, it is obvious that the time to failure of the LED is significantly different based on the material, structure and the driving strategy.

Bayesian modeling computes the LED reliability by combining prior published LED data with the current test data (such as life test to mimic the current application). While ample prior published LED data is available, it is very difficult to get prior data for the exact same material system, structure and driving strategy. Limited prior data

forces us to take two approaches. Either assume that the prior data is non-informative (such as using a uniform probability distribution function) or use prior data from a different LED material family, structure or driving strategy. Using non-informative prior distribution pretty much defeats the purpose of Bayesian modeling unless additional and successive Bayesian updating is used. Using prior data, which is not directly relevant to the medical application, will cause over estimation or under estimation of the LED reliability. This is a practical problem that applies to any application of Bayesian modeling.

9.2 The Solution: A Three Step Process

One approach to solving the above problem is using prior data for LEDs, which are similar but not identical to LEDs in the current application. It will be a 3-step process.

9.2.1 Step-1: Transform DC data to Pulse data by Multiplication

In Chapter 8, we transformed the prior data available for AlGaInP-MQW-DC in to AlGaInP-MQW-Pulse by multiplying it by a factor of 500. The rationale used was 1 hr at 100% duty cycle (i.e. DC) is equivalent to 500hrs at 0.2% duty cycle (medical application). While this is a good number to start with, an alternate approach to calculate the multiplier is to take a ratio of MTTF of Pulse testing to DC testing. Ratio of Weibull mean of AlGaInP-MQW-Pulse (from normalized ALT) to AlGaInP-MQW-DC (prior published) was used in this research. This computation (7.50E8/5.17E5) yields a multiplier of 1451. Both of these multipliers (500 and 1451) will be used in subsequent analysis in the following sections. Analysis of prior published data for LED life gave us a set of data consisting of time to failure

Set1={AlGaInP-DH-DC, AlGaInP-MQW-DC, GaN-MQW-DC} - (9.3)

GaN-DH-DC was ignored since limited data was available.

By using the two multipliers (500 and 1451), we go two additional data sets

Set2={AlGaInP-DH-DCx500, AlGaInP-MQW-DCx500, GaN-MQW-DCx500} - (9.4)

Set3={AlGaInP-DH-DCx1451, AlGaInP-MQW-DCx1451, GaN-MQW-DCx1451} - (9.5)

See Appendix 7 for Set1, Set2 and Set3 data.

9.2.2 Step-2: Use a Degree of Relevance Parameter R

A new parameter called degree of relevance 'R' is introduced which takes values between zero and one. The 'R' value will be used to modify the Bayesian model such that the influence of evidence is decreased as R approaches zero. The parameter 'R' can be estimated by engineering judgment and physics of semiconductor structures. Hypothetical values of 'R' based on LED material and structure will be used in this research to perform the analysis. Methods of estimating 'R' such as use of utility functions are left for future research and are briefly discussed in section 11.4.2.

9.2.3 Step-3: Changing the Likelihood function using R

In Bayesian modeling, the Likelihood function is generated from Evidence. One approach to using R in Bayesian modeling is changing the likelihood function as a function of R and then performing the Bayesian updating as shown below.

$$\pi\left(\alpha,\beta \mid E\right)=\frac{[L(E \mid \alpha,\beta)]^{R}\pi_{0}(\alpha,\beta)}{\int_{\beta}\int_{\alpha}[L(E \mid \alpha',\beta')]^{R}\pi_{0}(\alpha',\beta')d\alpha'\,d\beta'} \qquad \text{- (9.6)}$$

If R is 1, it becomes a standard Bayesian updating equation. As R approaches 0, the influence of likelihood function decreases. If R is 0, the posterior distribution becomes identical to prior distribution.

9.3 Results and Discussion

As described in section 8.2, Bayesian analysis started with a Uniform prior joint α-β distribution with α taking values between 5E7 to 9E9 and β taking values between 0.1 to 2. The DC data transformed to Pulse in Set2 (DCx500) and Set3 (DCx1451) was used as Evidence for the 1st Bayesian updating shown in Fig 8.1. The 2nd Bayesian updating is done using ALT data as evidence. Predictive Posterior distributions for LED TTF were computed using the SW developed (described in Appendix 6).

The results are described in Table 9.1 below. Sr. #1a and 1b used AlGaInP-MQW-DCx500 data as 1st Evidence. The only difference is 1b used an R-value of 0.75. Sr. #2 used AlGaInP-MQW-DCx1451 data as 1st Evidence. In this case, R-value assessed is already equal to 1. Hence there was no need to perform a separate analysis. Sr.#3a and 3b used GaN-MQW-DCx500 data as 1st Evidence. The only difference is 3b used an R-value of 0.50. Sr. #4a and 4b used GaN-MQW-DCx1451 data as 1st Evidence. The only difference is 4b used an R-value of 0.75. Sr.#5a and 5b used AlGaInP-DH-DCx500 data as 1st Evidence. The only difference is 5b used an

R-value of 0.50. Sr.#6a and 6b used AlGaInP-DH-DCx1451 data as 1st Evidence. The only difference is 6b used an R-value of 0.75.

Sr .#.	**Prior**	**Evidence 1 with Likelihood^{R}**	**Deg of Rel.**	**Evid-ence 2**	**Predictive Posterior**		**Mean TTF**	**Ch-Sq Statistic**
			R		**α**	**β**	**hrs**	**< 4.6**
1a	Uniform*	AlGaInP-MQW-DCx500 with L^{R}	1.00	ALT$^{\Psi}$	1.17E9	0.547	6.00E8	0.392
1b	Uniform*	AlGaInP-MQW-DCx500 with L^{R}	0.75	ALT$^{\Psi}$	1.30E9	0.538	6.58E8	0.244
2	Uniform*	AlGaInP-MQW-DCx1451 with L^{R}	1.00	ALT$^{\Psi}$	1.57E9	0.601	8.76E8	0.741
3a	Uniform*	GaN-MQW-DCx500 with L^{R}	1.00	ALT$^{\Psi}$	6.70E8	0.415	2.63E8	1.598
3b	Uniform*	GaN-MQW-DCx500 with L^{R}	0.50	ALT$^{\Psi}$	1.06E9	0.437	4.60E8	0.272
4a	Uniform*	GaN-MQW-DCx1451 with L^{R}	1.00	ALT$^{\Psi}$	9.05E8	0.474	4.00E8	0.673
4b	Uniform*	GaN-MQW-DCx1451 with L^{R}	0.75	ALT$^{\Psi}$	1.05E9	0.477	4.87E8	0.314
5a	Uniform*	AlGaInP-DH-DCx500 with L^{R}	1.00	ALT$^{\Psi}$	4.85E8	0.358	1.74E8	2.889
5b	Uniform*	AlGaInP-DH-DCx500 with L^{R}	0.50	ALT$^{\Psi}$	8.90E8	0.387	3.46E8	0.725
6a	Uniform*	AlGaInP-DH-DCx1451 with L^{R}	1.00	ALT$^{\Psi}$	5.88E8	0.388	2.29E8	2.084
6b	Uniform*	AlGaInP-DH-DCx1451 with L^{R}	0.75	ALT$^{\Psi}$	7.43E8	0.395	2.94E8	1.886

Table 9.1 Summary of Bayesian Analysis using partially relevant data

* Uniform prior joint α-β distribution with α taking values between 5E7 to 9E9 and β taking values between 0.1 to 2.

$^{\Psi}$ Accelerated Life Test (ALT) data given in Sr. #5 of Table 8.1 used as evidence 2.

9.4 Conclusions

LED families are made from different material systems (AlGaInP, GaN, GaAs etc.) and are manufactured using different semiconductor structures such as Double Heterostructure (DH) and Multi Quantum Well (MQW). Further, they may be driven in pulse mode or DC mode. The time to failure of the LED is significantly different based on the material, structure and the driving strategy. While ample prior published LED data is available, it is very difficult to get prior data for the exact same material system, structure and driving duty cycle. Using prior data, which is not directly relevant to the application, will cause over estimation or under estimation of the LED reliability. A 3-step solution is proposed which includes using a multiplier to convert from DC to pulse data, estimating the degree of relevance parameter R (engineering judgment and physics of semiconductor structures) and then modifying the Likelihood function in the Bayesian model with R. The results are presented in Table 9.1.

All the posterior predictive results in section 9.3 pass the Chi-square statistic test (described in detail in chapter 10). This test was used to determine how closely the ALT data represents the predictive Posterior PDF of LED TTF. It was interesting to observe that the Chi-square value was lower in all the 5 cases when R was appropriately chosen (compared to R=1). Since a lower value implies a better fit, the least we can say is that use of R produced better results in this application.

Chapter 10: Bayesian Parameter Selection and Model Validation

10.1 Bayesian Subjectivity

While the Baye's theorem itself has a sound statistical background, assumptions made in the prior knowledge and in the underlying distribution bring in subjectivity in Bayesian modeling. The subjective nature of the prior distribution (which could be based on relatively sparse expert opinion) may raise doubts about the accuracy of Bayesian posterior distributions. In the current research, Uniform prior distribution was used for α and β of the Weibull model. However, the limits for α and β in the uniform distribution had to be assumed. Further, prior published data transformed to application conditions was used as Evidence in the 1st Bayesian updating. Errors in assumptions made at the start of Bayesian analysis can result in the posterior distribution being a poor representation of the data. Accordingly, the posterior predictive distribution needs to be subject to some sort of validation [8].

10.2 Validation approach

Work by Mosleh et al [8] has been relied upon for formulating the validation approach in this dissertation. In statistical analysis, a model is often used to represent data. Since the entire population data is rarely available, the model is generally developed based on a small sample data (extracted randomly out of the population). Deviations between actual data and a model that describes the data well are subject to the Chi-Square distribution. This is based on the assumption that any deviations in

observed data from the expected value predicted by the underlying distribution are normally distributed. This assumption is generally sound, as many errors in observation are resultant from the summation of many other random variables, and hence are subject to the central limit theorem. By inference, if these variations are described by the Chi-Square distribution, then the model being tested is most likely a good one. The Bayesian Chi-Square statistic is a single measure that quantifies how well the posterior predictive distribution agrees with the data [8].

To calculate the Chi-Square statistic, the x – axis (for the random variable) is divided into K distinct intervals that contain at least 5 data points each from the sample. The number of data points in each interval I_j is written as b_j (j = 1 , 2, … , k). The intervals do not need to be of equal width. Then, with the model distribution being tested, the number of expected data occurrences in each interval is calculated:

$$e_j = n\, p_j \qquad \text{- (10.1)}$$

where e_j is the expected number of occurrences of data in interval I_j, n is the sample size and $p_j = \int_{I_j} f_1(x \mid \theta) dx$

The Bayesian Chi-Square statistic is then defined as

$$\chi_0^2 = \sum_{j=1}^{k} \frac{(b_j - e_j)^2}{e_j} \sim \chi_{k-1}^2 \qquad \text{- (10.2)}$$

This value summarizes the magnitude of natural variations between observed data and the model being tested. Note that the expected value is used in the denominator in place of the variance in the definition of the Chi-Square random variable. This is because we do not know the variance of the data from model expected values. To

accommodate this lack of knowledge, we reduce the number of degrees of freedom by 1, so the Chi-Square statistic above should be described by the Chi-Square distribution with $k - 1$ degrees of freedom.

For model validation, a 'significance level' is introduced. The significance level, α (unrelated to the scale parameter of the Weibull distribution which uses the same symbol), is defined as the probability of data analysis returning a result at most as extreme as the calculated value for which the decision maker is willing to accept the null hypothesis. Generally, α is in the range of 1 – 10 %. One way of hypothesis testing is to calculate the upper limit 'c' of the Chi-Square statistic based on the significance level.

i.e. $$\Pr\left(\chi^2_{K-1} \le c\right) = 1 - \alpha \qquad \text{- (10.3)}$$

This means that if the Chi-Square statistic exceeds *c*, then the null hypothesis is rejected.

10.3 Validation phases in Bayesian modeling

Validation of Bayesian modeling occurs in various phases. These are

1. Selection of the distribution for the underlying failure distribution,
2. Suitability of the prior information and
3. Appropriateness of predictive posterior distribution against the test data.

10.3.1 Selection of underlying failure distribution

Many of the LED degradation mechanisms occur the same test parameter range. The dominant failure mechanism leads to failure. This leads us to believe that Weibull

distribution (with parameters α & β) is the most suitable distribution for time to failure of the LEDs. Levada et al. [34] carried out accelerated life tests on plastic transparent encapsulation and pure metallic package GaN LEDs. A consistent Weibull based statistical model was found for MTTF thereby giving credibility to our approach.

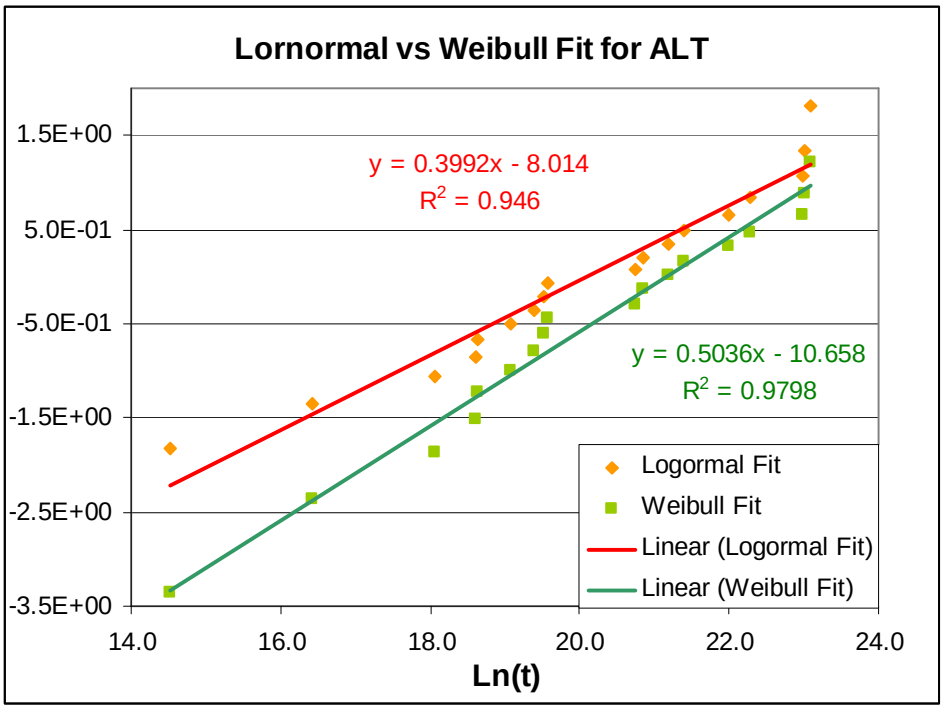

Fig 10.1 Lognormal vs. Weibull fit of ALT data

When the data from ALT performed in this research was analyzed, it revealed that Weibull is a slightly better fit compared to the Lognormal fit. See Fig 10.1. Thus the degradation mechanism of LEDs, published data and our ALT data all point to Weibull as the most suitable model for this data analysis.

10.3.2 Selection and verification of prior distribution

Uniform distribution was used as prior knowledge of parameters α and β of the Weibull model. The limits for α and β in the uniform distribution were selected such that they encompass the prior published data and the normalized life test data. In order to verify that the limits were selected correctly, an additional calculation was performed with the upper limits of α and β widened. See Table 10.1 and Fig 10.2. There was no difference in the predictive posterior CDF for LED time to failure. α stayed the same at 1.35E9. β changed slightly from 0.809 to 0.808. This proves that the limits on α and β in the uniform distribution were correctly chosen.

Property	**Used limits for prior of α and β**	**Wider limits for prior of α and β**
Samples	1 to 1E10, Total 800	1 to 1E10, Total 800
Prior	Uniform	Uniform
Alpha	5E7 to 9E9, Incr 5E6	5E6 to 9E10, Incr 5E6
Beta	0.1 to 2, Incr 0.1	0.1 to 4, Incr 0.1
Evidence Source	AlGaInP-MQW-DCx1451	AlGaInP-MQW-DCx1451
Evidence data	n=11, r=11, tc=4.829E+9	n=11, r=11, tc=4.829E+9
Alpha	1.13E+9	1.13E+9
Beta	0.89	0.89
Predictive Posterior		
Alpha	1.35E+09	1.35E+09
Beta	0.809	0.808

Table 10.1 Used vs. wider limits on prior of α and β

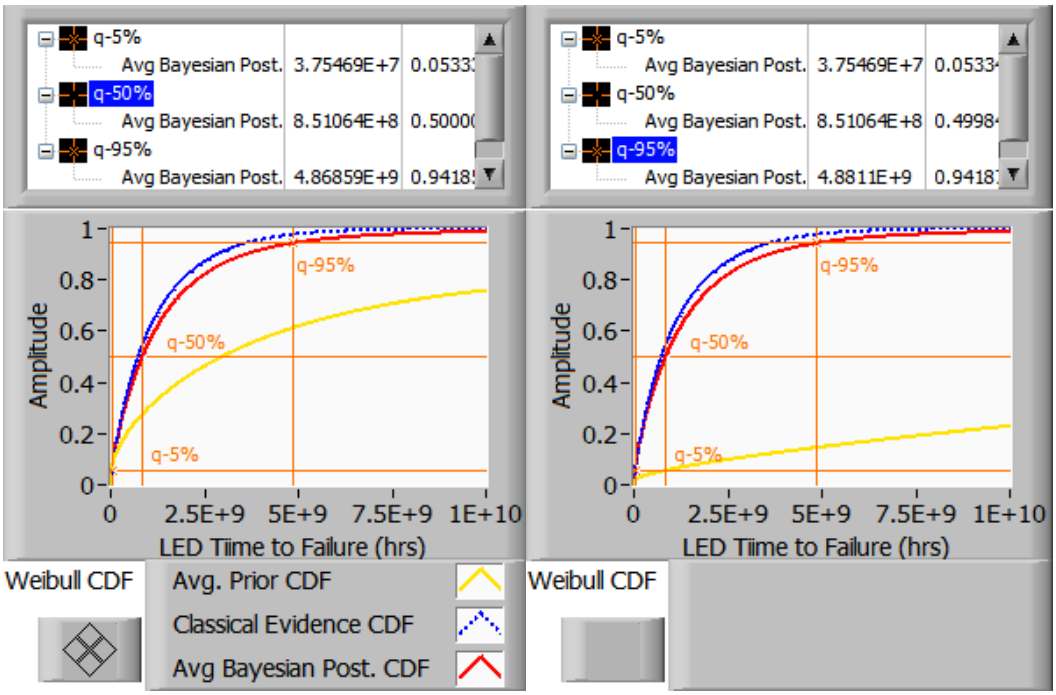

Fig 10.2 LED TTF with used vs. wider prior limits on α and β.
"Amplitude" refers to the magnitude of the cumulative distribution function.

10.3.3 Appropriateness of Predictive posterior distribution to test data

Validation approach using the Chi-square statistic as described in section 10.2 was used in order to check the appropriateness of predictive posterior distribution to the test data. Uniform distribution was used as the Prior for α and β as described in section 10.3.2. Prior published data for various LED materials, structure and driving (dc transformed in to pulse) was used as evidence for the 1st Bayesian updating. The 2nd Bayesian updating is done using ALT as evidence. See sections 8.3.2, 8.3.3, 9.2 and 9.3 for details. As described in section 9.3 and Appendix 8, Predictive Posterior distributions for LED TTF were computed by Evidence 1 taken from:

Set2: AlGaInP-MQW-DCx500

Set3: AlGaInP-MQW-DCx1451

Set2: GaN-MQW-DCx500

Set3: GaN-MQW-DCx1451

Set2: AlGaInP-DH-DCx500

Set3: AlGaInP-DH-DCx1451

The result of predictive posterior distribution for LED TTF is hypothesized as the population TTF. Using ALT as Test data (n=18, k=3), Chi-square statistic was computed as shown in Table 10.2.

Prior: Uniform	**Evid1: AlGaInP-MQW-DCx500**	**Evid2: ALT**	**Posterior->**	**Alpha**	**Beta**	**n**
				1.17E+09	0.547	18
Interval j	Lower Limit Xl	Upper Limit Xu	**pj**	**ej = npj**	**bj**	**(bj-ej)**2/ej**
1	0	2.00E+08	0.3165	5.70	6	0.016
2	2.00E+08	1.80E+09	0.4015	7.23	6	0.208
3	1.80E+09	8	0.2820	5.08	6	0.168
			1.0000		Chi-Statistic	**0.392**

Table 10.2 Computation of Chi-square statistic

Using the significance level of 10% and degrees of freedom as 2 (k-1), the c value is computed as 4.6. Since the chi-square statistic (0.392) is less than the ‘c’ value (4.6), the predictive posterior distribution (using Evidence 1 AlGaInP-MQW-DCx500) is an acceptable distribution to represent ALT data.

Taking a similar approach for the other data sets for Evidence1, Table 9.1 (included in chapter 9 and repeated in Appendix 8) was constructed. It can be seen that all of the data sets used for Evidence1 give an acceptable predictive posterior distribution. This means that the ALT data can be assumed as coming from a population

represented by the predictive posterior distributions predicted by various sources for Evidence 1.

Chapter 11: Conclusion

11.1 Summary

In a medical diagnostic application, the precise value of light intensity is used to interpret patient results for medical diagnostics. Hence understanding LED failure modes is very important. Failure Modes and Effects Criticality Analysis (FMECA) tool was used to identify critical LED failure modes. The next steps were Accelerated Life Testing (ALT), Accelerated Degradation Testing (ADT) and Bayesian analysis. ALT/ADT was performed on the LEDs by driving them in pulse mode at higher current density J and elevated temperature T. Inverse Power Law model with J as the accelerating agent and the Arrhenius model with T as the accelerating agent were used. The optical degradation during ALT was found to be logarithmic and this property was used for the degradation analysis using a log-linear degradation model. Further, the LED bandgap temporarily shifts towards the longer wavelength at high current. This shift was dependent on junction temperature. Empirical coefficients for Varshini's equation were determined.

The Bayesian analysis starting point was to identify pertinent published data which may be used for developing the prior information. From the published data, the time required for the optical power output to degrade by 20 percent was extracted LEDS with different active layers (AlGaInP, GaN, AlGaAs), different LED structures (DH, MQW) and bias conditions (DC, Pulsed). The degradation mechanism of LEDs, published literature and our ALT data all indicate that Weibull is the most suitable

model for this data analysis. This rationale was used to develop the Weibull based Bayesian likelihood function. For the first Bayesian updating, Uniform distribution was used as the Prior for α-β parameters of the Weibull model. Prior published data was used as Evidence to get the first posterior joint α-β distribution. For the second Bayesian updating, ALT data was used as Evidence to get the second posterior joint α-β distribution. This joint α-β distribution gave a series of Weibull time to failure distributions. The predictive posterior failure distribution for the LEDs was estimated by averaging over the range of α-β values. Lastly, a new parameter 'R' (degree of relevance) is used to transform partially relevant prior published data for use in Bayesian modeling.

Prior published data, the present ALT data, ADT analysis and Bayesian analysis indicate that the MTTF of AlGaInP-MQW LEDs when used in this specific medical application (pulse mode, on time 100us with 0.2% duty cycle, temperature = 35°C and current density = 21.6Amps/cm^2) is in excess of 1E8 hrs. This exceeds the warranty life of the medical diagnostic instrument by orders of magnitude and as such the LED is suitable for this application. The shape parameter β of the Weibull model is less than 1 in all cases indicating a decreasing failure rate. This may be explained by the observed logarithmic optical degradation of the present work. The initial high failure rate may be due to manufacturing defects, which were not properly screened, and hence the surviving population would be able to achieve a long life, since probability of surviving increases after the initial degradation.

11.2 Objectives and Accomplishments

The goal of this research was to deepen our understanding of AlGaInP LED performance over time for impulse currents (medical application), uncover unique failure mechanisms and generate a model of time to failure. Work carried out during this study resulted in the publication of three research papers and one poster presentation. The following are the answers to the questions we started with:

1. Will the LED intensity remain within acceptable limits? Yes it does.
2. Will the LED wavelength remain stable? Yes, if the junction temperature is maintained. Spectral shift investigation was performed during this research.
3. Will the Time to Failure of LEDs exceed the Life of the Medical Instrument? Yes, the LEDs will outlast the 7-year life of the medical instrument by orders of magnitude.
4. Will there be a cost benefit of using LEDs vs traditional light sources (flash lamps etc)? Traditional lamps have to be replaced every 3-6 months causing a major inconvenience to the customer. Use of LEDs will eliminate this replacement saving time and money needed for maintenance.
5. Will there be any critical failure modes for the medical application? A Failure Modes Effects and Criticality was performed for identifying critical failure modes which were found to be encapsulation degradation and active layer degradation. Even a worst case situation would only cause an unscheduled calibration of the medical instrument, which would delay medical test results.

In addition to meeting the stated objectives, extra work was carried out for using partially relevant prior data. A new parameter 'R' (degree of relevance) is used to control the influence of evidence (by adjusting the Likelihood function) in Bayesian modeling.

11.3 Research contribution and Significance

This Thesis represents the first measurements of AlGaInP LED reliability for the medical diagnostic application. This research will allow replacement of traditional light sources (filament or flash lamps) with LEDs. The lamps degrade and have to be replaced 3-6 months causing a major inconvenience to the customer whereas LEDs will outlast the 7-year life of the medical diagnostic instrument.

This research has produced significant contributions in the failure physics and analysis of LEDs for medical applications. We were able to combine the traditional ALT/ADT approach with FMECA and Bayesian analysis and hence have shown that this methodology is valid for such complex situations.

The research represents a new contribution to LED reliability for significantly different bias conditions. Our research used pulse driving with a very low duty cycle, and the failures were induced by the magnitude of the peak current. We have reported a decreasing failure rate β from the Weibull TTF model, through a unique combination of prior published data, ALT and Bayesian analysis. The cause was attributed to the observed optical degradation, which followed a logarithmic function with high degradation in the initial period.

We have reported that bandgap shift due to thermal effects can degrade the power output which may give an erroneous indication of “failure”. Upon returning to nominal junction temperature most of the wavelength shift is recoverable. The bandgap shifts toward longer wavelengths, but additional work must be carried out in order to understand this specific mechanism as well as the initial logarithmic degradation. Since the spectral performance is critical for the medical application, my spectral shift investigation will provide immense value to the designer. The junction temperature will need to be maintained.

11.4 Future Research

11.4.1 ALT at different duty cycles

LED life testing in prior published articles is done under DC conditions. Very few articles are available for pulse testing. Per the need of the medical application, ALT performed in this research was performed at very low duty cycles (0.2%). Performing ALT is difficult and time consuming. Since each experiment takes as high as 6 months, we could only perform ALT at the required low duty cycle conditions. It would be helpful to perform ALT at various duty cycles and estimate LED lifetime as a function of duty cycle. This would allow a designer to choose the correct duty cycle to maximize the reliability while meeting the LED application requirements.

11.4.2 Use of a Utility Function while estimating R

Insufficient data is a very common problem in Reliability studies. The conditions of prior published data rarely match application conditions. In Chapter 9, the concept of degree of relevance of prior published data was discussed. A 3-step approach is

proposed which includes using a multiplier to convert from DC to pulse data, estimating the degree of relevance parameter R and then modifying the Likelihood function in the Bayesian model with R. The three steps should be subjected to further scrutiny. Refinements may need to be carried out for use in applications other than LED reliability. One possible refinement is use of a Utility function while estimating R. This would allow a parametric relationship between individual relevance parameters for material (Rm), Structure (Rs) and Driving conditions (Rd) and the estimated R.

11.4.3 Other methods of using degree of Relevance 'R'

In addition to modifying the likelihood function by R, other methods of using 'R' should be studied. A common method is a Weighted posterior approach, which however was not considered during this research. An approach that we did consider (but which needs further development) is transforming the uncertain evidence itself based on the value of R. The purpose of transformation is to move the evidence data towards a Uniform distribution as R approaches 0. The transformed data when used as Evidence during Bayesian updating will make the computations much easier.

Boundary conditions for the data transformation are as follows:

If R=0. Transform the data in to 'Uniform distribution'

If R=1, Transformed data is identical to the original data

For $0 < R < 1$, move the PDF of the partially relevant data towards a Uniform distribution as R approaches 0.

During the Transformation of data, it is necessary to make

Mean of transformed data = M = Mean of ALT/Application data

If ti (t1, t2,…,tn) is a set of n partially relevant time to failure of LEDs, the transformed data set ti' is given by

$t_i' = [(2i-1)M/n]^{1-R} t_i^R$ - (11.1)

Again, the boundary conditions are

If R=0, $t_i' = [(2i-1)M/n]$ with Average = M

If R=1, $t_i' = t_i$

11.4.4 Failure Analysis

Additional failure analysis including microscopy is necessary in order to understand the role of dislocations and other defects in causing the initial decrease in power output. The diode surface can be analyzed through atomic force microscopy in order to understand the role of surface roughness in decreasing light output. The analysis should be designed so that one may differentiate between latent defects and manufactured in defects. Additional research should be carried out which goes beyond the surface of the die and into the interior of the die in order to totally characterize the physics of failure.

Appendix-1: Laboratory for LED Reliability Testing

Photos of laboratory test setup developed for LED reliability testing

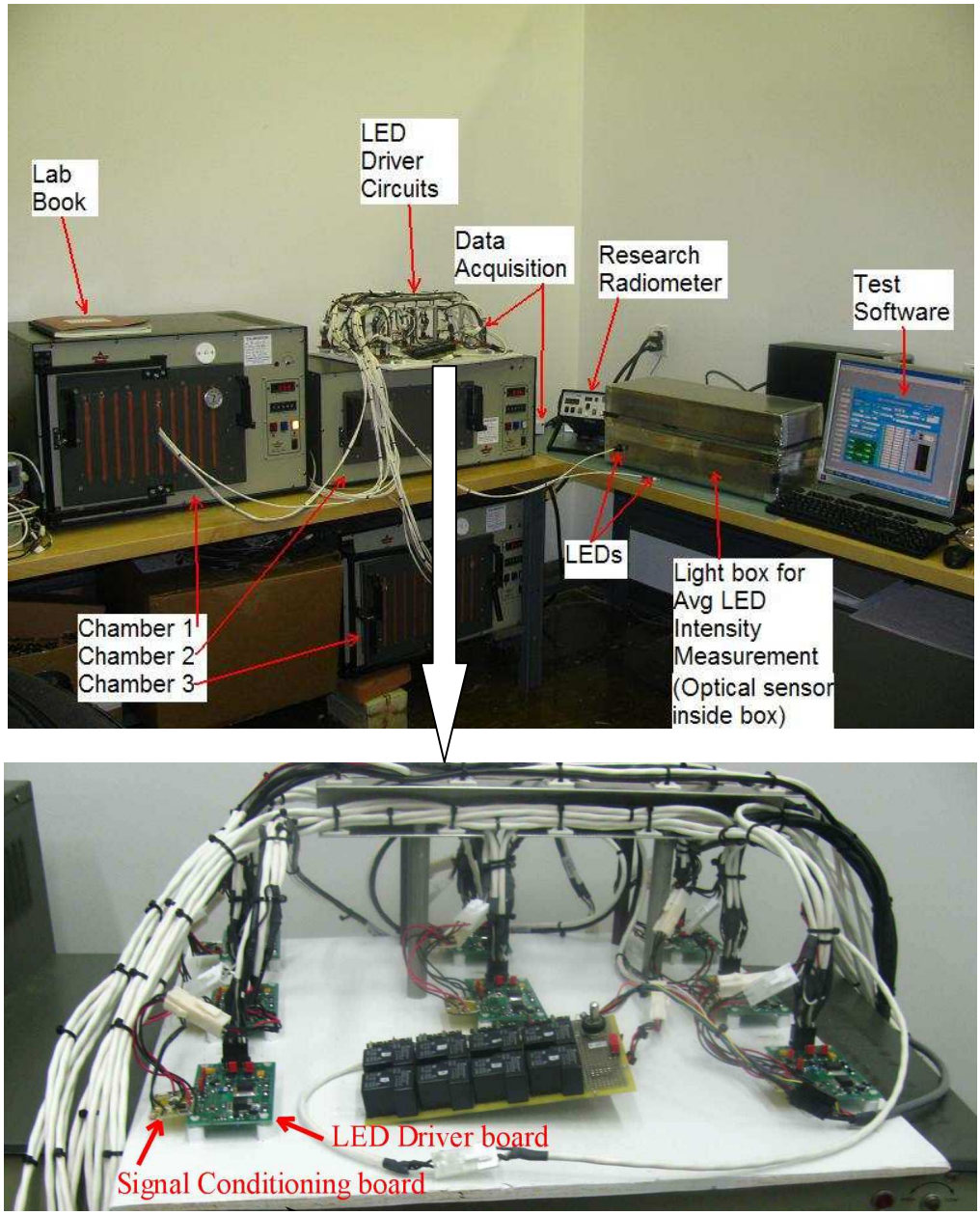

Fig A1.1 Laboratory photos of LED ALT setup

Appendix-2: Circuit Schematics for LED ALT

Wiring diagrams for LED ALT were used to connect the National Instruments Data acquisition board (PCI6025E) to the LED driver circuit, Signal conditioning circuit and the International Light Spectro-Radiometer (RPS900-R).

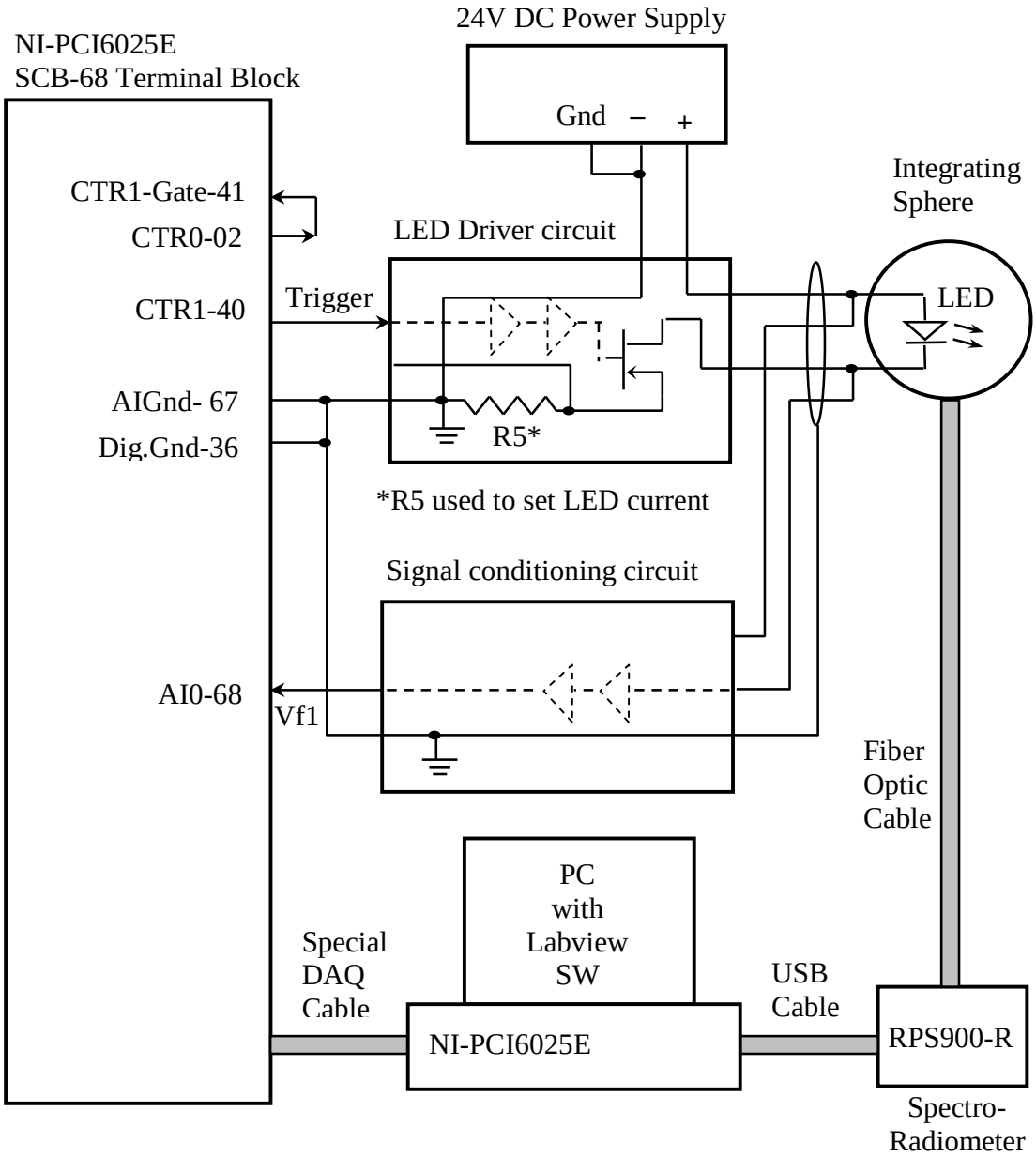

Fig A2.1 Circuit diagram for LED ALT setup

Appendix-3: Circuit diagram for Vf Signal conditioning

The following circuit was designed for this research. It measures the LED forward voltage while being driven in pulse mode. In the LED driver circuit, the cathode of the LED is pulled low to turn it on. For Vf measurement, this is fed to the op-amp (high input impedance) which controls the current through the current source at the output. This current source develops a voltage across the output resistor in proportion to the Vf swing. This Vf is measured by the data acquisition card. NI-PCI6025E.

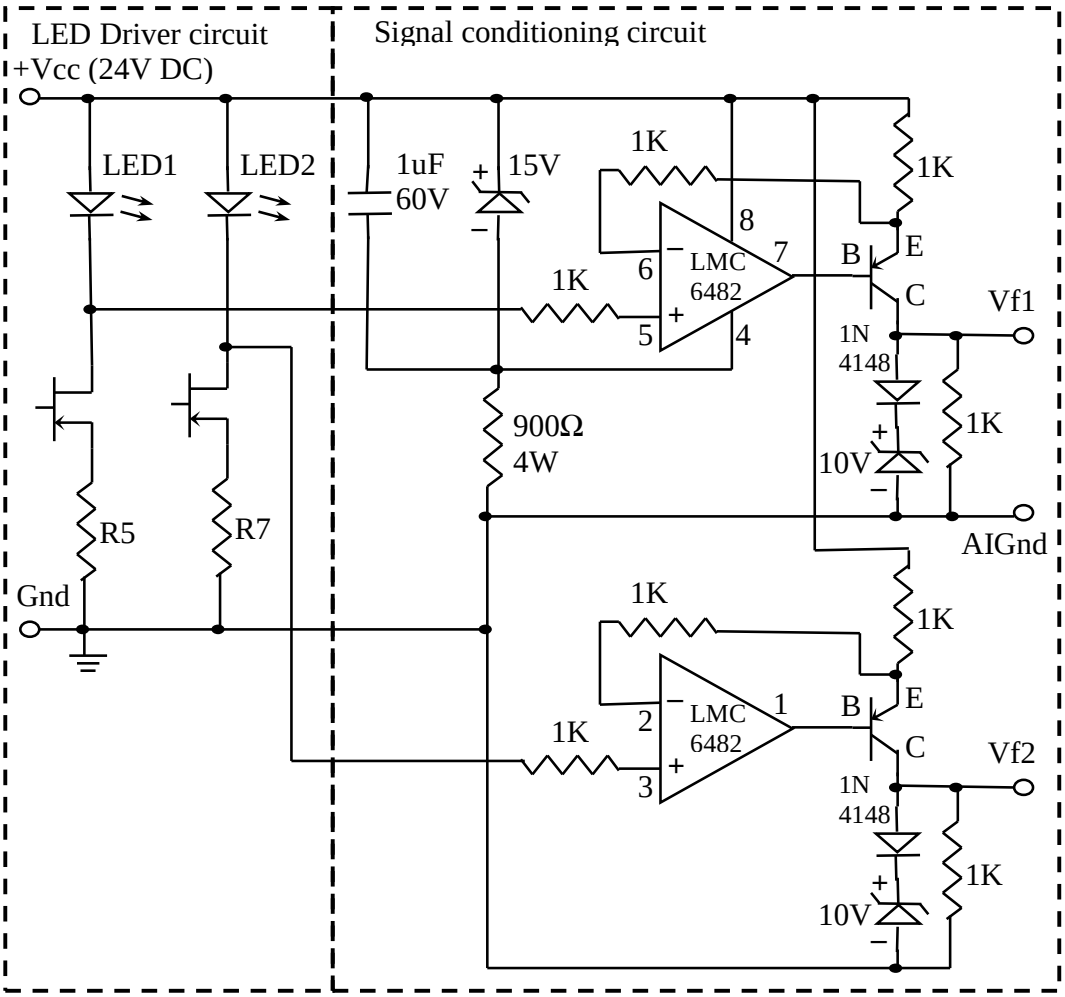

Fig A3.1 Circuit diagram for Vf Signal conditioning

Appendix-4: Photos of LED during ALT

The following LED photos were taken during the ALT.

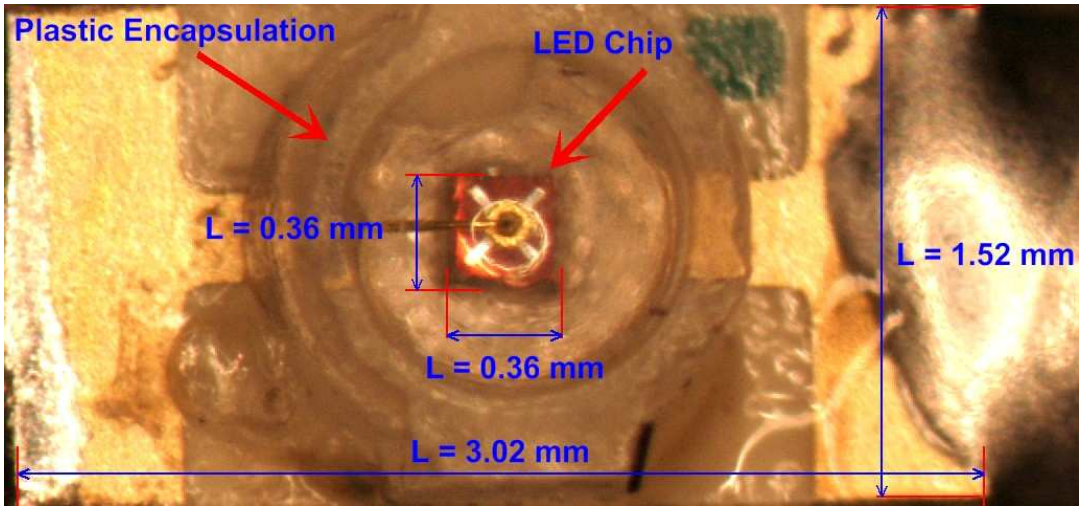

Fig A4.1 AlGaInP MQW SMD LED used in this research

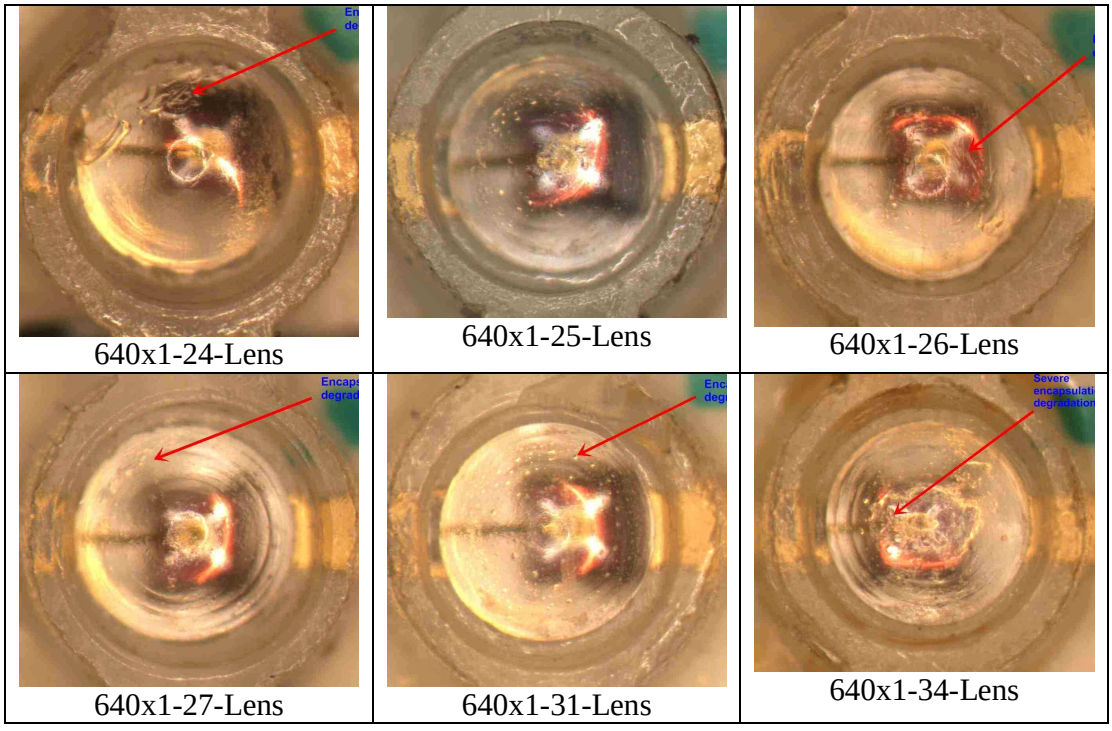

Fig A4.2 LED Photos from ALT Batch 2

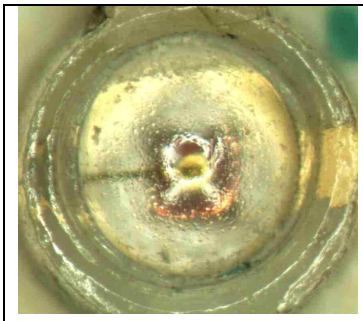 640x1-41-Lens	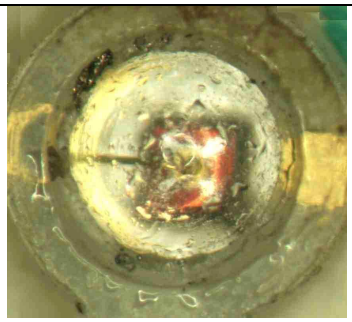 640x1-43-Lens	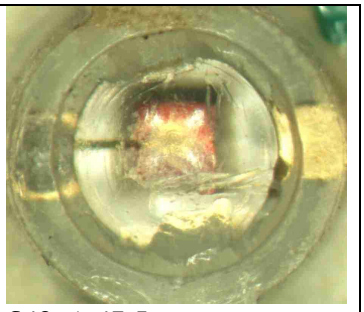 640x1-45-Lens
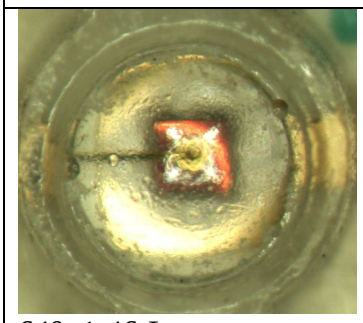 640x1-46-Lens	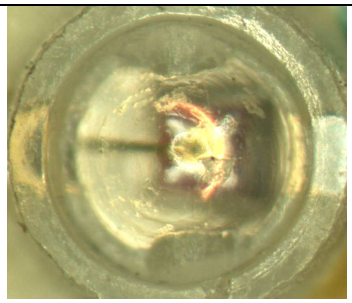 640x1-48-Lens	

Fig A4.3 LED Photos from ALT Batch 3

Appendix-5: Labview program for ALT

The following Labview program has been written exclusively for performing the Accelerated Life Test during this research. The labview programming language has been developed by National Instruments. Refer to http://www.ni.com/labview for details.

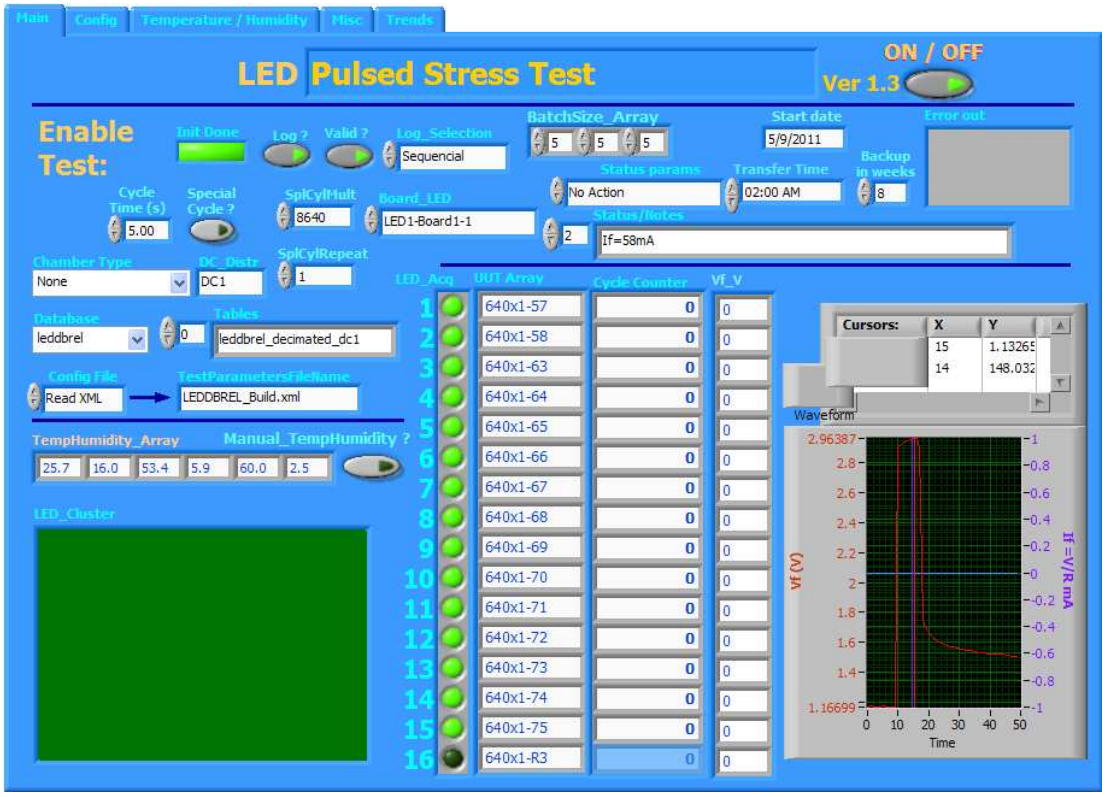

Fig A5.1 Front Panel of labview program for ALT

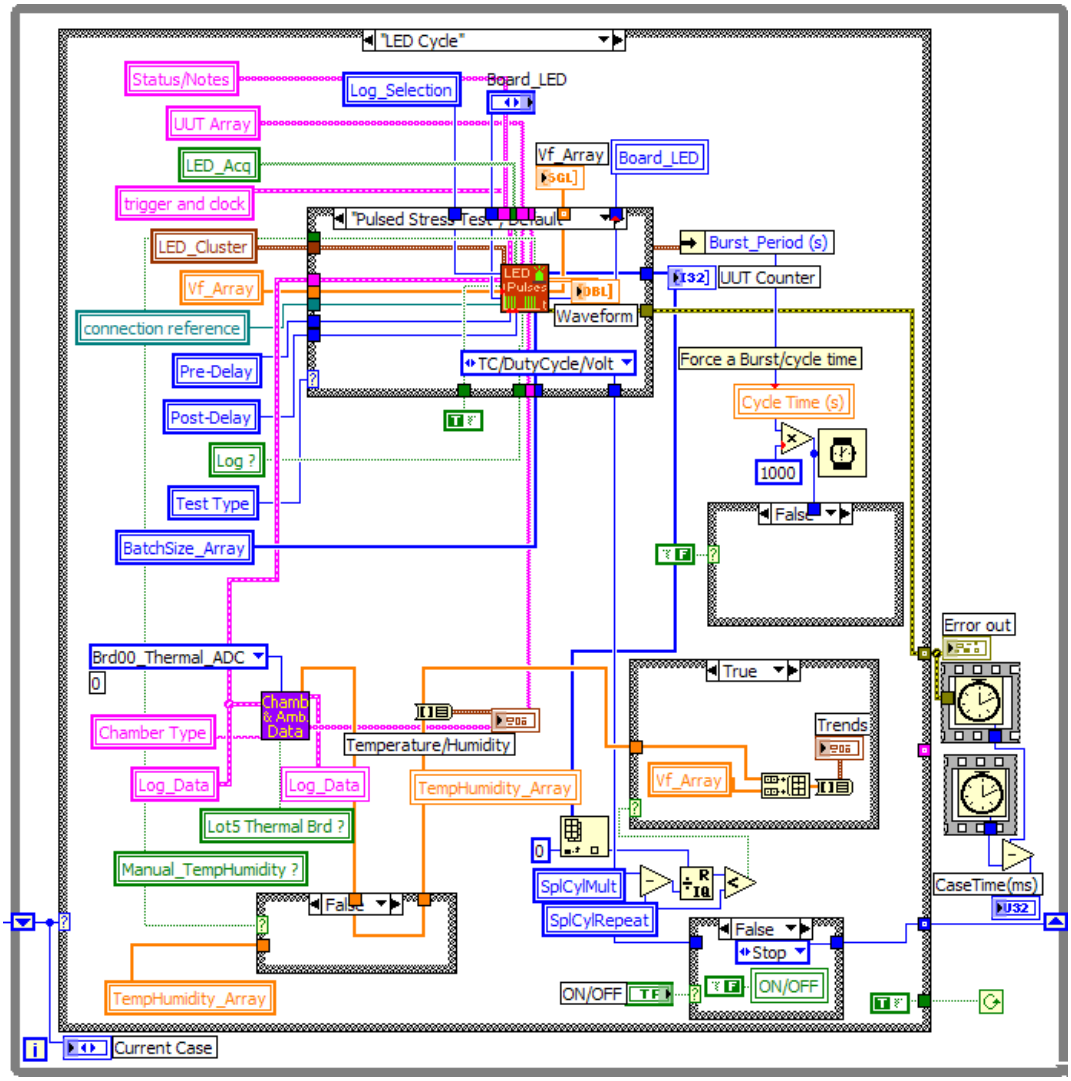

Fig A5.2 Block diagram of main labview program for ALT

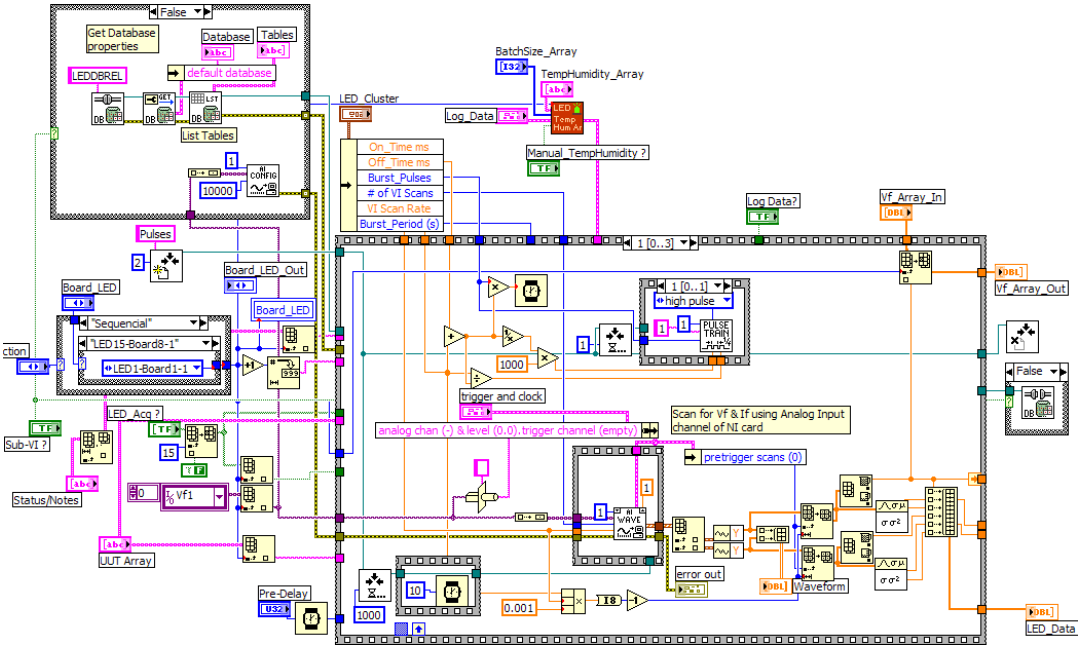

Fig A5.3 Block diagram of low level labview program for ALT

Appendix-6: Labview Program for Bayesian Modeling

The following Labview program has been written by us exclusively for the Bayesian modeling performed during this study. The labview programming language has been developed by National Instruments. Refer to http://www.ni.com/labview for details

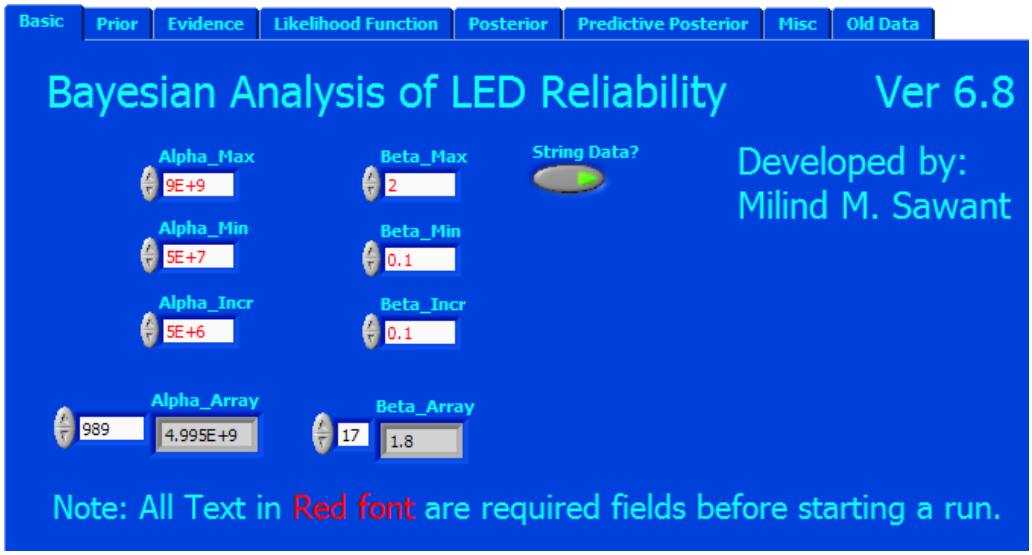

Fig A6.1 Front Panel Page 1 of labview program for Weibull Bayesian Analysis

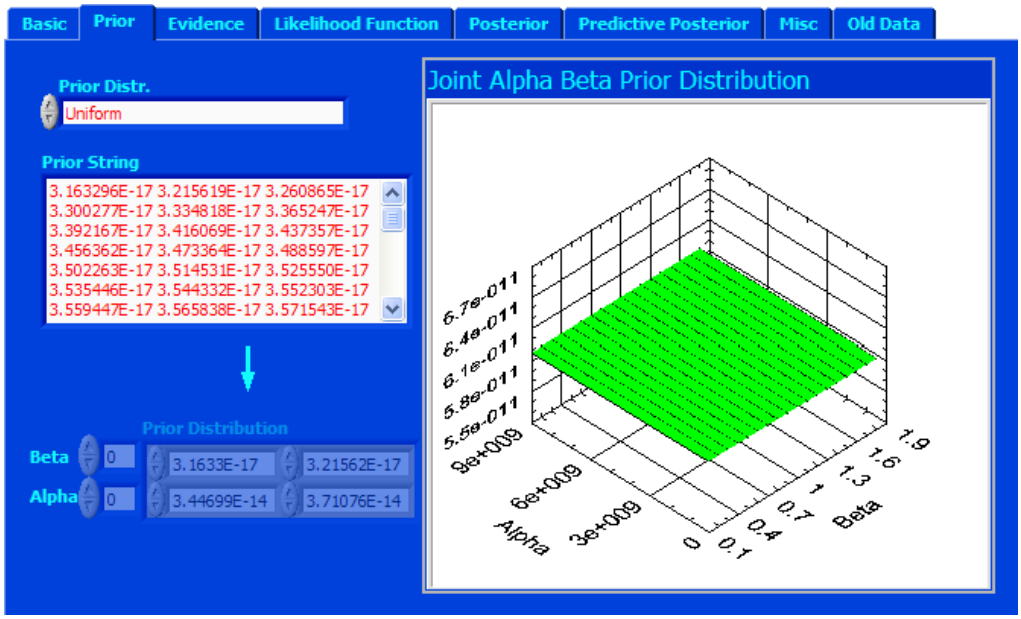

Fig A6.2 Front Panel Page 2 of labview program for Weibull Bayesian Analysis

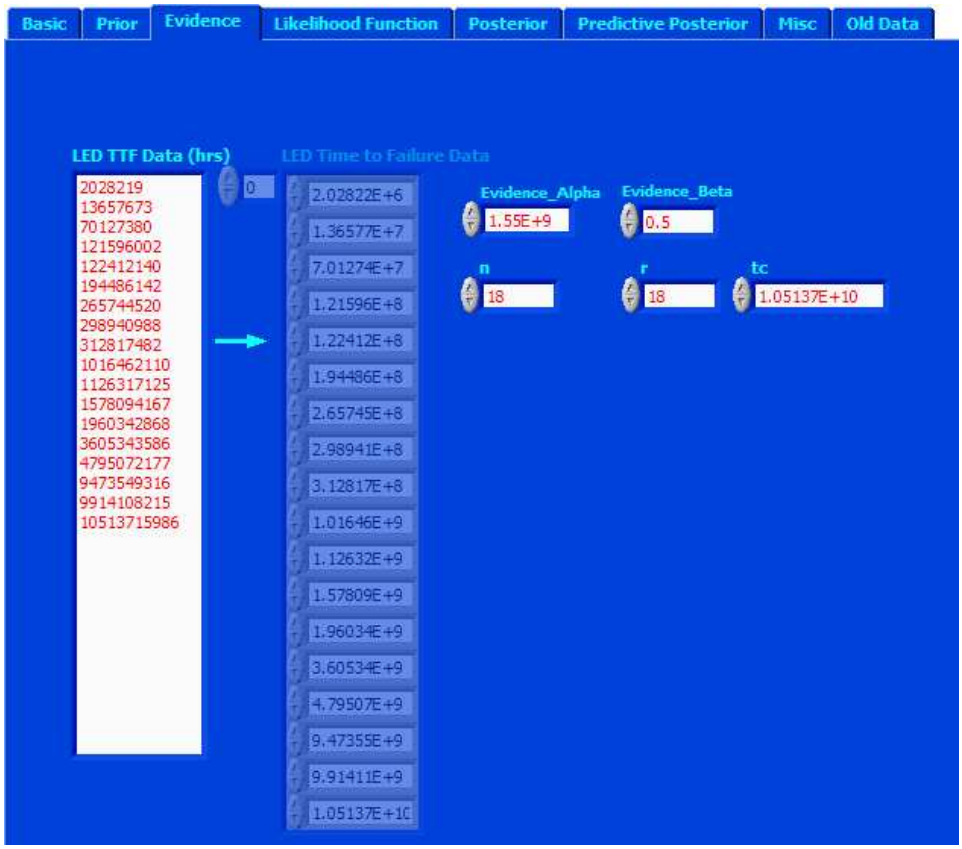

Fig A6.3 Front Panel Page 3 of labview program for Weibull Bayesian Analysis

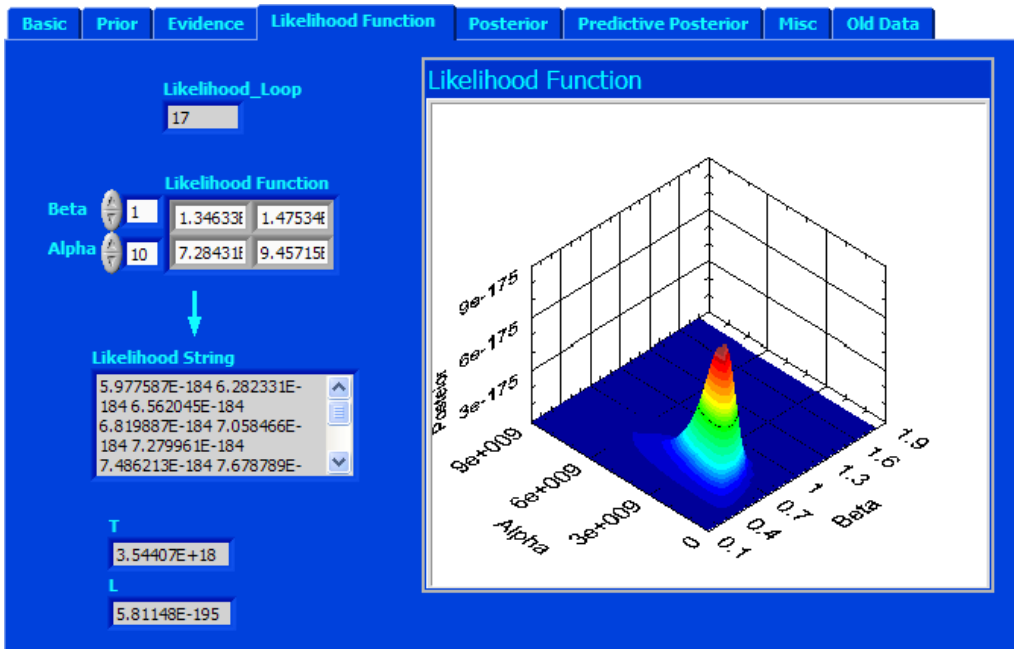

Fig A6.4 Front Panel Page 4 of labview program for Weibull Bayesian Analysis

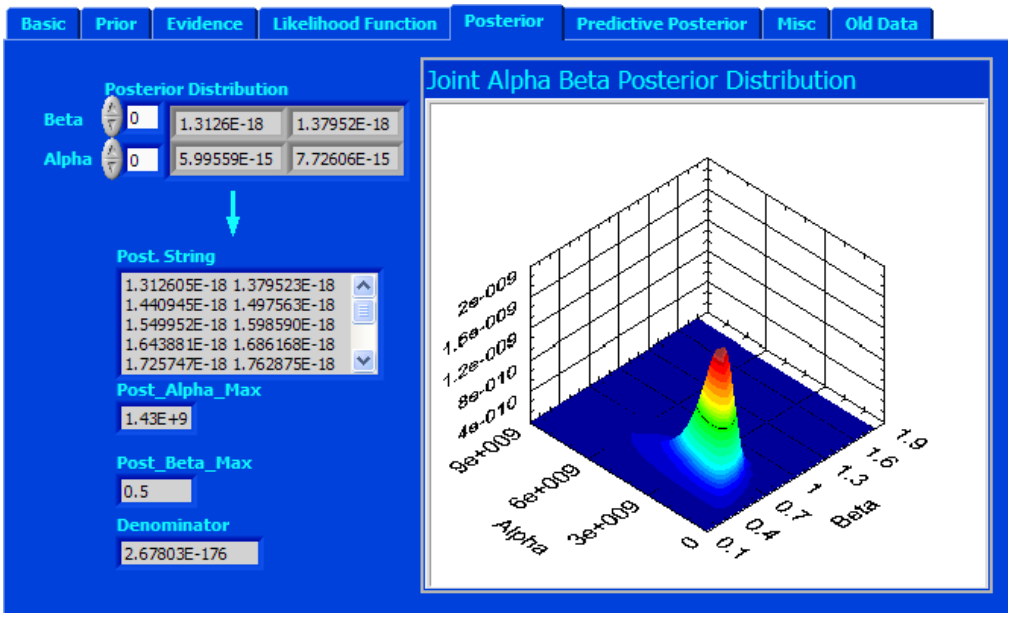

Fig A6.5 Front Panel Page 5 of labview program for Weibull Bayesian Analysis

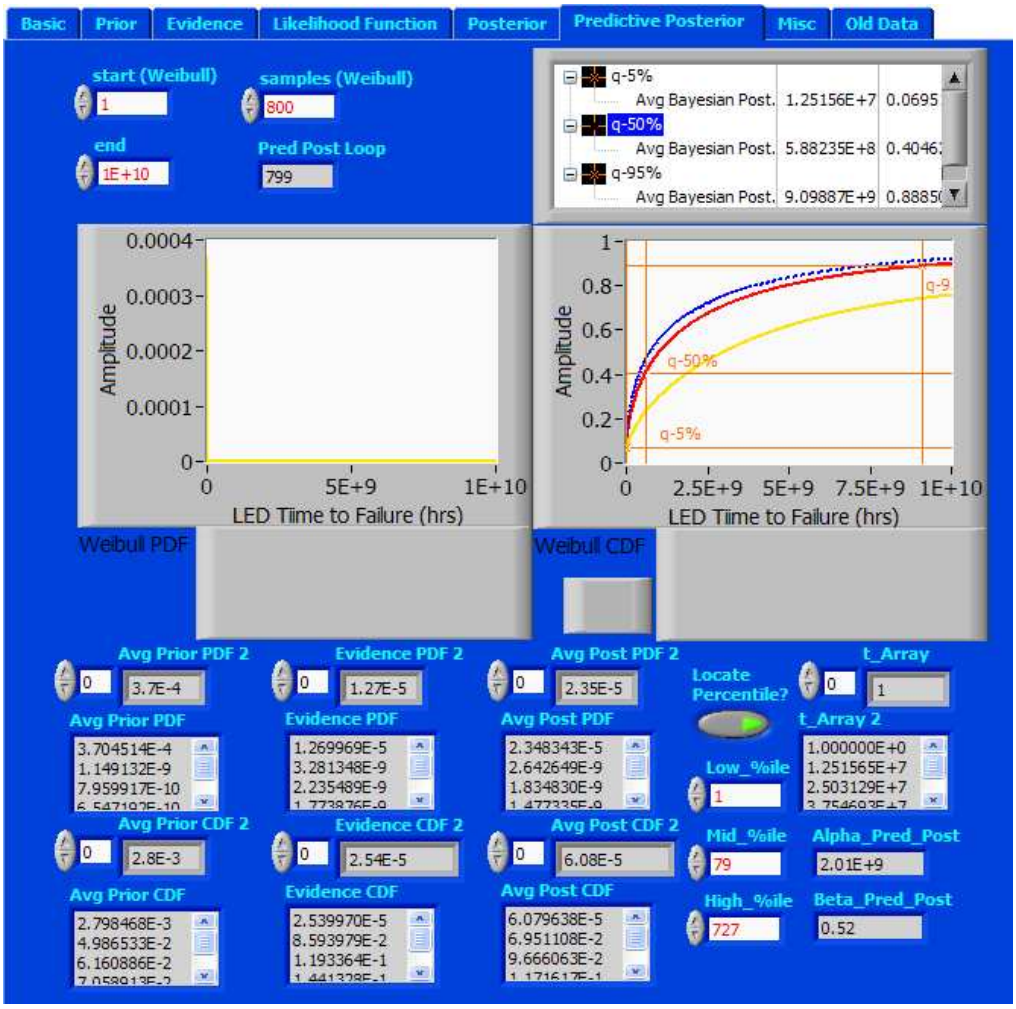

Fig A6.6 Front Panel Page 6 of labview program for Weibull Bayesian Analysis

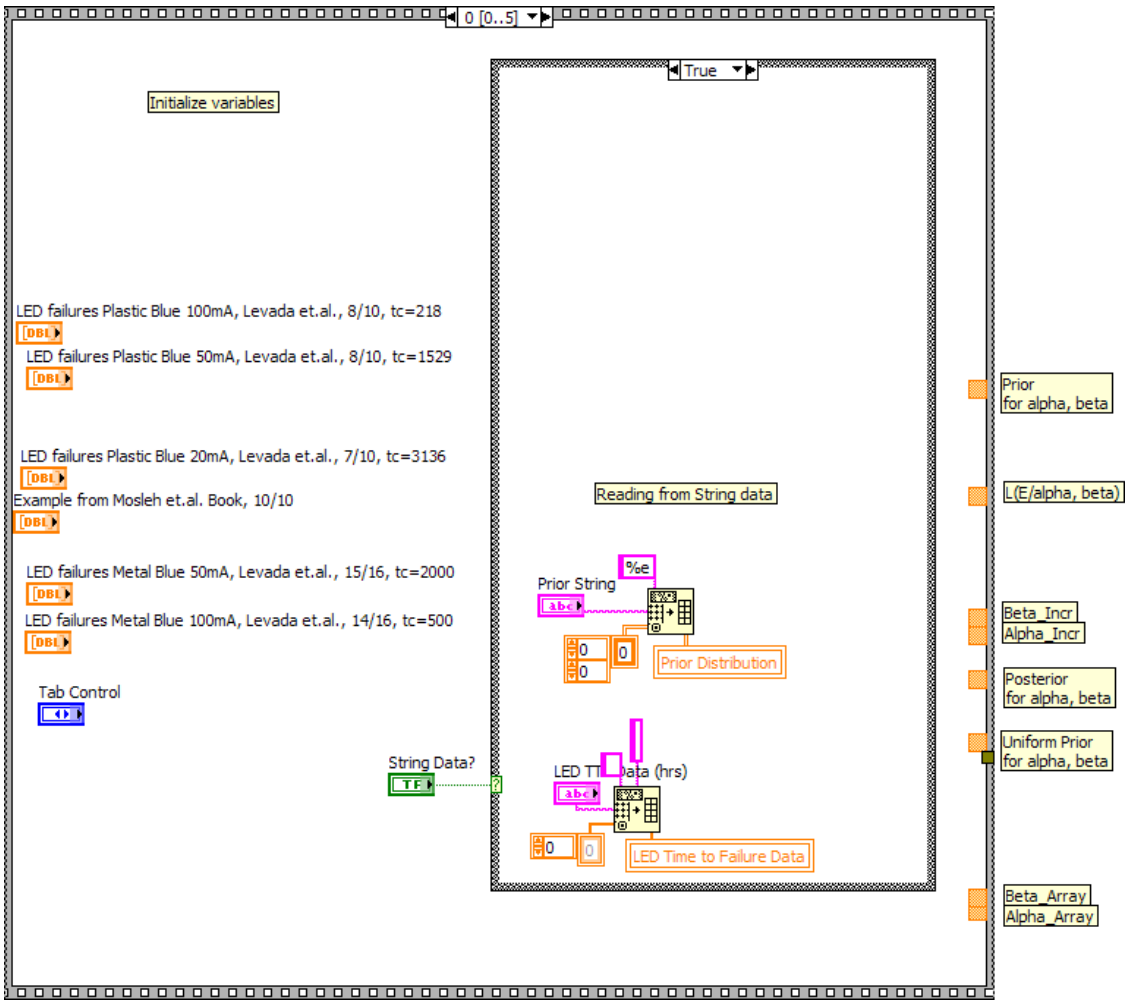

Fig A6.7 Block diagram Page 1 of labview program for Weibull Bayesian Analysis

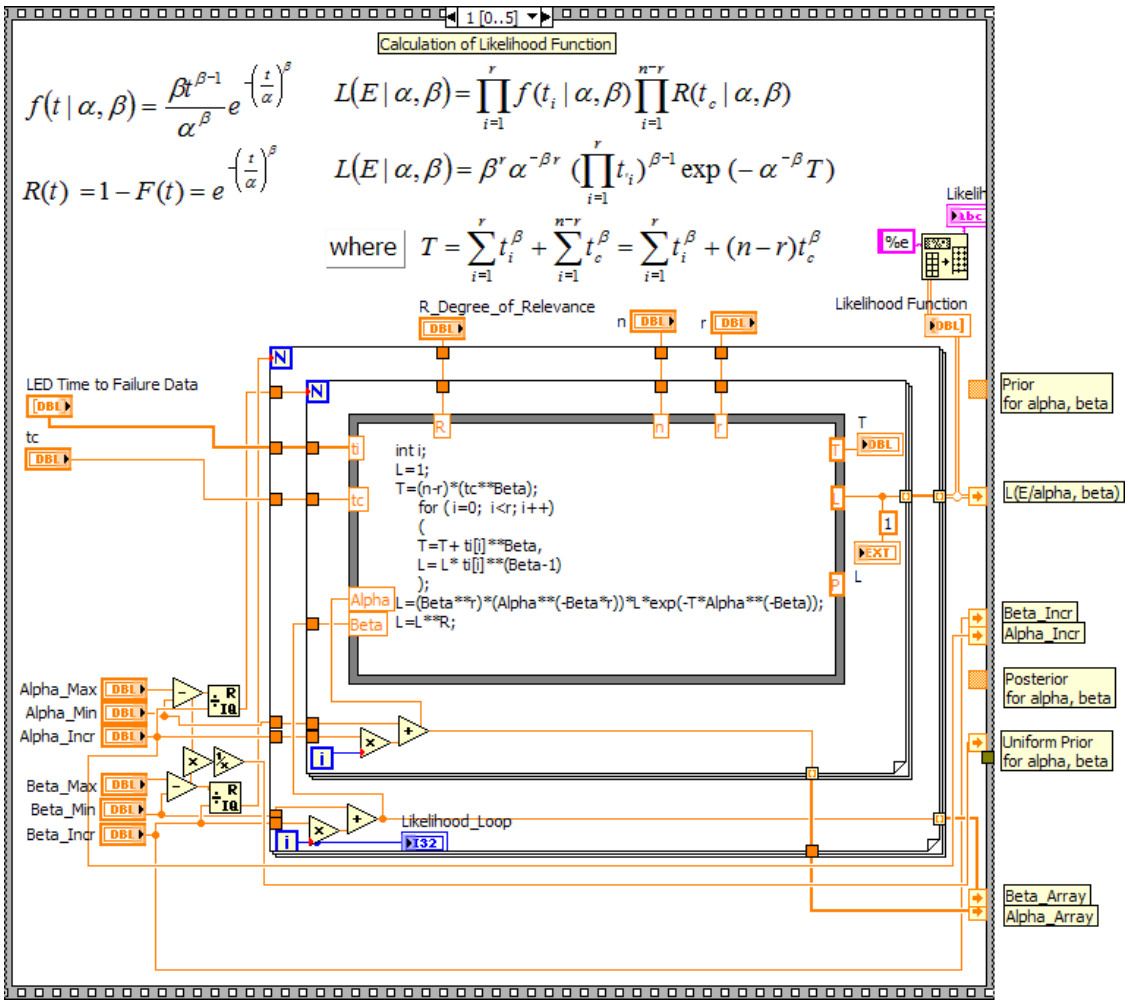

Fig A6.8 Block diagram Page 2 of labview program for Weibull Bayesian Analysis

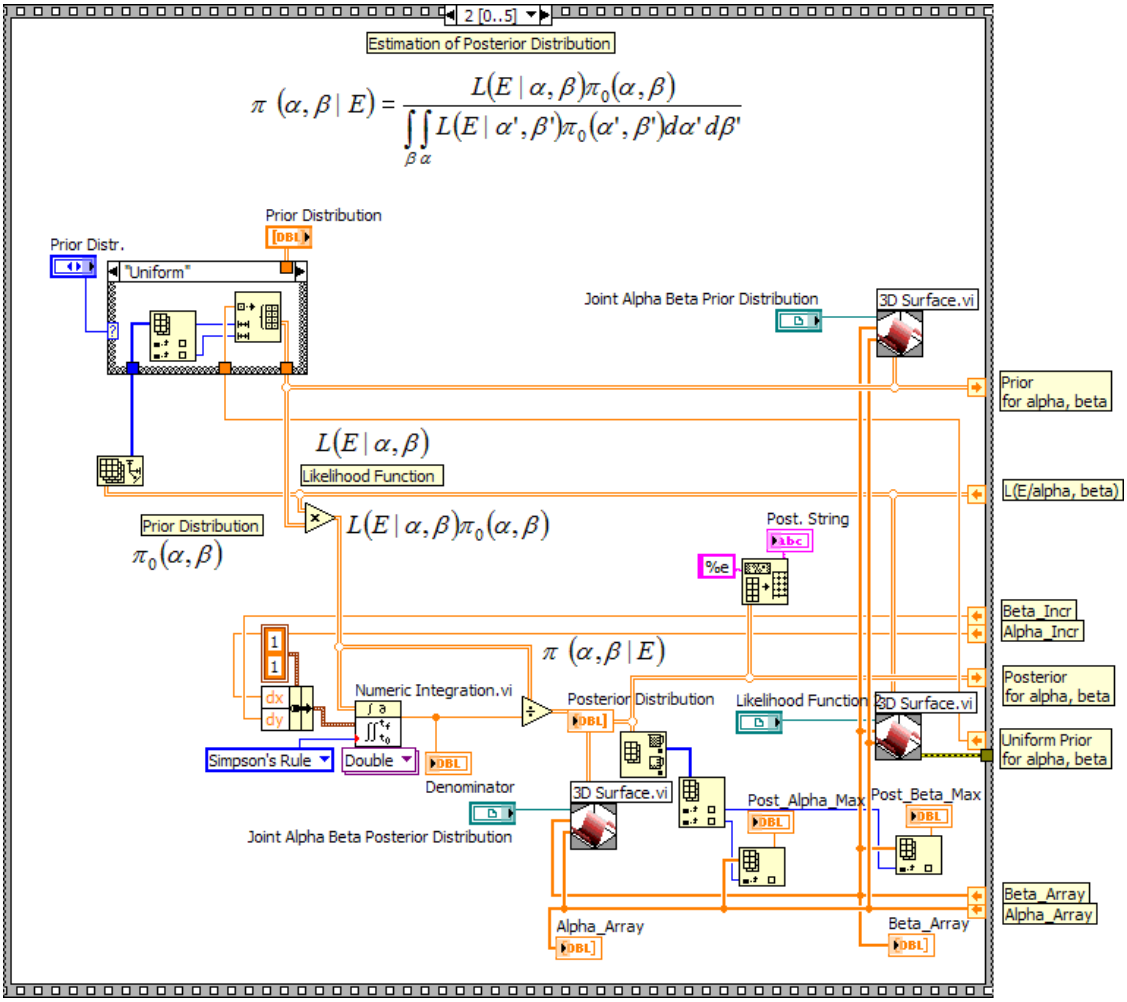

Fig A6.9 Block diagram Page 3 of labview program for Weibull Bayesian Analysis

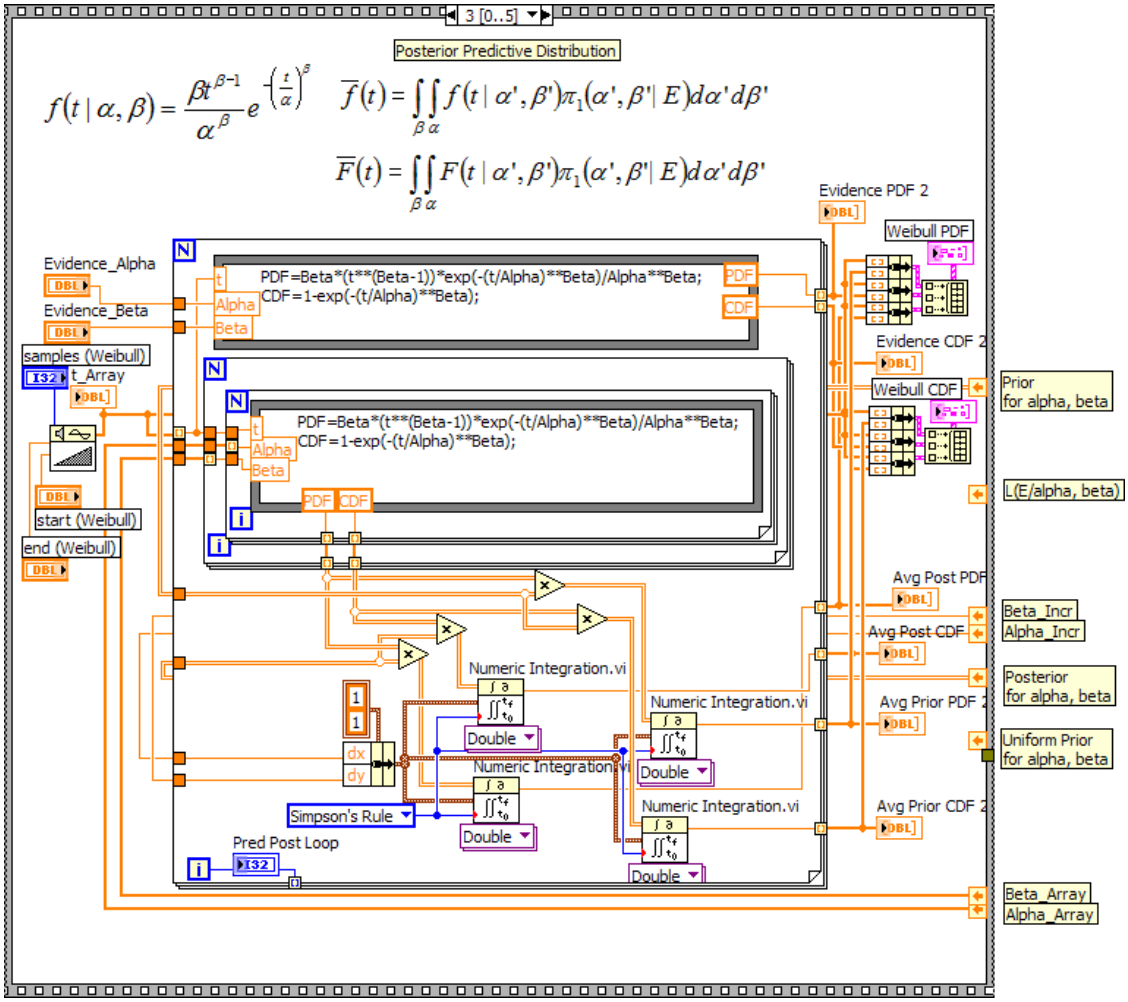

Fig A6.10 Block diagram Page 4 of labview program for Weibull Bayesian Analysis

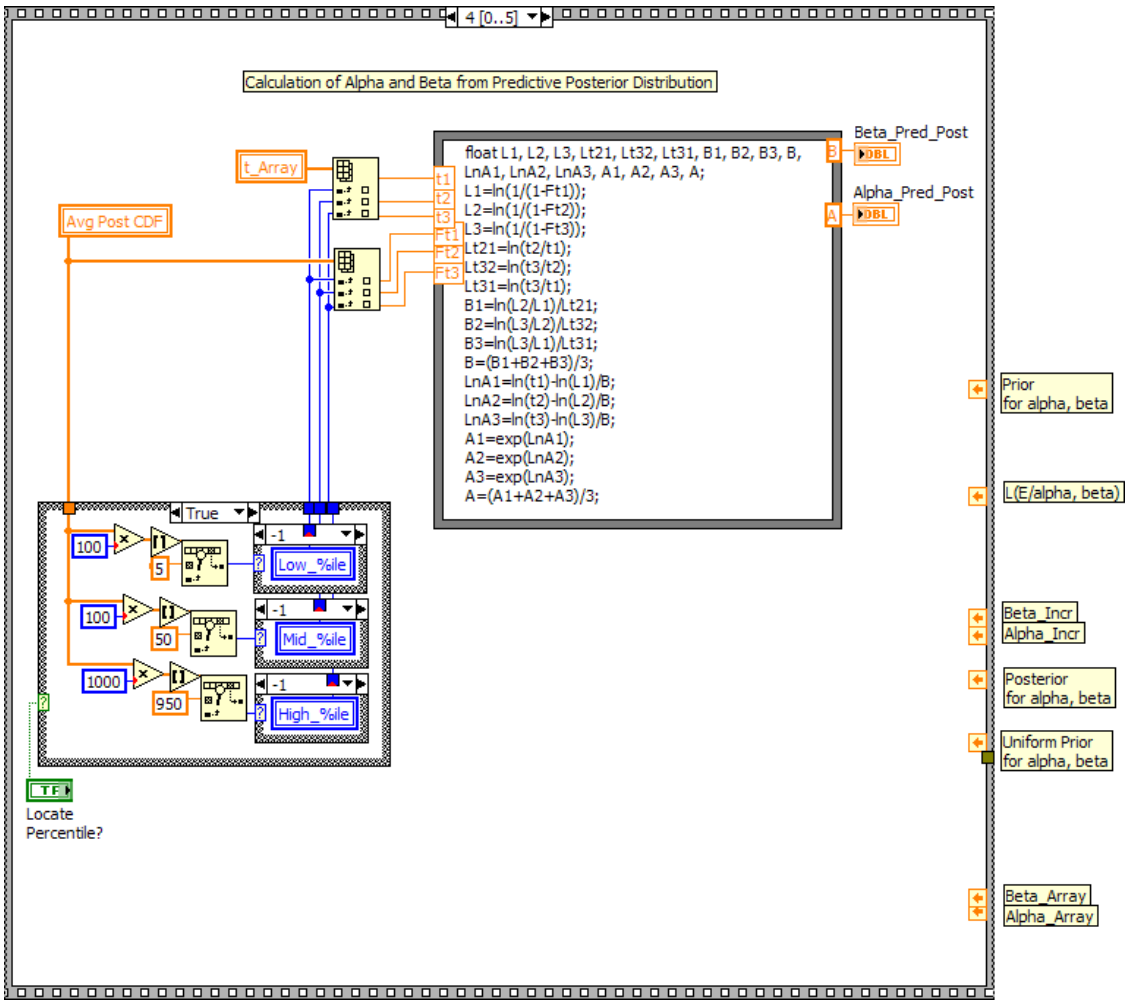

Fig A6.11 Block diagram Page 5 of labview program for Weibull Bayesian Analysis

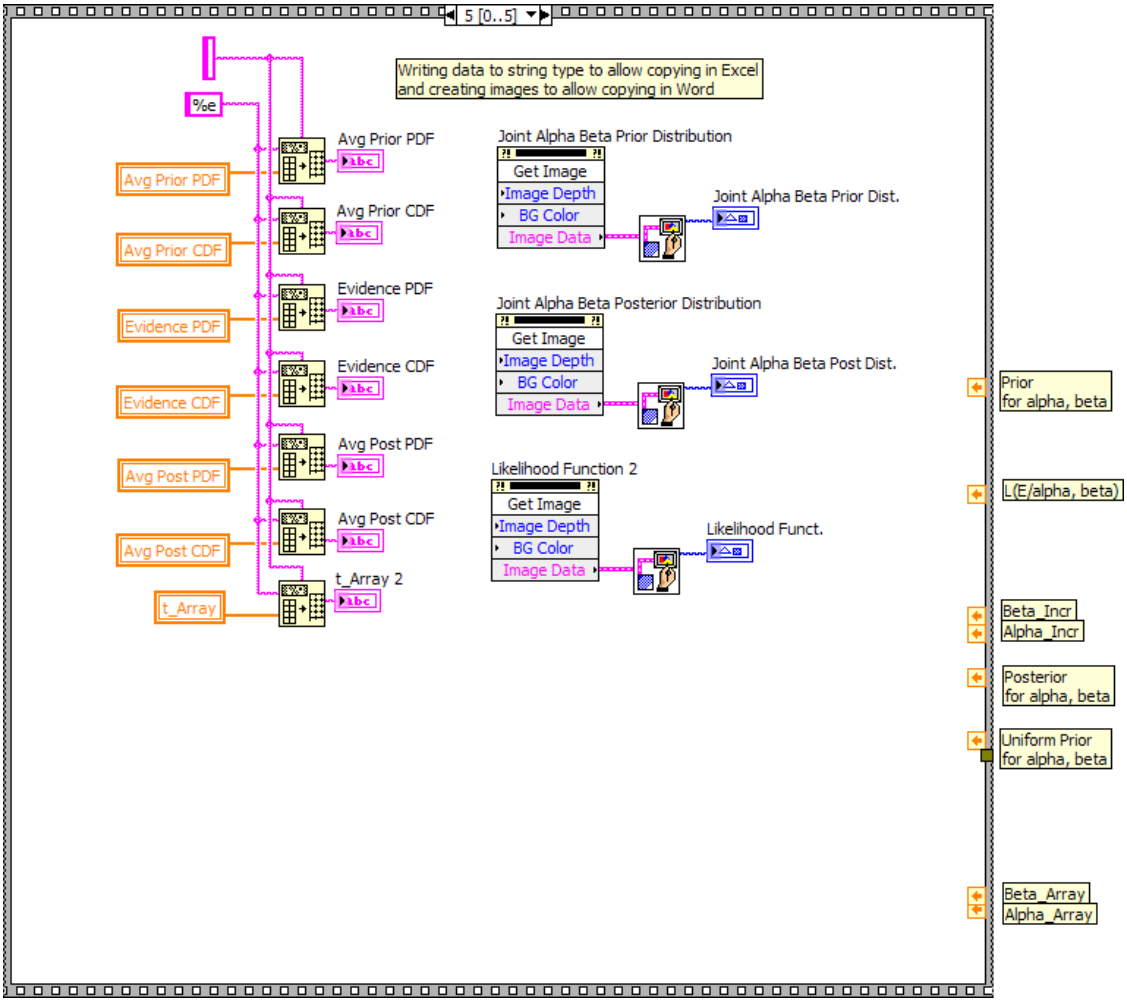

Fig A6.12 Block diagram Page 6 of labview program for Weibull Bayesian Analysis

Appendix-7: Transformation of Partially Relevant Data

The following data sets were generated for incorporating partially relevant data in Bayesian modeling.

Set1={AlGaInP-DH-DC, AlGaInP-MQW-DC, GaN-MQW-DC}

Also included in the table below is AlGaInP-MQW-Pulse-ALT data (normalized).

Weibull-Alpha	2.76E+04	7.82E+05	8.96E+03	1.61E+05	1.55E+09
Weibull-Beta	0.5	0.89	0.051	0.57	0.5
Weibull-MTTF	1.33E+04	5.17E+05	-	8.47E+04	7.50E+08
Degree of Relevance R	-	-	-	-	1
Multiplier-Transformation	1	1	1	1	1
Sr.#	AlGaInP-DH-DC-Prior	AlGaInP-MQW-DC-Prior	GaN-DH-DC-Prior	GaN-MQW-DC-Prior	AlGaInP-MQW-Pulse-ALT
1	517	200847	8914	8109	2028219
2	1546	200847	8936	8959	13657673
3	1785	204375	8950	9278	70127380
4	1890	236850	8957	10244	121596002
5	4348	236850	8958	13378	122412140
6	4364	273345	8966	15280	194486142
7	4527	304137		24998	265744520
8	5814	342795		132711	298940988
9	7095	807254		140061	312817482
10	16017	2446245		152794	1016462110
11	24825	3328400		189476	1126317125
12	33646			715395	1578094167
13	577168			966689	1960342868
14	577611			987052	3605343586
15					4795072177
16					9473549316
17					9914108215
18					10513715986

Table A7.1 Set 1 and ALT data

Set2={AlGaInP-DH-DCx500, AlGaInP-MQW-DCx500, GaN-MQW-DCx500}

Set3={AlGaInP-DH-DCx1451, AlGaInP-MQW-DCx1451, GaN-MQW-DCx1451}

Weibull-Alpha	1.38E+07	3.91E+08	8.05E+07	4.00E+07	1.13E+09	2.34E+08
Weibull-Beta	0.5	0.89	0.57	0.500	0.890	0.570
Weibull-MTTF	6.65E+06	2.59E+08	4.24E+07	1.93E+07	7.50E+08	1.23E+08
Degree of Relevance R	0.45	0.74	0.49	0.71	1.00	0.75
Multiplier-Transformation	500	500	500	1451	1451	1451
Sr.#	AlGaInP-DH-DCx500	AlGaInP-MQW-DCx500	GaN-MQW-DCx500	AlGaInP-DH-DCx1451	AlGaInP-MQW-DCx1451	GaN-MQW-DCx1451
1	258500	100423500	4054500	750167	291428997	11766159
2	773000	100423500	4479500	2243246	291428997	12999509
3	892500	102187500	4639000	2590035	296548125	13462378
4	945000	118425000	5122000	2742390	343669350	14864044
5	2174000	118425000	6689000	6308948	343669350	19411478
6	2182000	136672500	7640000	6332164	396623595	22171280
7	2263500	152068500	12499000	6568677	441302787	36272098
8	2907000	171397500	66355500	8436114	497395545	192563661
9	3547500	403627000	70030500	10294845	1171325554	203228511
10	8008500	1223122500	76397000	23240667	3549501495	221704094
11	12412500	1664200000	94738000	36021075	4829508400	274929676
12	16823000		357697500	48820346		1038038145
13	288584000		483344500	837470768		1402665739
14	288805500		493526000	838113561		1432212452

Table A7.2 Set 2 and Set3 data

Appendix-8: Bayesian updating using partially relevant data

Table 9.1 Summary of Bayesian Analysis using partially relevant data is reproduced here for convenience. The next few pages provide details for each analysis:

Sr .#.	**Prior**	**Evidence 1 with Likelihood^{R}**	**Deg of Rel.**	**Evid-ence 2**	**Predictive Posterior**		**Mean TTF**	**Ch-Sq Statistic**
			R		**α**	**β**	**hrs**	**< 4.6**
1a	Uniform*	AlGaInP-MQW-DCx500 with L^{R}	1.00	ALT$^{\Psi}$	1.17E9	0.547	6.00E8	0.392
1b	Uniform*	AlGaInP-MQW-DCx500 with L^{R}	0.75	ALT$^{\Psi}$	1.30E9	0.538	6.58E8	0.244
2	Uniform*	AlGaInP-MQW-DCx1451 with L^{R}	1.00	ALT$^{\Psi}$	1.57E9	0.601	8.76E8	0.741
3a	Uniform*	GaN-MQW-DCx500 with L^{R}	1.00	ALT$^{\Psi}$	6.70E8	0.415	2.63E8	1.598
3b	Uniform*	GaN-MQW-DCx500 with L^{R}	0.50	ALT$^{\Psi}$	1.06E9	0.437	4.60E8	0.272
4a	Uniform*	GaN-MQW-DCx1451 with L^{R}	1.00	ALT$^{\Psi}$	9.05E8	0.474	4.00E8	0.673
4b	Uniform*	GaN-MQW-DCx1451 with L^{R}	0.75	ALT$^{\Psi}$	1.05E9	0.477	4.87E8	0.314
5a	Uniform*	AlGaInP-DH-DCx500 with L^{R}	1.00	ALT$^{\Psi}$	4.85E8	0.358	1.74E8	2.889
5b	Uniform*	AlGaInP-DH-DCx500 with L^{R}	0.50	ALT$^{\Psi}$	8.90E8	0.387	3.46E8	0.725
6a	Uniform*	AlGaInP-DH-DCx1451 with L^{R}	1.00	ALT$^{\Psi}$	5.88E8	0.388	2.29E8	2.084
6b	Uniform*	AlGaInP-DH-DCx1451 with L^{R}	0.75	ALT$^{\Psi}$	7.43E8	0.395	2.94E8	1.886

Table 9.1 Summary of Bayesian Analysis using partially relevant data (Reproduced for convenience)

* Uniform prior joint α-β distribution with α taking values between 5E7 to 9E9 and β taking values between 0.1 to 2.

$^{\Psi}$ Accelerated Life Test (ALT) data given in Sr.# 5 of Table 8.1 used as evidence 2.

Details are provided in charts in the following pages

Sr .#.	Prior	Evidence 1 with Likelihood^{R}	Deg of Rel.	Evid-ence 2	Predictive Posterior		Mean TTF	Ch-Sq Statistic
			R		α	β	hrs	< 4.6
1a	Uniform*	AlGaInP-MQW-DCx500 with L^{R}	1.00	ALT$^{\Psi}$	1.17E9	0.547	6.00E8	0.392

1st Bayesian Updating

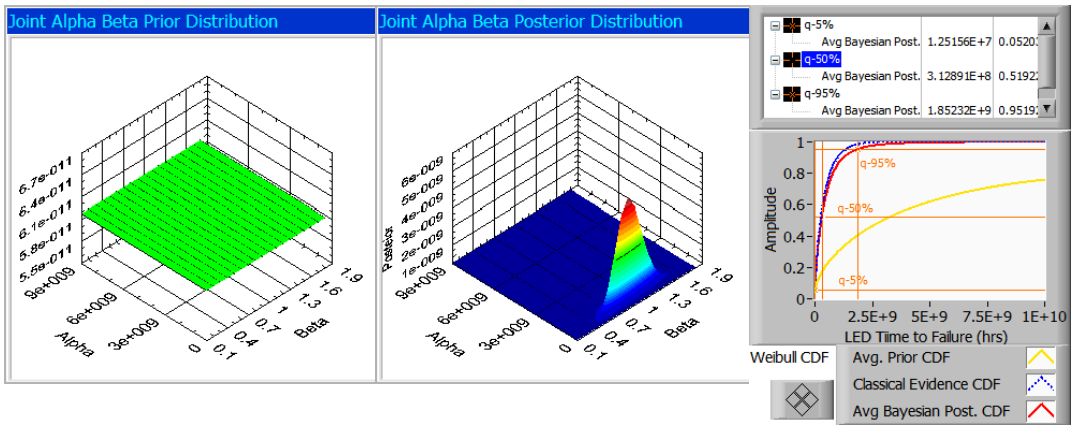

2nd Bayesian Updating

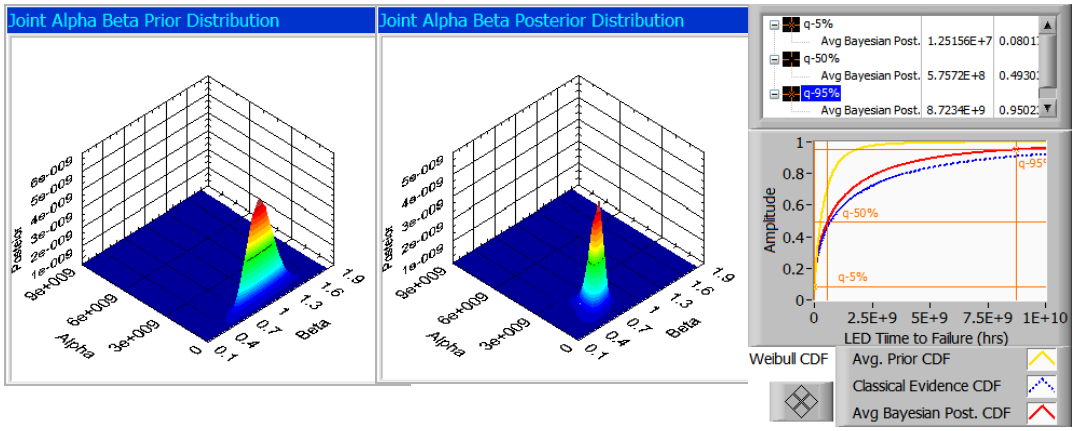

Sr .#.	Prior	Evidence 1 with Likelihood^{R}	Deg of Rel.	Evid-ence 2	Predictive Posterior		Mean TTF	Ch-Sq Statistic
			R		α	β	hrs	< 4.6
1b	Uniform*	AlGaInP-MQW-DCx500 with L^{R}	0.75	ALT$^{\Psi}$	1.30E9	0.538	6.58E8	0.244

1st Bayesian Updating

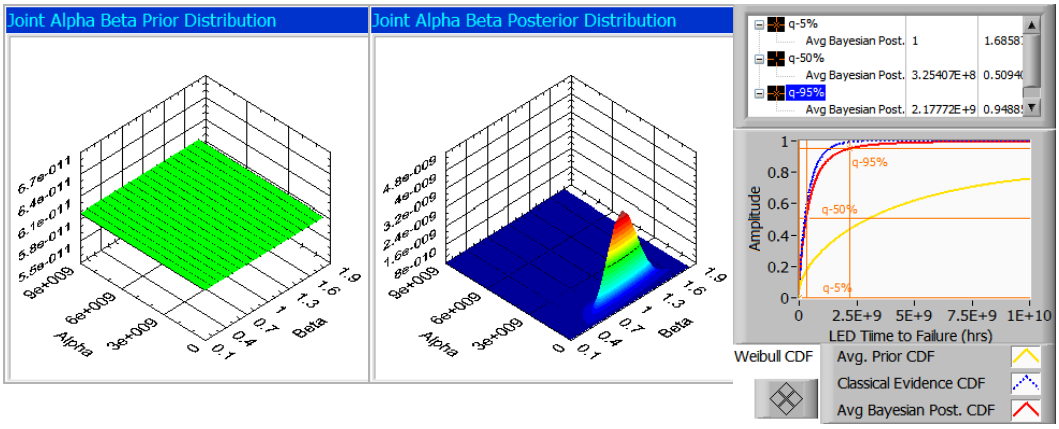

2nd Bayesian Updating

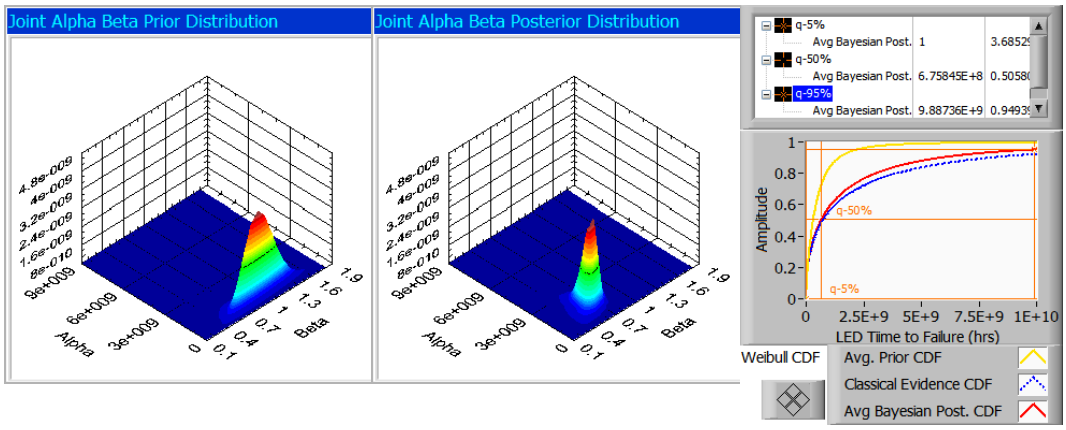

Sr .#.	Prior	Evidence 1 with Likelihood^{R}	Deg of Rel.	Evid-ence 2	Predictive Posterior		Mean TTF	Ch-Sq Statistic
			R		α	β	hrs	< 4.6
2	Uniform*	AlGaInP-MQW-DCx1451 with L^{R}	1.00	ALT^{Ψ}	1.57E9	0.601	8.76E8	0.741

1st Bayesian Updating

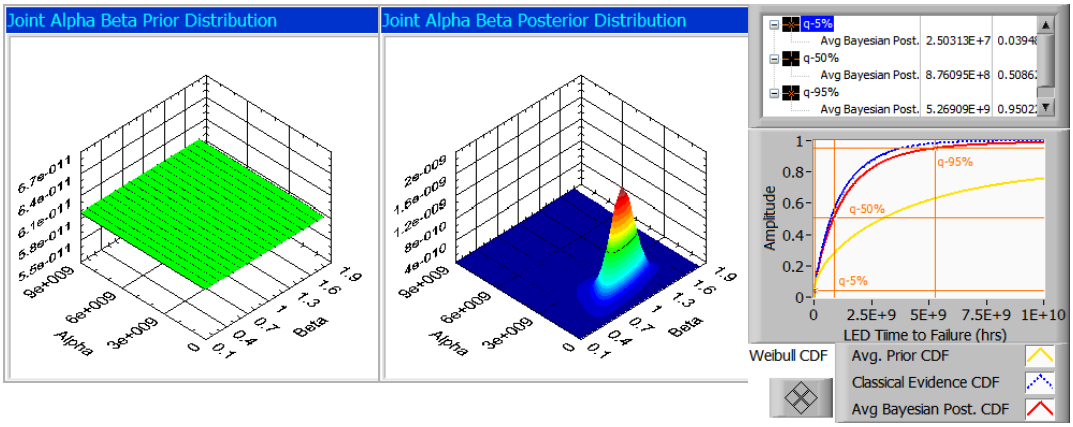

2nd Bayesian Updating

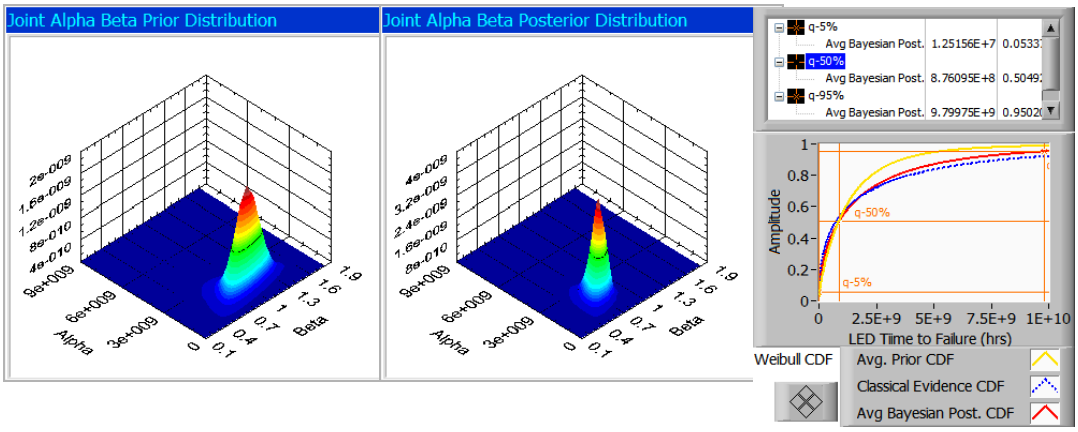

Sr .#.	Prior	Evidence 1 with Likelihood^{R}	Deg of Rel.	Evid-ence 2	Predictive Posterior		Mean TTF	Ch-Sq Statistic
			R		α	β	hrs	< 4.6
3a	Uniform*	GaN-MQW-DCx500 with L^{R}	1.00	ALT$^{\Psi}$	6.70E8	0.415	2.63E8	1.598

1st Bayesian Updating

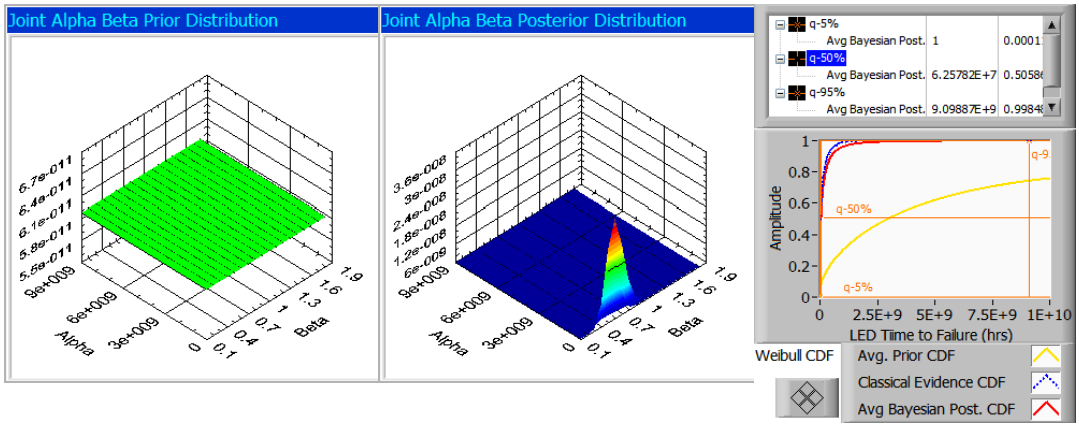

2nd Bayesian Updating

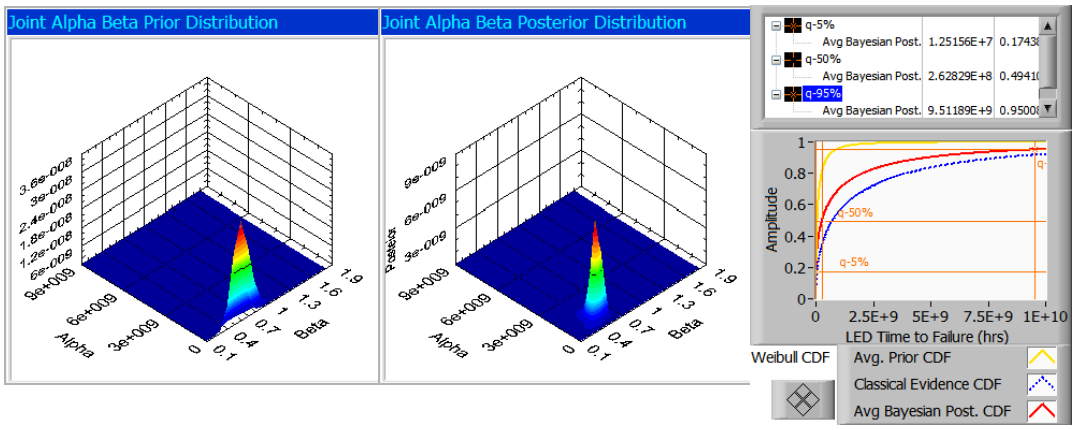

Sr .#.	Prior	Evidence 1 with Likelihood^{R}	Deg of Rel.	Evid-ence 2	Predictive Posterior		Mean TTF	Ch-Sq Statistic
			R		α	β	hrs	< 4.6
3b	Uniform*	GaN-MQW-DCx500 with L^{R}	0.50	ALT$^{\Psi}$	1.06E9	0.437	4.60E8	0.272

1st Bayesian Updating

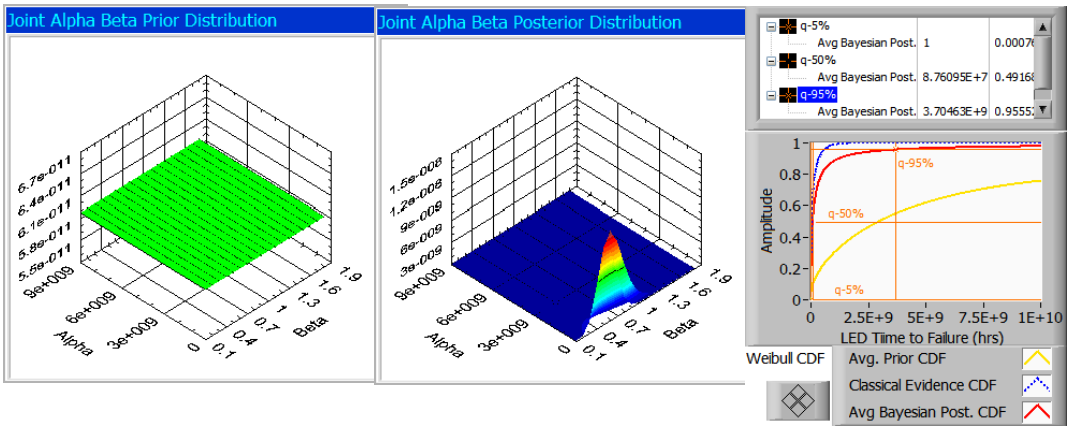

2nd Bayesian Updating

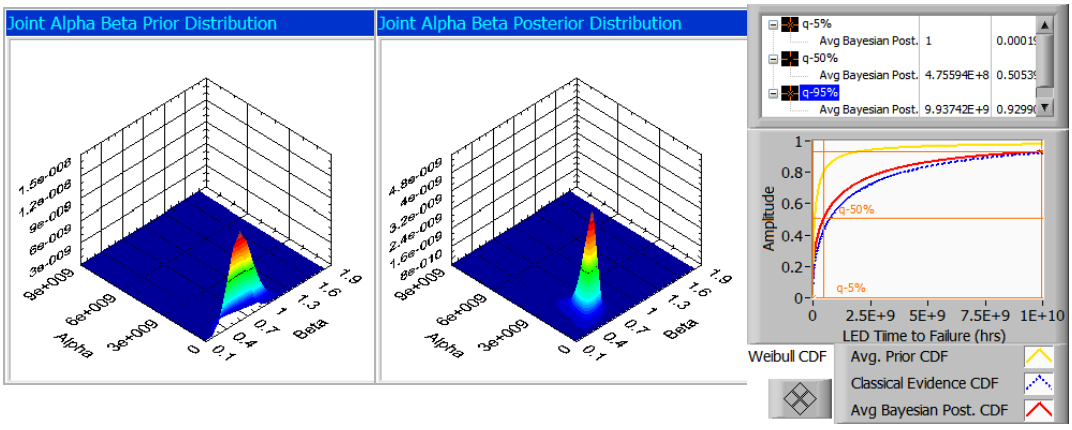

Sr .#.	Prior	Evidence 1 with Likelihood^{R}	Deg of Rel.	Evid-ence 2	Predictive Posterior		Mean TTF	Ch-Sq Statistic
			R		α	β	hrs	< 4.6
4a	Uniform*	GaN-MQW-DCx1451 with L^{R}	1.00	ALT^{Ψ}	9.05E8	0.474	4.00E8	0.673

1st Bayesian Updating

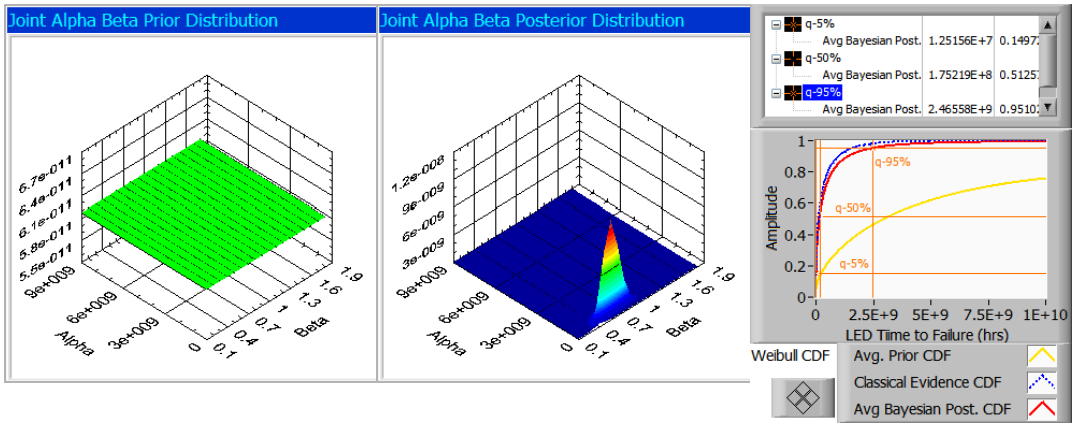

2nd Bayesian Updating

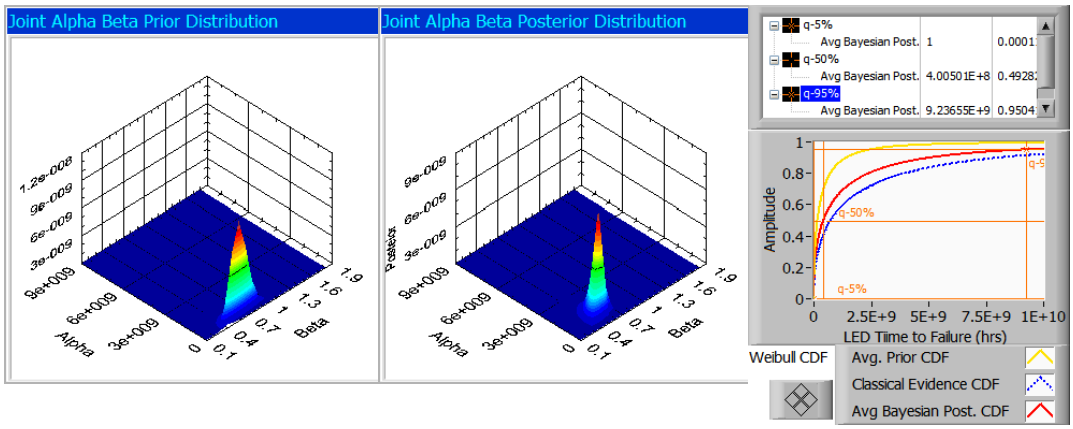

Sr .#.	Prior	Evidence 1 with Likelihood^{R}	Deg of Rel.	Evid-ence 2	Predictive Posterior		Mean TTF	Ch-Sq Statistic
			R		α	β	hrs	< 4.6
4b	Uniform*	GaN-MQW-DCx1451 with L^{R}	0.75	ALT$^{\Psi}$	1.05E9	0.477	4.87E8	0.314

1st Bayesian Updating

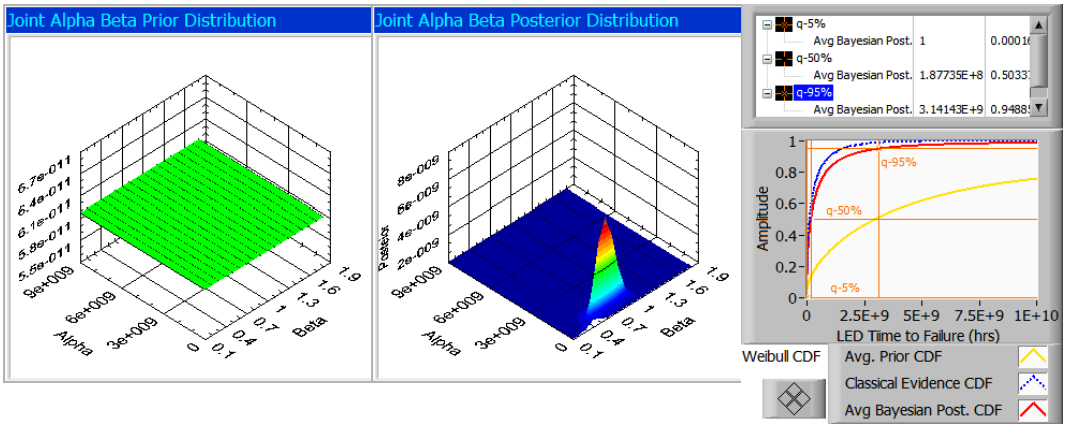

2nd Bayesian Updating

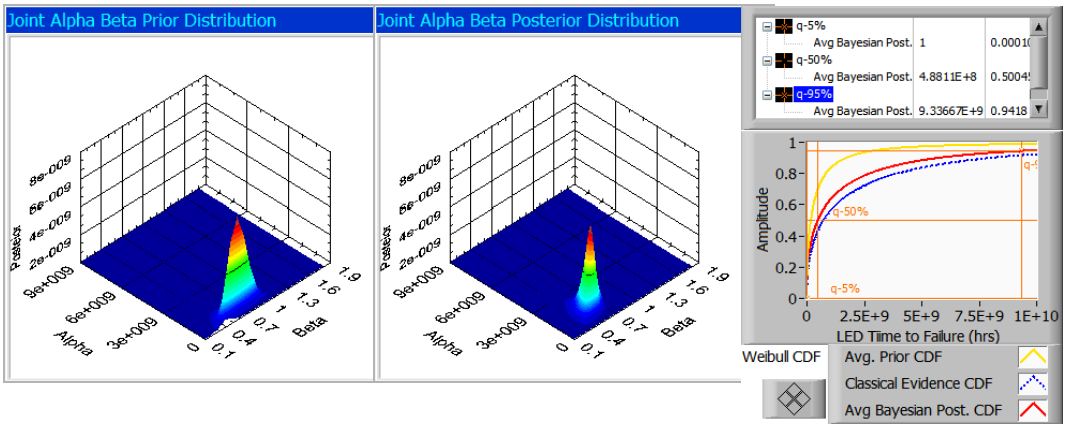

Sr .#.	Prior	Evidence 1 with Likelihood^{R}	Deg of Rel.	Evid-ence 2	Predictive Posterior		Mean TTF	Ch-Sq Statistic
			R		α	β	hrs	< 4.6
5a	Uniform*	AlGaInP-DH-DCx500 with L^{R}	1.00	ALT$^{\Psi}$	4.85E8	0.358	1.74E8	2.889

1st Bayesian Updating

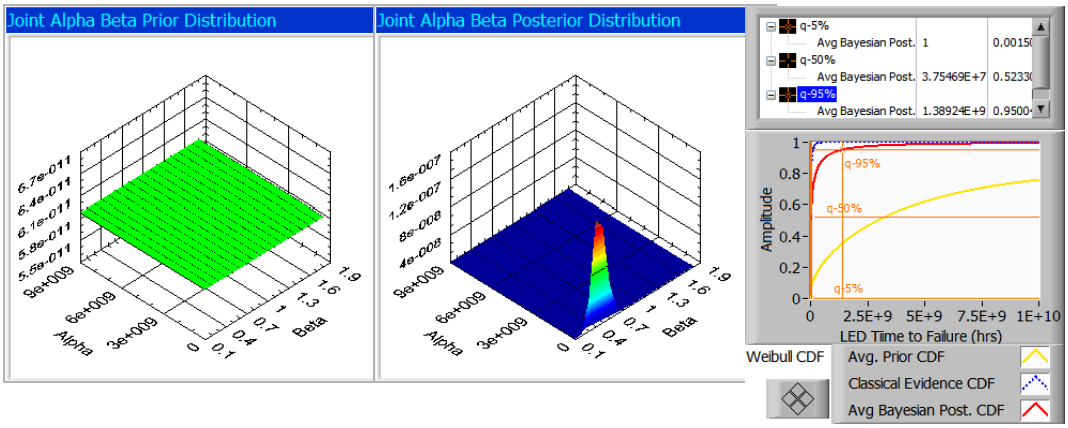

2nd Bayesian Updating

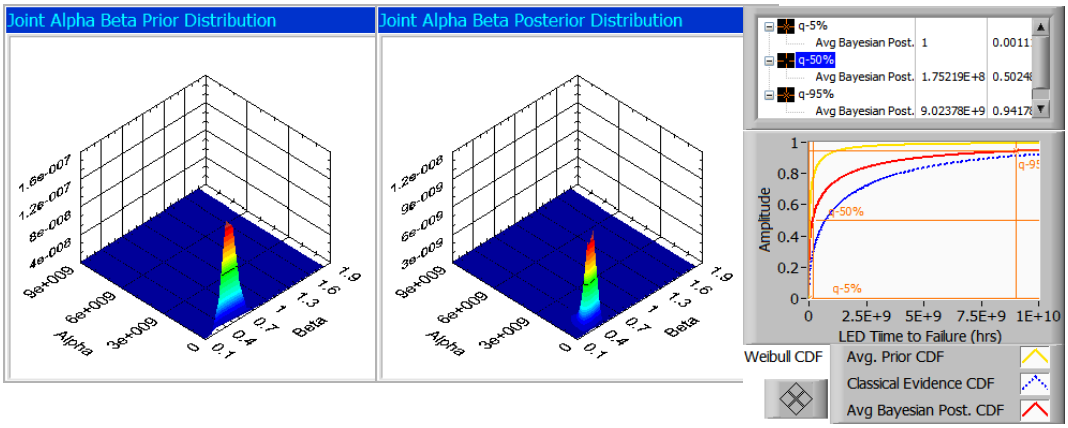

Sr .#.	Prior	Evidence 1 with Likelihood^{R}	Deg of Rel.	Evid-ence 2	Predictive Posterior		Mean TTF	Ch-Sq Statistic
			R		α	β	hrs	< 4.6
5b	Uniform*	AlGaInP-DH-DCx500 with L^{R}	0.50	ALT^{Ψ}	8.90E8	0.387	3.46E8	0.725

1st Bayesian Updating

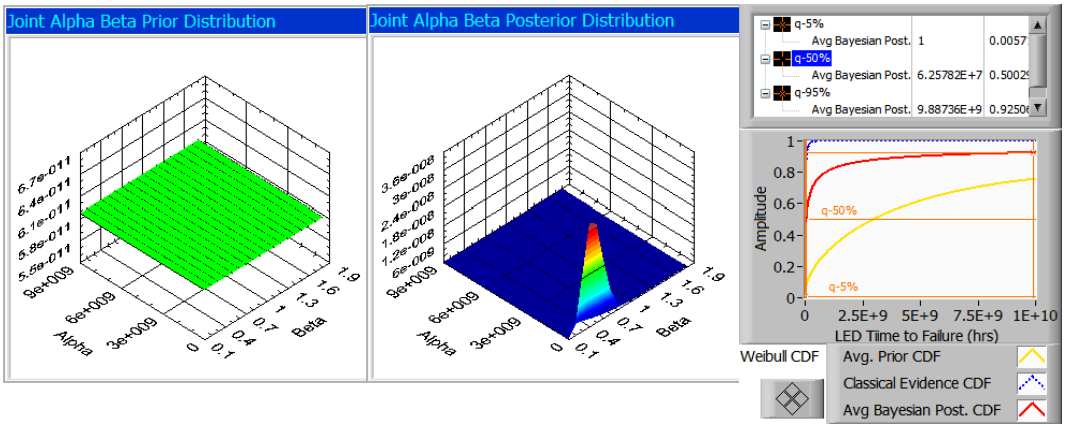

2nd Bayesian Updating

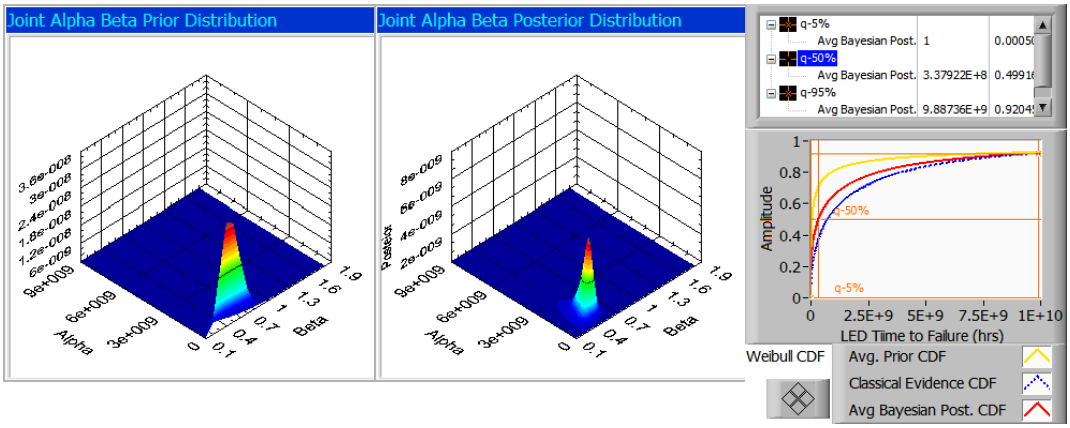

Sr .#.	Prior	Evidence 1 with Likelihood^{R}	Deg of Rel.	Evid-ence 2	Predictive Posterior		Mean TTF	Ch-Sq Statistic
			R		α	β	hrs	< 4.6
6a	Uniform*	AlGaInP-DH-DCx1451 with L^{R}	1.00	ALT$^{\Psi}$	5.88E8	0.388	2.29E8	2.084

1st Bayesian Updating

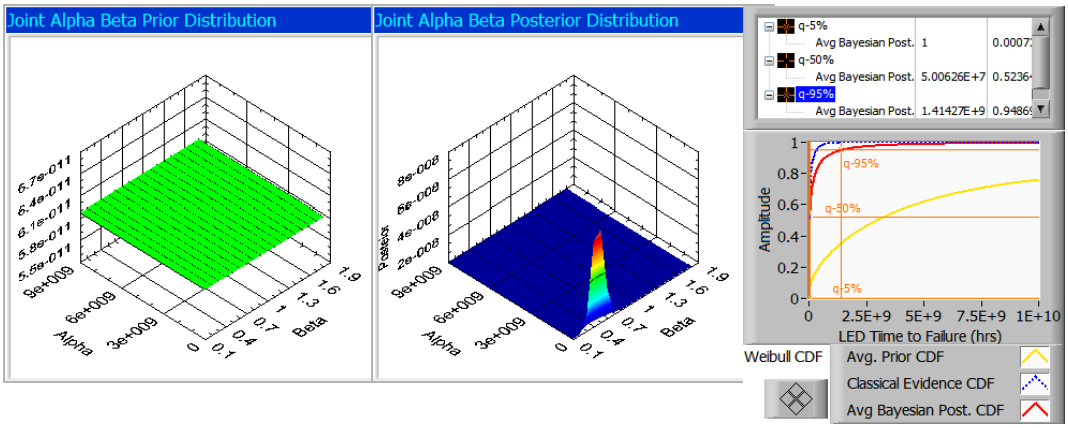

2nd Bayesian Updating

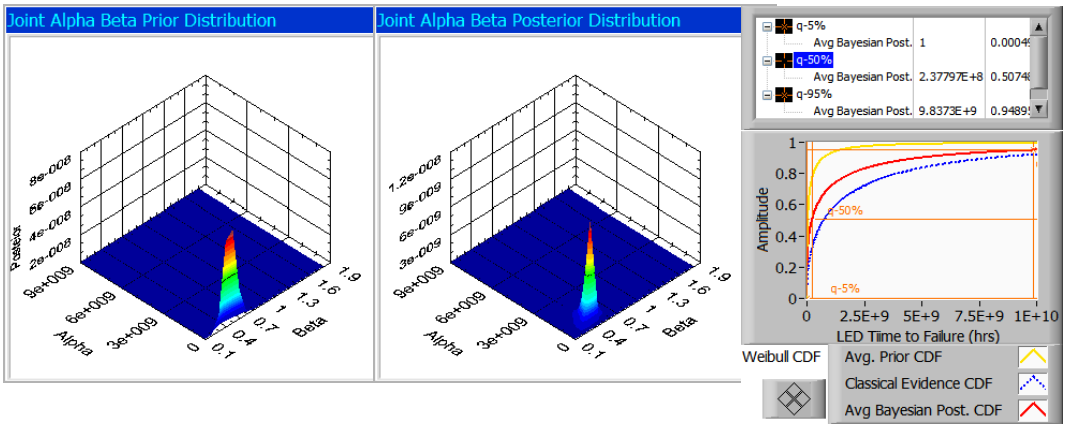

Sr .#.	Prior	Evidence 1 with Likelihood^{R}	Deg of Rel.	Evid-ence 2	Predictive Posterior		Mean TTF	Ch-Sq Statistic
			R		α	β	hrs	< 4.6
6b	Uniform*	AlGaInP-DH-DCx1451 with L^{R}	0.75	ALT^{Ψ}	7.43E8	0.395	2.94E8	1.886

1st Bayesian Updating

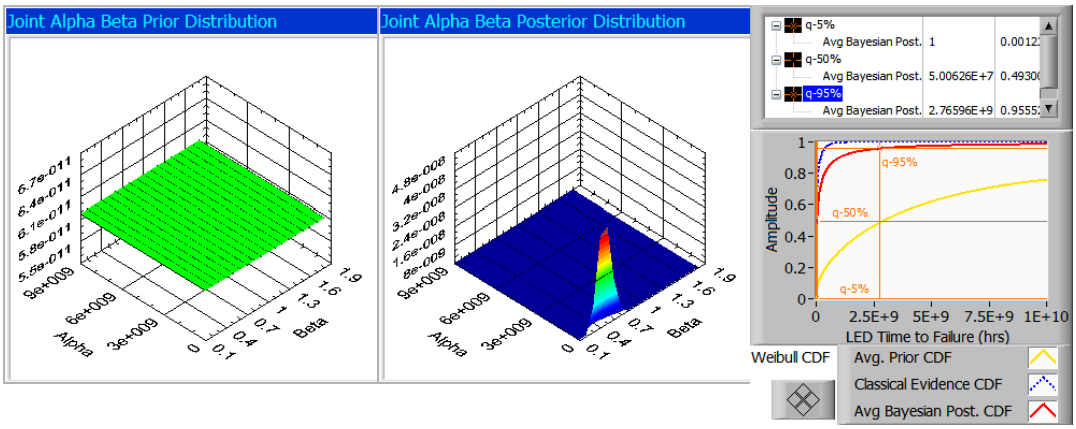

2nd Bayesian Updating

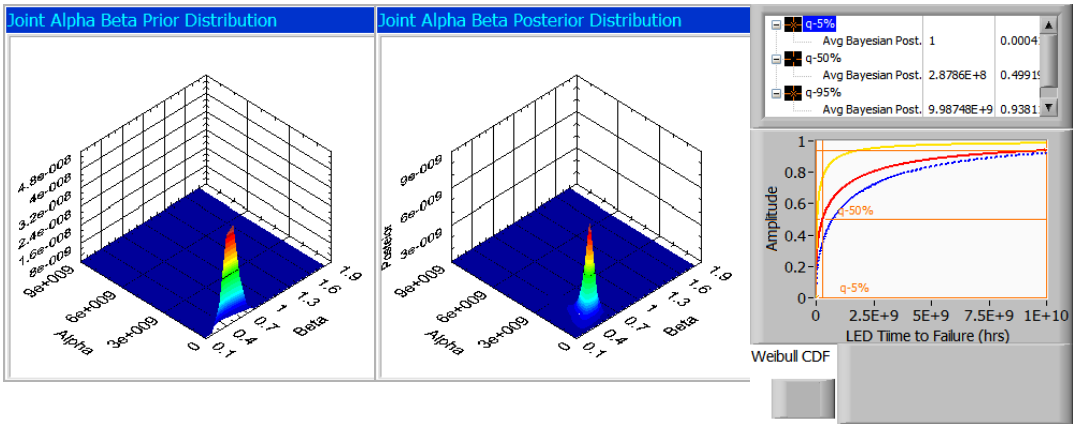

References

1. http://en.wikipedia.org/wiki/Beers_law.

2. Mitsuo Fukuda, ‘Reliability & Degradation of Semiconductor Lasers & LEDs’, 1991.

3. Shuji Nakamura & S.F. Chichibu, ‘Introduction to Nitride Semiconductor Blue Lasers & LEDs’, ‘Chpt. 7 Development & future prospects of InGaN based LEDs and LDs’, 2000.

4. Michael Stamatelatos et al, ‘Probabilistic Risk Assessment Procedures Guide for NASA Managers and Practitioners’, August 2002.

5. http://en.wikipedia.org/wiki/LED

6. H. Morkoc, ‘Nitride Semiconductors and Devices’, ‘Chpt. 11 Light Emitting Diodes’, Springer, 1999.

7. Bart Van Zeghbroeck, ‘Principals of Semiconductor Devices’, 2011.

8. Ali Mosleh, ‘Data Collection and Analysis for Risk and Reliability’, 2007.

9. http://en.wikipedia.org/wiki/Band_structure

10. http://en.wikipedia.org/wiki/Diode#Shockley_diode_equation

11. Sawant et al. ‘Failure modes and effects criticality analysis and accelerated life testing of LEDs for medical applications’, International Semiconductor Device Research Symposium (ISDRS), College Park, MD, Dec 2011.

12. Sawant et al. ‘Thermal shifts of active layer bandgap (Eg) during accelerated reliability testing of AlGaInP LEDs: A real or virtual failure mechanism?’, Workshop

on Compound Semiconductor Devices and Integrated Circuits (WOCSDICE), Island of Porquerolles, France, May 2012.

13. Sawant et al. ‘A Bayes approach and criticality analysis for reliability prediction of AlGaInP light emitting diodes’, Reliability of Compound Semiconductors Workshop (ROCS), Boston MA, April 2012.

14. Ott et al. 'Capabilities and Reliability of LEDs and Laser Diodes', NASA report, Technology Validation Assurance Group, updated 9/3/1997.

15. Vanderwater et al. ‘High-brightness AlGaInP light emitting diodes', Proceedings of the IEEE, Vol. 85, Issue 11, Pages 1752-1764, Nov. 1997.

16. Grillot et al. ‘Sixty Thousand Hour Light Output Reliability of AlGaInP LEDs', IEEE Trans. on Device and Mat. Reliability, Vol. 6, No.4, Pages 564-574, Dec 2006.

17. Kish et al. ‘Highly reliable and efficient semiconductor wafer-bonded AlGaInP/GaP LEDs', Electronics Letters, Vol. 32, Issue 2, Pages132–136, Jan 1996.

18. Hofler et al. ‘High-flux high-efficiency transparent-substrate AlGaInP/GaP LEDs', Electronics Letters, Vol. 34, Issue 18, Pages 1781-1782, September 1998.

19. Chang et al. ‘AlGalnP multiquantum well light-emitting diodes', IEE Proc.-Optoelectron., Vol. 144, No. 6, December 1997.

20. Kish et al. ‘High luminous flux semiconductor wafer-bonded AlGaInP/GaP large-area emitters', Electronics Letters, Vol. 30, Issue 21, Pages 1790-1792, October 1994.

21. Krames et al. ‘Status and Future of High-Power LEDs for Solid-State Lighting', Journal of Display Technology, Vol. 3, Issue 2, Pages 160–175, June 2007.

22. Streubel et al. ‘High Brightness AlGaInP Light-Emitting Diodes', IEEE Journal of Selected Topics in Quantum Electronics, Pages 321–332, March-April 2002.

23. Altieri et al. ‘Analysis of internal quantum efficiency of high-brightness AlGaInP LEDs', The 4th International Conference on Numerical Simulation of Optoelectronic Devices Proceedings NUSOD '04, Pages 13-14, August 2004.

24. Philips, ‘LUXEON Reliability Datasheet RD25’, Pages 9-10, July 2006.

25. Liang et al. ‘Comparison of temperature dependent electroluminescence of InGaN/GaN and AlGaInP based LEDs', Optoelectronics, The 6th Chinese Symposium Proceedings Pages 196-199, Sept. 2003.

26. Lin et al. ‘Highly reliable operation of indium tin oxide AlGaInP light emitting diodes', Electronics Letters, Vol. 30, No.21, October 1994.

27. Su et al. ‘High reliability of AlGaInP LEDs with tensile strain barrier-reducing Layer', IEEE Photonics Technology Letters, Vol. 16, Issue 1, Pages 30–32, Jan. 2004

28. Lacey et al. 'The reliability of AlGaInP visible LEDs', Quality & Reliability Engineering, Vol. 16, Issue 1, Pages 45 – 49, 2000.

29. Dutta et al. ‘High Brightness and Reliable AlGaInP-Based LED for POF Data Links', IEEE Photonics Technology Letters, Vol. 9, No 12, December 1997.

30. Nogueira et al. ‘Accelerated Life Testing LEDs on Temperature and Current', Proceedings of the 8th Spanish Conference on Electron Devices, Pages 1-4, Feb 2011.

31. Chen et al. 'Thermal resistance and reliability of low-cost high-power LED packages under WHTOL test', Int. Conf. on Electronic Materials and Packaging, EMAP 2008, Pages 271-276, Oct. 2008.

32. Meneghini et al. 'A review on the Reliability of GaN based LEDs', IEEE transactions on device and materials reliability, Vol. 8, No. 2, June 2008.

33. Meneghini et al. ' A review on the physical mechanisms that limit the reliability of GaN based LEDs', IEEE trans. on electron devices, Vol. 51, Issue. 1, Jan 2010.
34. Levada et al. ' Analysis of DC Current Accelerated Life Tests of GaN LEDs Using a Weibull-Based Statistical Model', IEEE transactions on device and materials reliability, Vol. 5, No. 4, Dec 2005.
35. Buso et al. 'Performance Degradation of High-Brightness LEDs Under DC and Pulsed Bias', IEEE trans. on device and materials reliability, Vol. 8, No. 2, June 2008.
36. Trevisanello et al. 'Accelerated life test of High Brightness LEDs', IEEE transactions on device and materials reliability, Vol. 8, No. 2, June 2008.
37. Meneghesso et al. 'Degradation mechanisms of GaN-based LEDs after accelerated DC current aging', Electron Devices Meeting Digest, Pages 103-106, Dec 2002.
38. Levada et al. ' High Brightness InGaN LED degradation at high injection current bias', 44th Ann. Int. Reliability Physics Symposium Proc., Pages 615-616, Mar 2006.
39. Meneghesso et al. 'Failure mechanisms of GaN-based LEDs related with instabilities in doping profile and deep levels', 42nd Annual International Reliability Physics Symposium Proceedings, Pages 474-478, April 2004.
40. Trevisanello et al. 'Thermally activated degradation and package instabilities of low flux LEDS ', Ann. Int. Reliability Physics Symp. Proc, Pages 98-103, April 2009.
41. Meneghini et al. 'High Temperature Degradation of GaN LEDs related to passivation', IEEE transactions on electron devices, Vol. 53, No. 12, Dec 2006.
42. Osinski et al. 'AlGaN/InGaN/GaN blue light emitting diode degradation under pulsed current stress', Applied Physics Letters, 69 (7), August 1996.

43. Barton et al. 'Life tests and failure mechanisms of GaN-AlGaN-InGaN LEDs', 35th Ann. Int. Reliability Physics Symposium Proc, Pages 276-281, April 1997.

44. Barton et al. 'Degradation mechanisms in GaN/AlGaN/InGaN LEDs and LDs', 10th Conf. on Semiconducting & Insul. Materials Proc., Pages 259-262, June 1998.

45. Wang et al. 'Device design and simulation for GaN based dual wavelength LEDs', Applied Optics, Vol. 48, No. 6, February 2009.

46. Shuji Nakamura, 'High-power InGaN/AlGaN double-heterostructure blue-LEDs, 'IEDM '94. Technical Digest', Dec 1994.

47. Yanagisawa T., 'Estimation of the degradation of InGaN/A1GaN Blue LEDs', Microelectronic Reliability, Vol. 37, No. 8, pp. 1239-1241, 1997.

48. Yanagisawa T. ' The degradation of GaAlAs red LEDs under continuous and low-speed pulse operations ', Microelectronics Reliability 38, pp. 1627-1630, 1998.

49. Narendran et al. 'Life of LED-Based White Light Sources', IEEE/OSA journal of display technology, Vol. 1, NO. 1, September 2005.

50. Narendran et al. 'Performance characteristics of high power LEDs', 3rd International conference on solid state lighting. Proc. of SPIE 5187: 267-275, 2004.

51. Tsai et al. 'Decay of radiation pattern and spectrum of high-power LED modules in aging test', IEEE Lasers and Electro-Optics Society, 2008. LEOS 2008. 21st Annual Meeting of the 9-13 Nov. 2008 Page(s):658 - 659.

52. Yoshi Ohno, 'Optical metrology for LEDs and solid state lighting', Fifth Symposium Optics in Industry, Proceedings of SPIE Vol. 6046, 604625, (2006).

53. Miller et al. ' LED Photometric Calibrations at the NIST and Future Measurement Needs of LEDs', Proc. of SPIE Vol. 5530 2004.

54. Miller et al. 'Luminous Intensity Measurement of LEDs at NIST' Proc. 2nd CIE Expert Symposium on LED Measurement, May 2001, Gaithersburg, MD, USA.

55. Miller et al. ' Luminous Flux calibration of LEDs at NIST' Proc. 2nd CIE Expert Symposium on LED Measurement, May 2001, Gaithersburg, MD, USA.

56. Getty et al. 'Electroluminescent measurement of the internal quantum efficiency of light emitting diodes', Applied Physics Letters, 94, 181102, 2009.

57. Park et al. 'Uncertainty evaluation for the spectro-radiometric measurement of the averaged LED intensity', Applied Optics, Vol. 46, No. 15, May 2007.

58. Brian Hall. ‘Methodology for evaluating reliability growth programs of discrete systems', Ph.D. Dissertation, Mechanical Engineering, University of Maryland, 2008.

59. Hall et al. ‘A Reliability Growth Projection Model for One-Shot Systems', IEEE transactions on reliability, Vol. 57, No.1, March 2008.

60. Hurtado-Cahuao, ‘Airframe Integrity Based on Bayesian Approach', Ph.D. Dissertation, Mechanical Engineering, University of Maryland, 2006.

61. Wang et al. ‘A probabilistic-based airframe integrity management model', Reliability Engineering & System Safety, Vol. 94, Issue 5, Pages 932-941, 2009.

62. R. Bris ‘Bayes approach in RDT using accelerated and long-term life data' Reliability Engineering & System Safety, Vol. 67, Issue 1, Pages 9-16, January 2000.

63. Anduin E. Touw ‘Bayesian estimation of mixed Weibull distributions' Reliability Engineering & System Safety, Vol. 94, Issue 2, Pages 463-473, Feb 2009.